NASA Contractor Report 3309

Atmospheric Turbulence Simulation Techniques With Application to Flight Analysis

Show-Tien Wang and Walter Frost

CONTRACT NAS8-32692
SEPTEMBER 1980

NASA

NASA Contractor Report 3309

Atmospheric Turbulence Simulation Techniques With Application to Flight Analysis

Show-Tien Wang and Walter Frost
The University of Tennessee Space Institute
Tullahoma, Tennessee

Prepared for
Marshall Space Flight Center
under Contract NAS8-32692

National Aeronautics
and Space Administration

**Scientific and Technical
Information Branch**

1980

AUTHORS' ACKNOWLEDGMENTS

This research was supported under NASA Contract No. NAS8-32692. The authors are grateful for the support of John H. Enders, Solomon Weiss and A. Richard Tobiason of the Office of Aeronautical and Space Technology, NASA Headquarters, Washington, DC. Special thanks go to Dennis W. Camp of the Space Sciences Laboratory, Atmospheric Sciences Division, NASA/George C. Marshall Space Flight Center, Alabama, who monitored the research program.

TABLE OF CONTENTS

LIST OF TABLES

LIST OF FIGURES

NOMENCLATURE

$A,B,C,D,$ a,b,c,d }	Constants
E	TKE density function
f	Cyclic frequency
f_c	Cut-off frequency, $f_c = 1/(2\Delta t)$
H	Filter function
K	Wavenumber, $K = \omega/V$
K_o	von Karman constant
L	Monin Obukhov length scale
N	Total number of signals
P	Probability density function
R	Correlation function
Ri	Gradient Richardson number
r	Non-Gaussian parameter
s	Laplace transform operator, $s = j\omega$
t	Time
Δt	Sampling time
U_i	i-component velocity
u_i	i-component fluctuation
u_*	Friction velocity given by $u_* = (t_o/\rho)^{1/2}$
V	Reference velocity
x,y	Time history function of random signal
X,Y	Frequency function of random signal
z	Height
z_o	Surface roughness

Greek Letters

γ	Coherence function
η	Reduction frequency, $\eta = fz/V$
Λ	Turbulence integral length scale
ρ	Density
σ^2	Variance
ϕ	Turbulence energy spectrum function
θ	Phase angle
ω	Angular frequency, $\omega = 2\pi f$

Subscripts

ℓ,m,n	Integer numbers
i	Direction indicator
i=1	Longitudinal component
i=2	Lateral component
i=3	Vertical component

CHAPTER I

INTRODUCTION

The effects of atmospheric turbulence on many of the modern sophisticated technological systems have become an important design parameter from both structural and performance aspects. Techniques for simulating atmospheric turbulence have therefore been developed in an attempt to provide reliable design criteria. Turbulence simulation is achieved by the generation of an analog or digital signal which has equivalent statistical characteristics to the true atmospheric turbulence. The degree of complexity and mathematical involvement of the models has increased with each successive generation, from a simple, one-component wind speed having a Gaussian distribution and a Dryden turbulence spectra to multi-component models having non-Gaussian probability distribution, more complex spectra, and simulation of other statistical properties, such as coherence. The simulated turbulence can then be used to predict the behavior of airplanes, bridges, buildings, etc., under the influence of a turbulent atmosphere. The purpose of this study is to investigate the effects of three turbulence models of various complexity on the performance of a simulated aircraft landing under an automatic controlled system. The work compares the aircraft landing under a

simple "Z-transform" simulation technique [1],[1] a non-Gaussian simulation technique [2], and a simulation which incorporates vertical coherence [3].

The basic simulation procedure is shown in Figure 1-1. Random signals are computer generated and passed through shaping filters to provide the output which is the simulated time history of turbulence. The degree of complexity of the system is internal to the filter system. Through the appropriate design of the filter, however, the turbulence signal output is designed to have certain statistical properties which are the same as those that have been measured and verified for atmospheric turbulence.

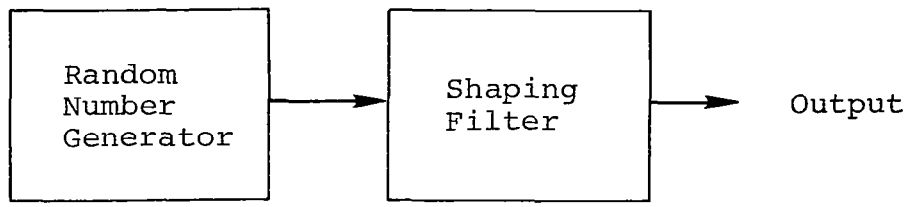

Figure 1-1. Turbulence simulation system.

This report first reviews the statistical properties of atmospheric turbulence, in particular the probability distribution, the spectra, and the coherence in Chapter II. The three different simulation techniques investigated in the study are then described in Chapter III,

---

[1]Numbers in brackets refer to similarly numbered references in the Bibliography.

and appropriate statistical analyses are carried out to verify validity of the models in Chapter IV. Finally, in Chapter V, the models are incorporated into a computer model of aircraft flight dynamics; and statistical landing results for simulated flights of an aircraft having characteristics of a DC-8 are made for the different turbulence simulation techniques. The significance of the various degrees of sophistication introduced into the simulation technique on the landing performance of the aircraft is discussed.

CHAPTER II

ATMOSPHERIC TURBULENCE AND MODELS

This chapter presents the basic expressions involved in mathematically describing atmospheric turbulence. In particular, the statistical properties such as the probability density distribution of wind speeds, the turbulence energy spectrum functions, and the spatial coherence are discussed.

A. Atmospheric Turbulence Spectra

In developing the atmospheric turbulence statistics, the wind velocity is written as

$$U_i = \overline{U}_i + u_i \ , \qquad (2\text{-}1)$$

where U_i is the instantaneous velocity, $\overline{U}_i$ is the average velocity, and u represents the fluctuating component. The subscript i denotes the i^{th} direction of the wind velocity. The intensity of the fluctuations in wind speed is expressed by the root-mean-square value

$$\sigma_i = (\overline{u_i^2})^{1/2} \ . \qquad (2\text{-}2)$$

The mean turbulence kinetic energy, TKE, is proportional to the value of u'^2 and includes contributions from all frequencies of eddies making up the turbulent

motion. If the time history of the velocity fluctuations is processed through a filter which passes only a small selected band of frequencies, $\Delta\omega$, the mean square value of the wind fluctuation in that frequency range will be proportional to the turbulence kinetic energy of gusts or perturbation in the wind having that frequency. The value of the turbulence kinetic energy density function at the midpoint of the band is then given by

$$E_{ij}(\omega) = \overline{u_i\, u_j} \;/\; \Delta\omega \;. \qquad (2\text{-}3)$$

The function $E_{ij}(\omega)$ forms the spectrum tensor having nine components. The function $E_{ii}(\omega)$ defined by Equation (2-3) for i = j is called the one-dimensional energy spectrum function. It follows that

$$\overline{u_i^2} = \int_0^\infty E_{ii}(\omega)\; d\omega \;. \qquad (2\text{-}4)$$

Frequently the energy spectral density is normalized as

$$\phi_i(\omega) = E_{ii}(\omega) \;/\; \overline{U}^2 \;, \qquad (2\text{-}5)$$

and thus,

$$\int_0^\infty \phi_i(\omega)\; d\omega = \overline{u_i^2} \;/\; \overline{U}^2 = \sigma_i^2 \;/\; \overline{U}^2 \;, \qquad (2\text{-}6)$$

where σ_i^2 is called the variance.

For $i \neq j$, the function $E_{ij}(\omega)$ is related to the cross-correlations and is called the cross-spectrum.

The energy spectrum tensor can be considerably simplified if the atmospheric turbulence is homogeneous and isotropic, for which there is no mean rate of transfer of momentum across shearing surfaces or, more specifically, the Reynolds or eddy shearing stresses, $-\rho\overline{u_i u_j}$, vanish. For this case, a three-dimensional energy spectrum function E(K) is defined as

$$E(K) = 2\pi K^2 [\, E_{11}(K) + E_{22}(K) + E_{33}(K) \,] , \qquad (2\text{-}7)$$

where K is the wave number defined as $K = \omega/V$, and V is the reference velocity; therefore, $E_{ij}(K) = VE_{ij}(\omega)$.

Figure 2-1 shows the typical form of the three-dimensional energy spectrum.

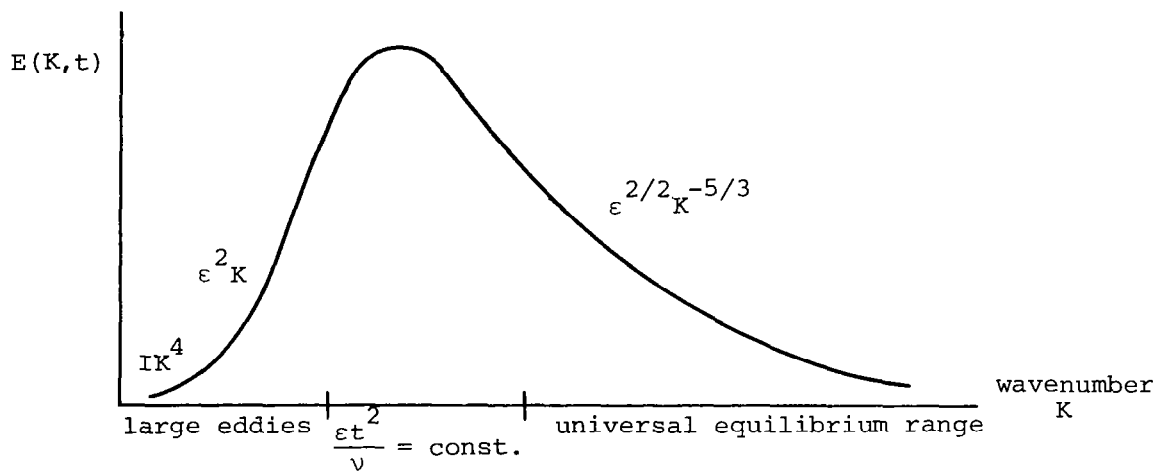

Figure 2-1. Typical three-dimensional energy spectrum function [4].

Physical argument coupled with dimensional analysis has provided basic insight into the behavior of E(K). The mathematical form of E(K) adopted by von Karman [5] is

$$E(K) = c \frac{(K/K_o)^4}{[1 + (K/K_o)^2]^{17/6}}, \qquad (2\text{-}8)$$

where $c = (55/9)(\Lambda/\rho)\sigma^2$, $K_o = 1/(1.339\Lambda)$, and Λ is the integral length scale defined by the correlation function R as

$$\Lambda = \int_o^\infty R(t)dt \ . \qquad (2\text{-}9)$$

This von Karman spectrum function exhibits a K^4 and $K^{-5/3}$ behavior at low and high frequencies, respectively, which represents the limiting conditions of the spectrum for these wave number ranges. Also, the one-dimensional spectrum function, ϕ, becomes

$$\phi_1(K) = \sigma_1^2 \frac{2\Lambda_1}{\pi} \frac{1}{[1 + (1.339\ \Lambda_1 K)^2]^{5/6}}$$

$$\phi_2(K) = \sigma_2^2 \frac{\Lambda_2}{\pi} \frac{1 + 8/3\ (1.339\ \Lambda_2 K)^2}{[1 + (1.339\ \Lambda_2 K)^2]^{11/6}} \qquad (2\text{-}10)$$

$$\phi_3(K) = \sigma_3^2 \frac{\Lambda_3}{\pi} \frac{1 + 8/3\ (1.339\ \Lambda_3 K)^2}{[1 + (1.339\ \Lambda_3 K)^2]^{11/6}},$$

where the subscripts 1, 2, and 3 represent longitudinal, lateral, and vertical fluctuations, respectively.

Also, Dryden [5] points out that for laboratory-type flow the shape of the velocity correlation curve can be approximated by an exponential function. In this case the one-dimensional Dryden spectra become

$$\phi_1(K) = \sigma_1^2 \frac{2\Lambda_1}{\pi} \frac{1}{1 + \Lambda_1^2 K^2}$$

$$\phi_2(K) = \sigma_2^2 \frac{\Lambda_2}{\pi} \frac{1 + 3\,\Lambda_2^2 K^2}{(1 + \Lambda_2^2 K^2)^2} \qquad (2\text{-}11)$$

$$\phi_3(K) = \sigma_3^2 \frac{\Lambda_3}{\pi} \frac{1 + 3\,\Lambda_3^2 K^2}{(1 + \Lambda_3^2 K^2)^2} .$$

Simulation of atmospheric turbulence usually employs the Dryden spectrum which exhibits a K^{-2} fall-off at high frequencies and is, therefore, easier to handle mathematically, as described later. However, as Figure 2-2 shows, the von Karman spectrum gives a better description of the measured data than the Dryden spectrum.

In a recent paper describing the spectral properties of atmospheric turbulence over a flat homogeneous field site, Kaimal [6] shows that with proper nondimensionalization, spectra in the stable atmospheric

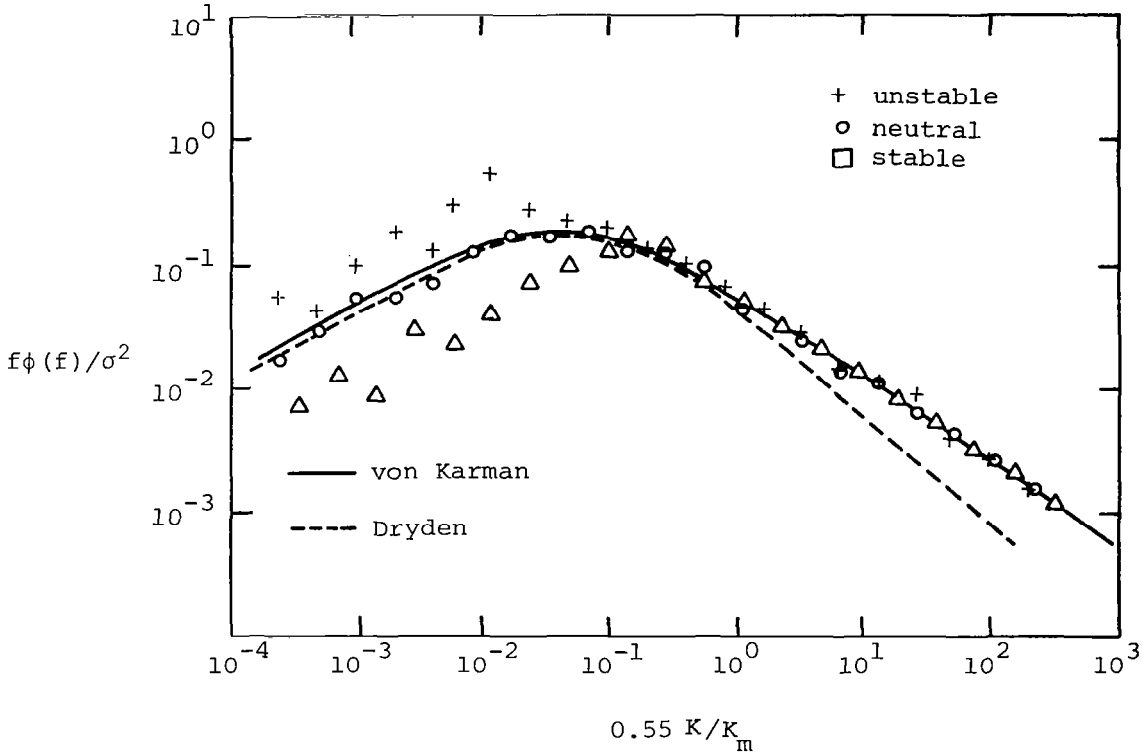

Figure 2-2. Longitudinal velocity spectra compared with the von Karman and Dryden spectra (wave-number normalized by the peak scale K_m of the vertical spectra) [8].

surface layer can be reduced to a universal curve having the empirical formula

$$\frac{f}{\sigma^2}\,\phi(f) = \frac{0.164\,(\eta/\eta_o)}{1 + 0.164\,(\eta/\eta_o)^{5/3}}\,, \qquad (2\text{-}12)$$

where f is the cyclic frequency, $\eta = fz/V$ is the reduced frequency, z is height, and η_o is a scaling parameter related to the atmospheric stability condition. Figure 2-3 shows η_o plotted both against the ratio of height to Monin Obukhov length scale, z/L, and against the gradient Richardson number, Ri. For neutral conditions, the values of η_o recommended by Frost, et al. [7] are

$$\begin{aligned} \eta_{o_1} &= 0.0144 \\ \eta_{o_2} &= 0.0265 \\ \eta_{o_3} &= 0.0962\,. \end{aligned} \qquad (2\text{-}13)$$

Figure 2-4 shows experimental data for atmospheric turbulence compared with Equation (2-12).

B. Filter Theory for Simulation Applications

The principal use of power spectral density functions is to establish the frequency composition of the data which, in turn, bears an important relationship to the basic characteristics of a physical system exposed to interaction with the turbulence. For example, consider a system

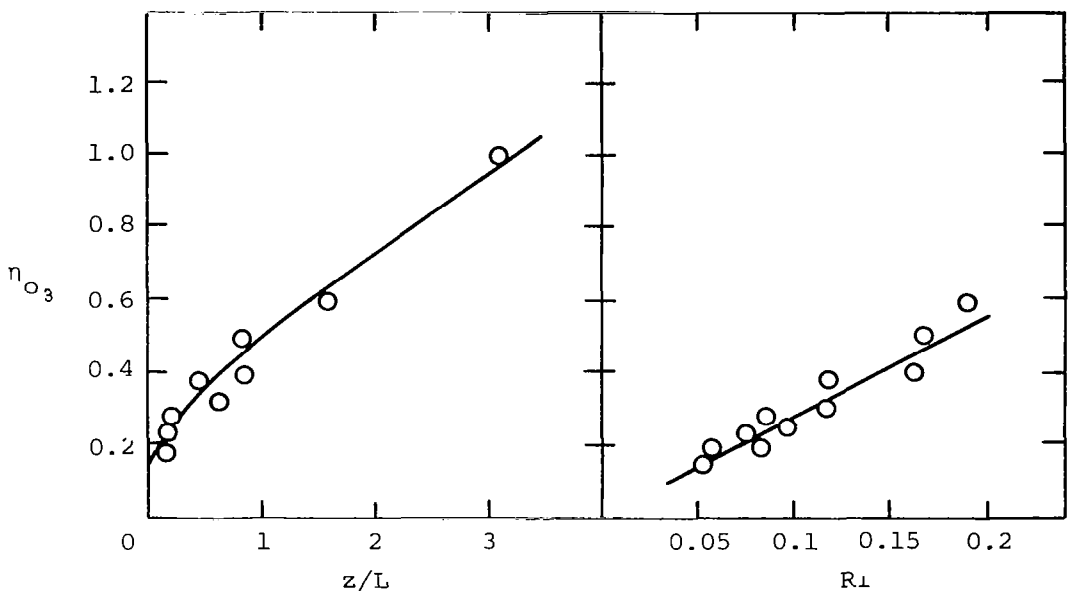

Figure 2-3. The scale parameter η_{o3} of vertical component as a function of z/L and of Ri [6].

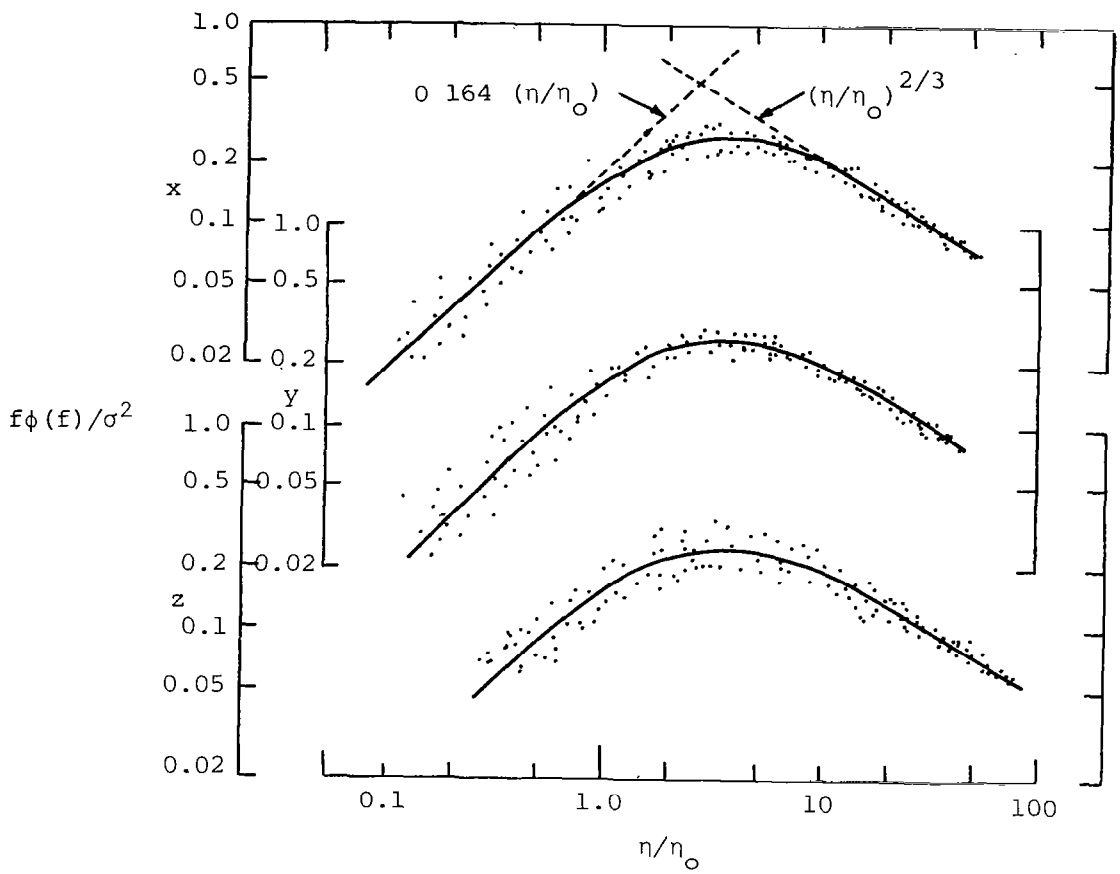

Figure 2-4. Measured turbulent data compared with Equation (2-12) [6].

exposed to interaction with the turbulence. For example, consider a system as shown in Figure 1-1, page 2, with a frequency response function $H(\omega)$. Assume that a stationary random signal with a power spectral density function $\phi_x(\omega)$ is applied as an input to this system. The output from the system will be a stationary random signal with a power spectral density function $\phi_y(\omega)$ given by

$$\phi_y(\omega) = |H(\omega)|^2 \phi_x(\omega) \quad . \tag{2-14}$$

One can obviously design a filter function to obtain the form of the output spectrum $\phi_y(\omega)$ desired for any given known input $\phi_x(\omega)$. For example, if the desired output is the longitudinal or lateral component of the Dryden spectrum given by Equation (2-11), then Equation (2-14) becomes

$$\begin{aligned} \phi_x(\omega) \ |H_1(\omega)|^2 &= \frac{\sigma_1^2 2\Lambda_1}{V\pi} \frac{1}{1 + (\Lambda_1\omega/V)^2} \\ \phi_x(\omega) \ |H_2(\omega)|^2 &= \frac{\sigma_2^2 \Lambda_2}{V\pi} \frac{1 + 3(\Lambda_2\omega/V)^2}{[1 + (\Lambda_2\omega/V)^2]^2} \quad . \end{aligned} \tag{2-15}$$

Introducing the input as wide-band white noise for which the spectrum $\phi_x(\omega)$ is a constant, adjustable to unity, gives

$$|H_1(\omega)|^2 = \frac{c_1}{a_1^2 + \omega^2}$$

$$|H_2(\omega)|^2 = \frac{c_2 (b^2 + \omega^2)}{(a_2^2 + \omega^2)^2}, \qquad (2\text{-}16)$$

where

$$c_1 = \frac{2a_1\sigma_1^2}{\pi}, \quad a_1 = \frac{V}{\Lambda_1}$$

$$c_2 = \frac{3a_2\sigma_2^2}{\pi}, \quad b = \frac{a_2}{\sqrt{3}}, \quad a_2 = \frac{V}{\Lambda_2}.$$

One solution for $H(\omega)$ is

$$H_1(\omega) = \frac{\sqrt{c_1}}{a_1 + j\omega}$$

$$H_2(\omega) = \frac{\sqrt{c_2}\,(b + j\omega)}{[a_2 + j\omega]^2}. \qquad (2\text{-}17)$$

The complex polar notation gives the frequency response function in terms of a gain factor $|H(\omega)|$ and a phase factor $\theta(\omega)$ as

$$H(\omega) = |H(\omega)|e^{-j\theta(\omega)} \qquad (2\text{-}18)$$

Thus,

$$|H_1(\omega)| = \frac{\sqrt{c_1}}{[a_1^2 + \omega^2]^{1/2}}$$

$$\theta_1(\omega) = \tan^{-1}(\omega/a_1)$$

and (2-19)

$$|H_2(\omega)| = \left[\frac{c_2(b^2 + \omega^2)}{(a_2^2 + \omega^2)^2}\right]^{1/2}$$

$$\theta_2(\omega) = \tan^{-1}\left[\frac{(2a_2b - (a_2^2 - \omega^2))\omega}{2a_2\omega^2 - (a_2^2 - \omega^2)b}\right].$$

These gain factors and phase factors are plotted in Figure 2-5. Because of the irrational form of the Kaimal and von Karman spectra, approximate forms of $H(\omega)$ are used. Equation (2-20) is a modified Kaimal spectrum with a Dryden form:

$$\frac{f\phi(f)}{\sigma^2} = 1.9\,\frac{(\eta/\eta_o)}{(3.8)^2 + (\eta/\eta_o)^2}\,. \qquad (2\text{-}20)$$

Figure 2-6 shows a comparison of this approximate form with the original spectrum.

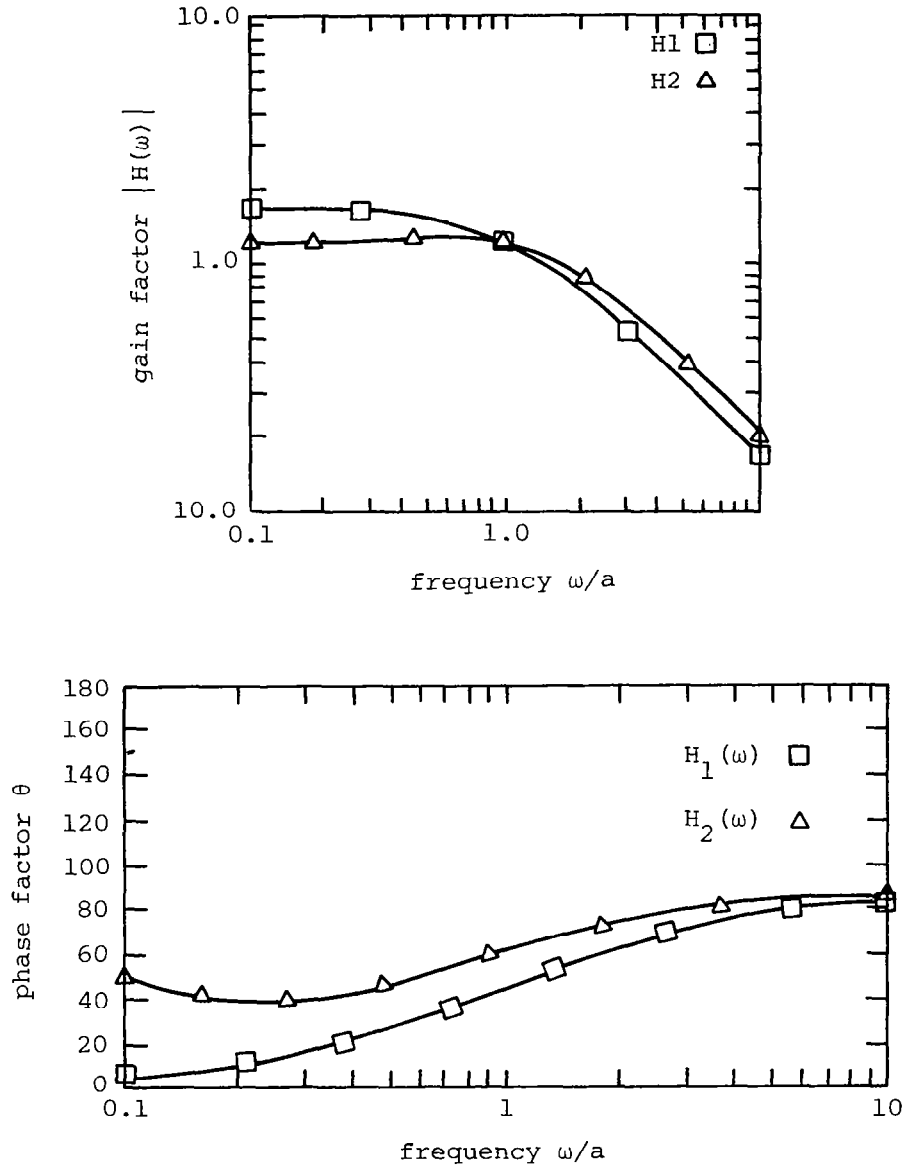

Figure 2-5. The gain and phase factor for $H_1(\omega)$ and $H_2(\omega)$ of the Dryden spectrum; Λ = 700 m and V = 150 m/s.

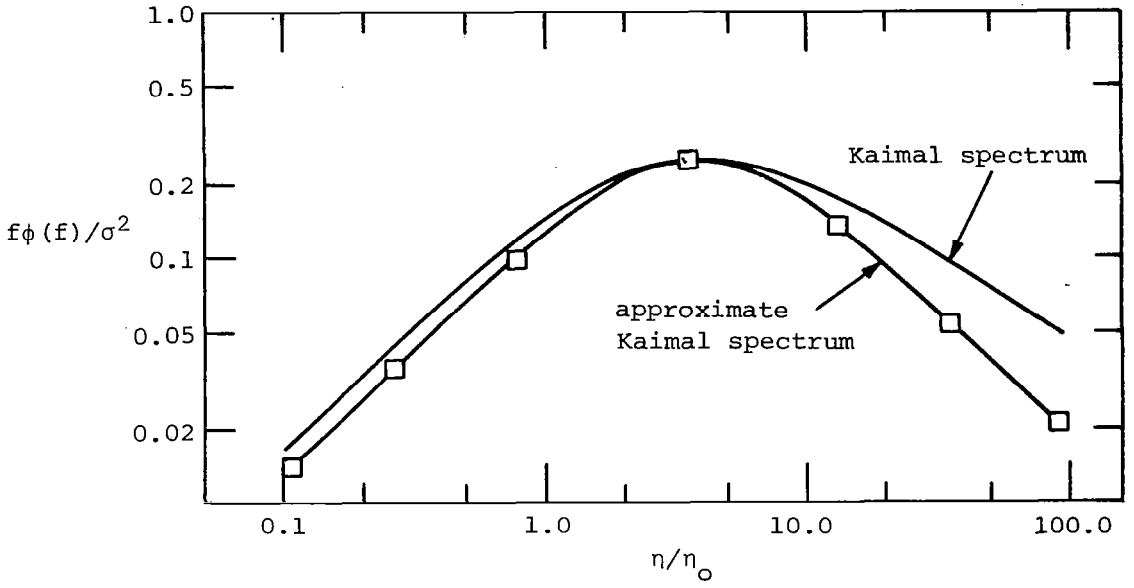

Figure 2-6. The Kaimal spectrum, Equation (2-12), compared with the approximation form, Equation (2-20).

From Kaimal [6] a definition of Λ is given as $0.041\ (z/\eta_o)$, which gives

$$\eta/\eta_o = \frac{f\Lambda}{0.041\ V} \ . \qquad (2\text{-}21)$$

Substituting Equation (2-21) into Equation (2-20) and replacing f with $\omega/2\pi$ gives

$$\phi(\omega) = \frac{c}{a^2 + \omega^2} \ , \qquad (2\text{-}22)$$

where

$$c = \frac{0.156\ \sigma^2 \pi V}{\Lambda} \quad , \quad a = \frac{0.312 \cdot \pi V}{\Lambda} \ .$$

Recalling Equation (2-16), it follows that the frequency response function $H(\omega)$ for the approximate Kaimal spectrum can be solved in the same manner as that used to obtain Equation (2-17).

The approximate von Karman spectrum, as shown in [9] is

$$\phi(f) = \frac{1.942\ \sigma^2\ \frac{\Lambda}{V}\left[1 + \left(3.496\ \frac{\Lambda}{V}\ f\right)^2\right]}{\left[1 + \left(3.496\ \frac{\Lambda}{V}\ f\right)^2\right]^2}\ , \qquad (2\text{-}23)$$

which can also be written as

$$\phi(\omega) = c\ \frac{\left(b^2 + \omega^2\right)}{\left[a^2 + \omega^2\right]^2}\ . \qquad (2\text{-}24)$$

The filter function $H(\omega)$ in this case is therefore similar to the lateral component of Equation (2-17). Figure 2-7 compares the approximate expression with the actual von Karman longitudinal spectrum given by Equation (2-10).

C. Multi-Filter System for Non-Gaussian Turbulence and Turbulence with Interlevel Coherence

Additional turbulence characteristics can be taken into account with more complex filter systems. A filter system which gives a non-Gaussian turbulence output and a turbulence output with interlevel coherence, respectively, is described in this section. Both simulations use the

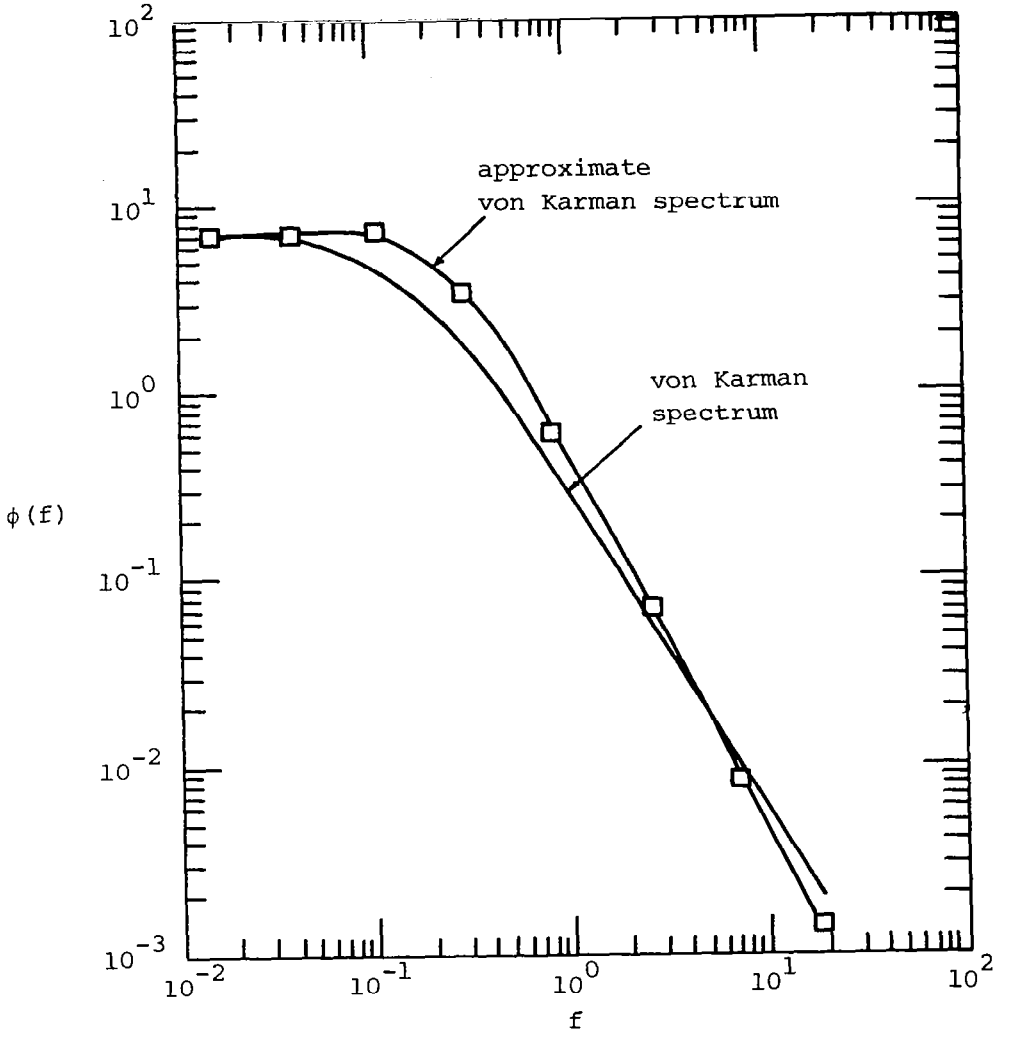

Figure 2-7. The von Karman spectrum compared with the approximate form, Equation (2-23); V = 180 m/s, Λ = 195 m.

same Dryden spectrum. The frequency response function for each filter can no longer be derived from the simple relation given in Equation (2-14).

The non-Gaussian output filter, Figure 2-8, combines three filter functions, H_a, H_b, and H_c, for each of the three wind speed components being simulated. This nonlinear system allows the probability density function to be adjusted through the parameter r. Figures 2-9 and 2-10 show the comparison of measured atmospheric turbulence with a Gaussian distribution curve, and the comparison of the same turbulence with the probability density function simulated by selecting different values of r, respectively.

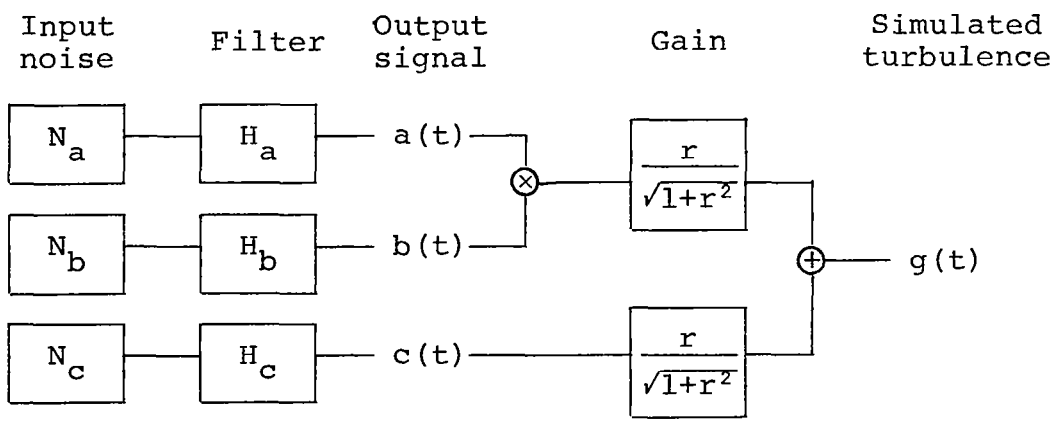

Figure 2-8. The non-Gaussian multi-filter system.

To determine the frequency response functions, H_a, H_b, and H_c, the correlation function is first derived from the Fourier transform of the spectrum to be simulated:

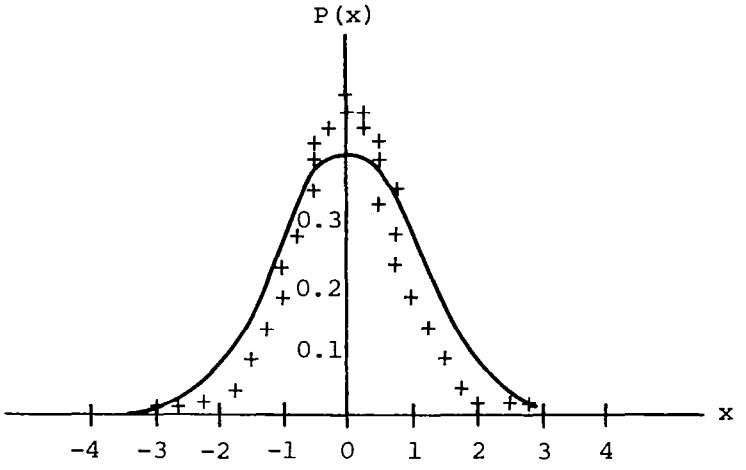

Figure 2-9. Comparison of the Gaussian distribution with measured gust velocity distribution [10].

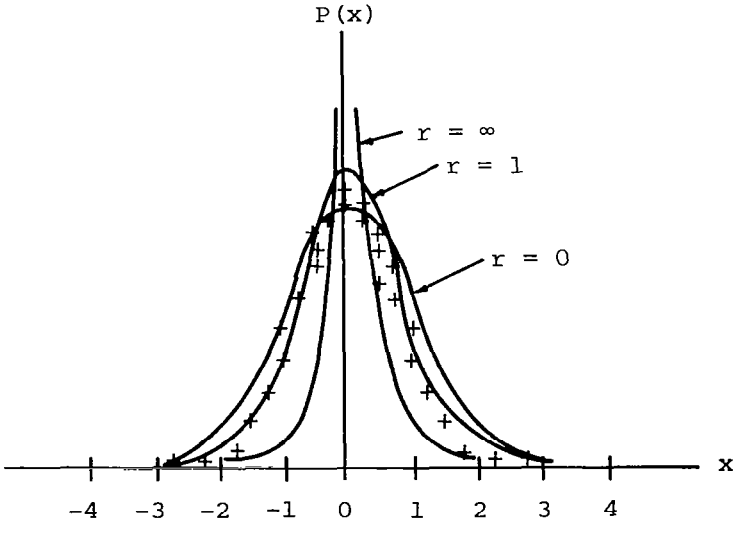

Figure 2-10. The probability distribution function for different values of r.

$$R(t) = \int_{-\infty}^{\infty} \phi(K) \exp(iVKt)\, dK \quad . \qquad (2\text{-}25)$$

Considering the Dryden spectra, Equation (2-11), the correlation becomes

$$R_1(t) = \sigma_1^2 \exp[-V/\Lambda\, |t|]$$
$$R_2(t) = \sigma_2^2 \left[1 - \frac{V|t|}{2\Lambda}\right] \exp[-V/\Lambda\, |t|] \quad . \qquad (2\text{-}26)$$

The correlation function of the simulated turbulence time history can also be determined from (see Figure 2-8)

$$R_{gg}(\tau) = E[g(t)\, g(t+\tau)] \quad , \qquad (2\text{-}27)$$

where

$$g(t) = a(t)\, b(t) \frac{r}{[1+r^2]^{1/2}} + c(t) \frac{1}{[1+r^2]^{1/2}} \quad . \qquad (2\text{-}28)$$

Since $a(t)$, $b(t)$, and $c(t)$ are independent, random processes with zero mean, the correlation function can be written as

$$R_{gg}(t) = R_{aa}(t)\, R_{bb}(t) \frac{r^2}{[1+r^2]} + R_{cc} \frac{1}{[1+r^2]} \quad , \qquad (2\text{-}29)$$

and each function can be related to a spectrum function through Equation (2-30):

$$R_{aa}(t) = \int_{-\infty}^{\infty} \phi_{aa}(K) \exp(iVKt)\, dK , \qquad (2\text{-}30)$$

where $\phi_{aa}(K)$ can be replaced by the filter function $H(iVK)$, i.e.,

$$|H_a(iVK)|^2 = \phi_{aa}(K) . \qquad (2\text{-}31)$$

Similar results apply to R_{bb} and R_{cc}. Reeves, et al. [2] assume the general form of the response function to be

$$H_a(s) = \frac{N_1}{1 + D_1 s}$$

$$H_b(s) = \frac{N_2 + N_3 s}{(1 + D_2 s)^2} \qquad (2\text{-}32)$$

$$H_c(s) = \frac{N_4 + N_5 s}{(1 + D_3 s)^2} ,$$

where s is the Laplace transform variable $s = j\omega$.

Substituting Equation (2-32) into Equation (2-31) and transforming as shown by Equation (2-30) yields the following correlation functions:

$$R_{aa}(t) = \frac{N_1^2}{2D_1} \exp\left[- \frac{|t|}{D_1} \right]$$

$$R_{bb}(t) = \left(\frac{N_3}{2D_2} \right)^2 \left\{ |t| \left[\left(\frac{N_2}{N_3} \right)^2 - \left(\frac{1}{D_2} \right)^2 \right] + \left[\frac{1}{D_2} + D_2 \left(\frac{N_3}{N_2} \right)^2 \right] \right\} \exp\left[- \frac{|t|}{D_2} \right] \qquad (2\text{-}33)$$

$$R_{cc}(t) = \left(\frac{N_5}{2D_3} \right)^2 \left\{ |t| \left[\left(\frac{N_4}{N_5} \right)^2 - \left(\frac{1}{D_3} \right)^2 \right] + \left[\frac{1}{D_3} + D_3 \left(\frac{N_4}{N_5} \right)^2 \right] \right\} \exp\left[- \frac{|t|}{D_2} \right] .$$

These particular expressions for the response functions have been chosen because they will give the correct Dryden spectrum. Also, to eliminate the r appearing in Equation (2-29), the following choices are made for the constants in Equation (2-32):

$$N_1 = 4\sigma_1 \frac{\Lambda}{V} \quad , \quad N_2 = 1.0 \quad , \quad N_3 = \frac{2\Lambda}{V} \quad , \quad N_4 = \sigma_1 \left(\frac{2\Lambda}{V} \right)^{1/2}$$

$$N_5 = \sigma_1 \left(\frac{2\Lambda^3}{V^3} \right)^{1/2} \quad , \quad D_1 = \frac{2\Lambda}{V} \quad , \quad D_2 = \frac{2\Lambda}{V} \quad , \quad D_3 = \frac{\Lambda}{V} .$$

The resulting correlation functions of the model become

$$R_{aa}(t)\, R_{bb}(t) = R_{cc}(t) = R_{gg}(t) = \sigma_1^2 \exp\left[- \frac{V}{\Lambda} |t| \right] . \qquad (2\text{-}34)$$

This is the desired form of the longitudinal gust correlation function for a Dryden spectrum. Similarly, the lateral and vertical components can be simulated correctly by proper choice of constants. These constants are listed in Table 2-1.

Atmospheric turbulence near the ground has been shown to have strong coherence between vertically separated layers of air. Many researchers [11, 12, 13] have found that the coherence near the ground ($z \leq 150$ m) behaves as

$$\gamma_o\ (K,\ \Delta z) = \exp\ [-a\ |K\Delta z|\ ]\ . \qquad (2\text{-}35)$$

Therefore, this statistical property should be included in a valid turbulence simulation.

Perlmutter, Frost, and Fichtl [3] developed a multi-filter system to provide turbulence simulation including coherence function. They defined the two-point spectral function $\phi(K,z_1,z_2)$ at different height z_1,z_2 to be

$$\phi(K,z_1,z_2) = A^2 H(K,z_1) H^*(K,z_2) \sum_{m=-P}^{P} D_m(K,z_1) D_m^*(K,z_2)\ , \qquad (2\text{-}36)$$

where $H(K,z)$ is the frequency response function, and $D(K,z)$ is a level frequency factor, as shown in Figure 2-11.

Table 2-1. Transfer Functions for the Non-Gaussian Model

	H_a	H_b	H_c
Longitudinal	$\frac{4\sigma_1(\frac{\Lambda}{V})}{1+2(\frac{\Lambda}{V})s}$	$\frac{1}{1+2(\frac{\Lambda}{V})s}$	$\frac{\sigma_1(\frac{2\Lambda}{V})^{1/2}}{1+(\frac{\Lambda}{V})s}$
Lateral	$\frac{\sigma_2(128)^{1/2}(\frac{\Lambda}{V})^2}{1+2(\frac{\Lambda}{V})s}$	$\frac{s}{(1+2\frac{\Lambda}{V}s)^2}$	$\frac{\sigma_2(\frac{\Lambda}{V})^{1/2}(1+\sqrt{3}\frac{\Lambda}{V}s)}{(1+(\frac{\Lambda}{V})s)^2}$
Vertical	$\frac{\sigma_3(128)^{1/2}(\frac{\Lambda}{V})^2}{1+2(\frac{\Lambda}{V})s}$	$\frac{s}{(1+2\frac{\Lambda}{V}s)^2}$	$\frac{\sigma_3(\frac{\Lambda}{V})^{1/2}(1+\sqrt{3}\frac{\Lambda}{V}s)}{(1+(\frac{\Lambda}{V})s)^2}$

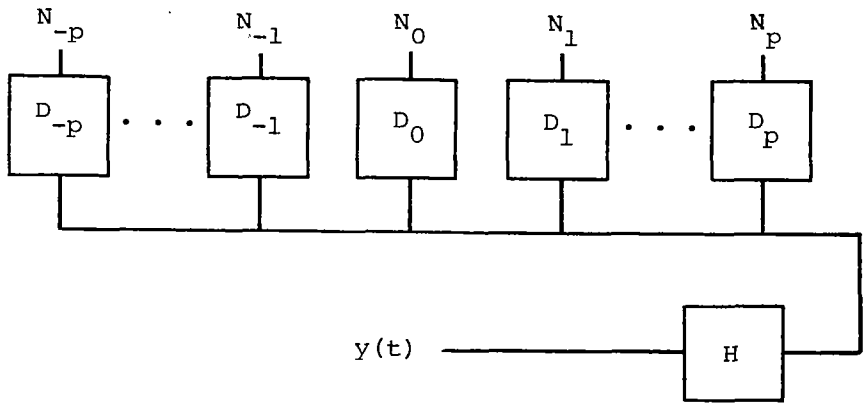

Figure 2-11. The interlevel coherence model.

The coherence function $\gamma(K,z_1,z_2)$ is defined as

$$\gamma(K,z_1,z_2) = \frac{\phi(K,z_1,z_2)\,\phi^*(K,z_1,z_2)}{\phi(K,z_1,z_1)\,\phi(K,z_2,z_2)} \quad . \tag{2-37}$$

The level frequency factor is therefore assumed to have the form

$$D_m(K,z) = c_m \exp\,[\,j\ k\ z\ d_m\,]\ , \tag{2-38}$$

where

$$d_m = \frac{m\pi}{(K\Delta z)_{max}} \quad .$$

Therefore, Equation (2-36) becomes

$$\phi(K,z_1,z_2) = A^2 H(K,z_1) H^*(K,z_2) \sum_{m=-P}^{P} c_m^2 \exp[jk(z_1-z_2)d_m] \quad .$$

Substituting this into Equation (2-37) yields

$$\gamma(K,\Delta z) = \frac{\left[\sum_{m=-P}^{P} c_m^2 \exp(jK\Delta z d_m)\right]\left[\sum_{\ell=-P}^{P} c_\ell^2 \exp(-jK\Delta z d_\ell)\right]}{\left[\sum_{m=-P}^{P} c_m^2\right]\left[\sum_{\ell=-P}^{P} c_\ell^2\right]} . \quad (2\text{-}39)$$

Notice that c_m and d_m are equal for D_m and D_{-m}; therefore, Equation (2-39) can be rewritten as

$$\gamma(K,\Delta z) = \frac{\left[c_o^2 + 2\sum_{m=1}^{P} c_m^2 \cos(K\Delta z d_m)\right]^2}{\left[c_o^2 + 2\sum_{m=1}^{P} c_m^2\right]^2} . \quad (2\text{-}40)$$

The error between this equation and the true wind coherence exponential function given by Equation (2-35) is

$$E_{rr} = \int_0^1 \left[\gamma(K,\Delta z) - \gamma_o(K,\Delta z)\right] d\xi , \quad (2\text{-}41)$$

where

$$\xi = \frac{K\Delta z}{(K\Delta z)_{max}} .$$

Values of c_m which cause E_{rr} to be a minimum are found by setting $dE_{rr}/dc_m = 0$. The result is:

$$c_o^2 = 2\xi_o \left[1 - \exp\left(-\frac{1}{2\xi_o}\right) \right]$$

$$c_m^2 = \frac{2\xi_o \left[1 - (-1)^m \exp\left(-\frac{1}{2\xi_o}\right) \right]}{\left[1 + \left(2m\pi\xi_o \right)^2 \right]}, \qquad (2\text{-}42)$$

where

$$\xi_o = \frac{1}{a(K\Delta z)_{max}} .$$

Values of the c_m's for the set $\xi_o = 0.1$ are shown in Figure 2-12.

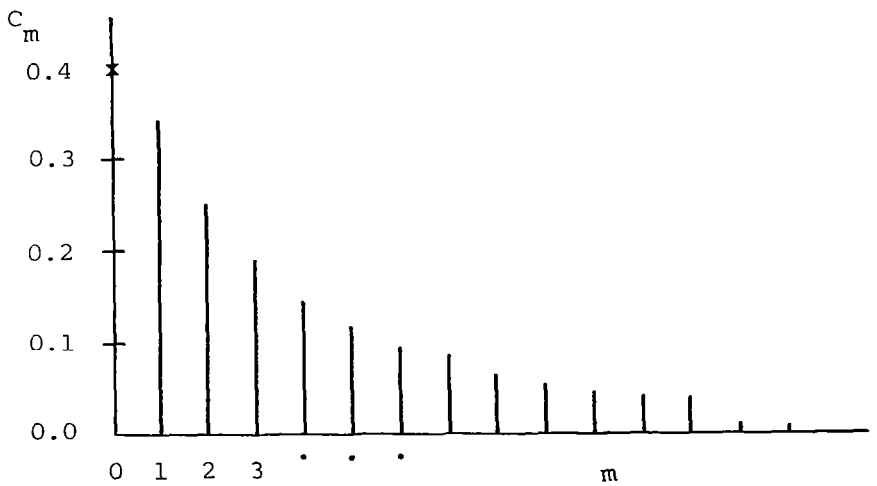

Figure 2-12. Values of the parameter c_m.

To determine the value of the parameter A in Equation (2-36), consider that Equation (2-36) must reduce to the one-level auto-spectral function when $\Delta z = 0$. Equation (2-36) then takes on the new form of

$$\phi(K,z_1,z_1) = A^2 H(K,z_1)H^*(K,z_1)\left[c_o^2 + 2\sum_{m=1}^{P} c_m^2\right] . \qquad (2\text{-}43)$$

Comparing Equation (2-43) with a single filter system for which the spectrum is

$$\phi(K,z_1) = |H(K,z_1)|^2 , \qquad (2\text{-}44)$$

then A can be obtained as

$$A^2 = \frac{1}{\left[c_o^2 + 2\sum_{m=1}^{P} c_m^2\right]} . \qquad (2\text{-}45)$$

Therefore, the two-point interlevel coherence model reduces, as necessary, to the one-level auto-spectrum at $\Delta z = 0$.

CHAPTER III

DIGITAL SIMULATION TECHNIQUES

This chapter describes the basic methods and problems associated with digital simulation of random processes. Topics discussed are the generation of a random signal and the calculation of the necessary transformation functions used in later work.

A. Generation of a Random Signal

The method used to generate random numbers with a digital computer is based on the formula

$$x_{n+1} = a\,x_n + b \pmod{m} \quad . \tag{3-1}$$

This technique is called the mixed congruential method and provides a simple and fast computation procedure. It also has the advantage that it can be repeated for several cycles by using different values of a and b. Moreover, it can be analyzed theoretically. The period at which the random numbers repeat cannot be greater than the module number m; thus, m is usually selected to be the largest integer possible with the capability of the computer used. The value of m in this study is 2,147,483,647, which is equal to $(2^{31} - 1)$, the largest possible number allowed on the IBM 360/65 system.

Frequently, it is desired that the sequences generated be bounded by zero and unity and be uniformly distributed within this interval. This bounding requirement is accomplished easily by normalizing the output data with respect to the largest possible number m.

$$x_n' = x_n/m \ , \tag{3-2}$$

where x_n is generated from Equation (3-1).

Since

$$0 \leq x_n \leq m \ ;$$

therefore,

$$0 \leq x_n' \leq 1 \ .$$

The constants a and b in Equation (3-1) are selected to provide speed of computation and good statistical properties, such as uniform distribution and maximum period.

Results presented by Chambers [14] and Hamming [15] show that a maximum period can be achieved if a and b are selected as

$$\begin{cases} a = 4 \cdot I + 1 & I = 1,2,3,... \\ b = \text{odd} \end{cases}$$

or (3-3)

$$\begin{cases} a = 8 \cdot I \pm 3 \\ b = 0 \ . \end{cases}$$

The computer program RANDU used for generating random numbers was combined in subroutine GAUSS, as discussed in the following text. The value a is selected equal to 65539 which follows the second rule of Equation (3-3) by setting I equal to 8192 and provides the best statistical results using the IBM 360 computer.

As mentioned earlier, Gaussian distributed numbers are required as the input white noise. The probability density function of the numbers must, therefore, have the form

$$P(x) = \frac{1}{\sigma_x\sqrt{2\pi}} \exp\left[-\frac{(x-\bar{x})^2}{2\sigma_x^2}\right], \qquad (3\text{-}4)$$

where σ_x is the standard deviation and $\bar{x}$ is the mean value of the variate.

If $x_i'(i = 1,2,\ldots N)$ are N uniformly distributed numbers over the interval 0 to 1, the central limit theorem yields the following formula:

$$x_j'' = \sigma_x \left[\frac{12}{N}\right]^{1/2} \left[\sum_{i=1}^{N} x_i' - N/2\right] + \bar{x}, \qquad (3\text{-}5)$$

where $x_j''(j = 1,2,\ldots M)$ is a set of random numbers having an approximate Gaussian distribution with the mean value equal to $\bar{x}$, and the standard deviation equal to σ_x.

The value of N indicates the number of terms used for each output. Figure 3-1 compares the approximation

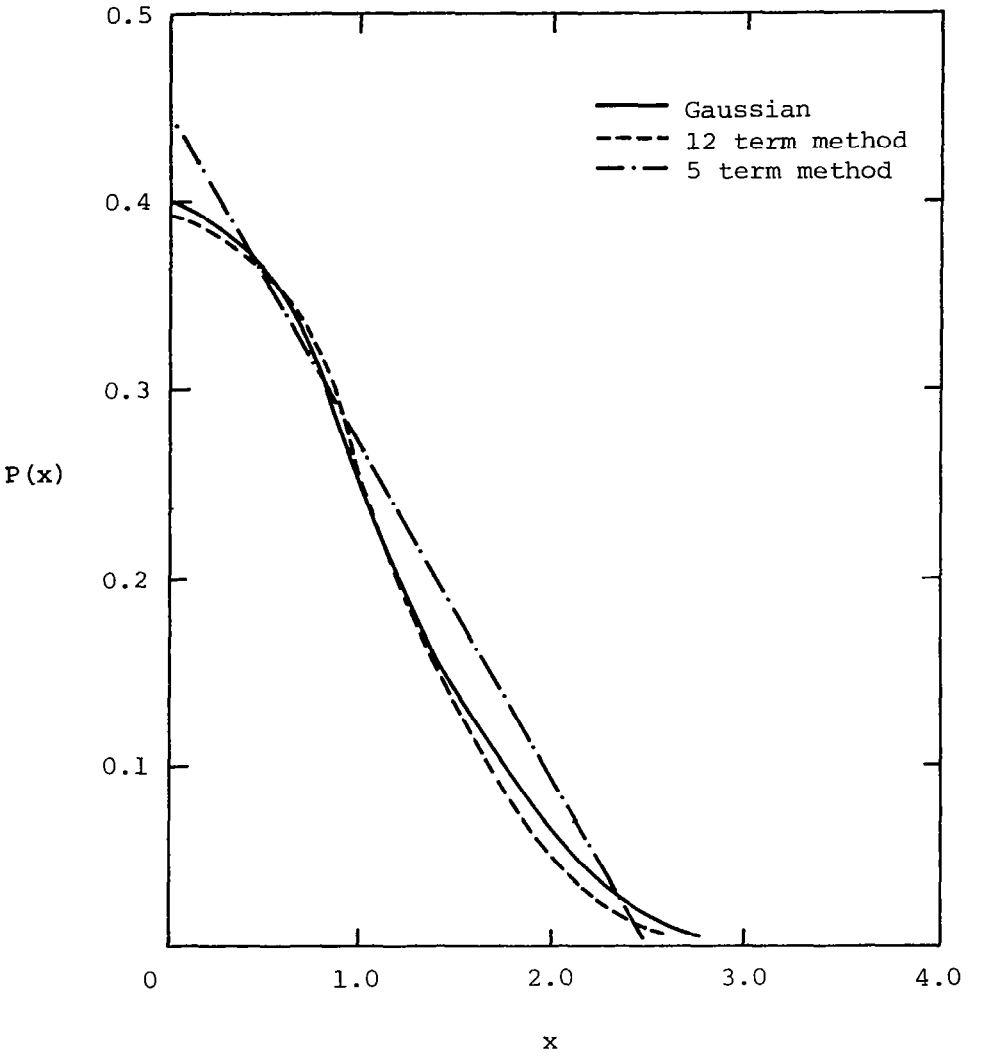

Figure 3-1. The Gaussian distribution compared with the approximation, Equation (3-5) [16].

given by Equation (3-5) for 5 terms and 12 terms with the true Gaussian distribution function.

The computer program for generating Gaussian random numbers also appears in the IBM scientific subroutine package. The N value of Equation (3-5) is selected equal to 12 in order to simplify the computations. Equation (3-5) then reduces to

$$x''_j = \sigma_x \left[\sum_{i=1}^{N} x'_i - 6 \right] + \bar{x} . \qquad (3\text{-}6)$$

The computer subroutine is called GAUSS and is given in Appendix A, Section A-1.

B. Calculation of the Required Discrete Transformations

The filter system shown in Figure 3-2 consists of an input and an output history function x(t), y(t), respectively, and a system response function h(t).

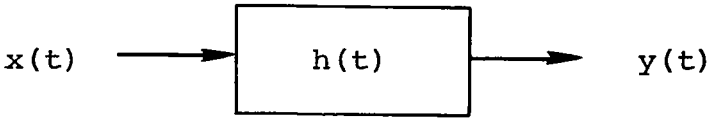

Figure 3-2. Simple filter system.

The output y(t) is given by the convolution integral

$$y(t) = \int_{-\infty}^{\infty} h(\tau)\, x(t-\tau)\, d\tau . \qquad (3\text{-}7)$$

The Fourier transformation of Equation (3-7) is [17]

$$Y(\omega) = H(\omega)\ X(\omega)\ . \qquad (3\text{-}8)$$

Since the filter function $H(\omega)$ can be designed to simulate most forms of the spectrum desired, as described in Chapter II, Section B, the calculation of a simulated time history of turbulence relies mainly on the Fourier transformation of the input function $x(t)$ to $X(\omega)$. The inverse transformation of the $Y(\omega)$ back to $y(t)$ is also of equal importance to the computational effort. These two procedures will be discussed in detail in the following, as they pertain to transformation of digital data.

The Discrete Fourier Transformation

For cyclic frequency f, the infinite range Fourier transform of a real valued or a complex valued record $x(t)$ is defined by

$$X(f) = \int_{-\infty}^{\infty} x(t)\ e^{-j2\pi ft}\ dt\ . \qquad (3\text{-}9)$$

It is physically impossible to calculate this transformation since an infinite number of digitized data does not exist in reality. However, by restricting the limits to a finite time interval of $x(t)$, say in the range $(0,T)$, then the finite range Fourier transform will exist as defined by Bendat and Piersol [17]

$$X(f,T) = \int_0^T x(t)\ e^{-j2\pi ft}\ dt\ . \qquad (3\text{-}10)$$

Assume now that x(t) is sampled at N equally spaced points separated by a distance Δt apart, where Δt has been selected to produce a high cut-off frequency to avoid aliasing. The cut-off frequency (Nyquist frequency) and the aliasing problem are discussed in a later section. The discrete values of x_n thus become

$$x_n = x(n\ \Delta t) \qquad n = 1,1,2,\ldots N\text{-}1\ , \qquad (3\text{-}11)$$

and the discrete version of Equation (3-10) becomes

$$X(f,t) = \Delta t \sum_{n=0}^{N-1} x_n \exp\ [-j\ 2\pi\ f\ n\ \Delta t]\ . \qquad (3\text{-}12)$$

A basic frequency f_o is defined as

$$f_o = \frac{1}{T}\ , \qquad (3\text{-}13)$$

and the discrete frequency value f_m is defined in terms of f_o as

$$f_m = m\ f_o = \frac{m}{N\Delta t} \qquad m = 0,1,2,\ldots N\text{-}1\ . \qquad (3\text{-}14)$$

The discrete frequency f_m is substituted into the discrete Fourier components, X_m, defined as

$$X_m = \frac{X(f_m\ T)}{\Delta t}\ . \qquad (3\text{-}15)$$

Therefore,

$$X_m = \sum_{n=0}^{N-1} x_n \exp\left[-j \frac{2\pi mn}{N}\right] . \qquad (3\text{-}16)$$

To simplify the notation, let

$$W_{mn} = \exp\left[-j \frac{2\pi mn}{N}\right] . \qquad (3\text{-}17)$$

Then Equation (3-16) becomes in tensor form,

$$X_m = W_{mn}\, x_n . \qquad (3\text{-}18)$$

This is the equation for the discrete, finite-range Fourier transform. No difficulty is involved in carrying out calculation of the Fourier transform with the equation using a digital computer. Equation (3-8) can now be written in discrete form as

$$Y_m = H_m\, X_m . \qquad (3\text{-}19)$$

This equation gives the discrete Fourier components of the output to be simulated. To invert the output Fourier components into the desired time domain, the discrete inverse Fourier transform is applied, which can be derived similar to Equation (3-18). The result is

$$y_n = \frac{1}{N} W^*_{mn} Y_m \ , \qquad (3\text{-}20)$$

where

$$W^*_{mn} = \exp \left[j \frac{2\pi mn}{N} \right] .$$

These three steps complete the calculation; that is, the simulated discrete data y_n are obtained by one Fourier transform, Equation (3-18), one multiplication, Equation (3-19), and one inverse Fourier transform, Equation (3-20). To calculate Equation (3-18) or Equation (3-20) requires N^2 times of complex multiplication and N(N-1) complex additions to transform N discrete values.

Since the value of W_{mn} repeats for certain combinations of m and n, some additions and multiplications can be eliminated. The Fast Fourier Transform (FFT) is an algorithm based on this principle which allows computation of the transformation much more rapidly than the direct method in Equation (3-18) or Equation (3-20). The FFT performs a series of computations by rearranging the matrix W_{mn} to save the calculation of dual node pairs. For N discrete points, where N is a power of 2, namely,

$$N = 2^P \ , \qquad (3\text{-}21)$$

the FFT method requires only P·N/2 complex multiplications and P·N complex additions. Thus, the approximate ratio of

computing time for the direct method compared to the FFT method is

$$\frac{\text{Direct Method}}{\text{FFT}} = \frac{2N}{P} \quad . \tag{3-22}$$

Figure 3-3 illustrates the difference between the number of multiplications required for each method.

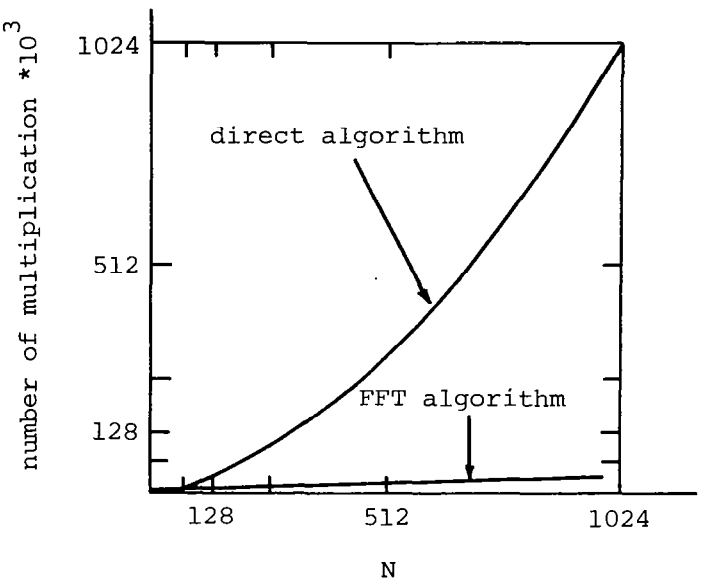

Figure 3-3. Comparison of the number of multiplications required for a Fourier transform by the direct algorithm and the FFT algorithm.

The Z-Transformation

Another useful discrete transformation technique is the Z-transformation which is defined as

$$X(z) = \sum_{m=0}^{\infty} x(m\ \Delta t)\, z^{-m} \quad , \tag{3-23}$$

where X(z) is called the Z-transform function of X(t). Actually, the Z-transformation is the Laplace transform of digitized data. It can be derived from the Laplace transformation defined as

$$X(s) = \int_{o}^{\infty} x(t)\ e^{-st}\ dt\ . \tag{3-24}$$

Consider the data x(t) digitized as

$$x'(t) = \sum_{m=0}^{\infty} x(m\ \Delta t)\,\delta(t-m\ \Delta t)\ , \tag{3-25}$$

where

$$\delta(a) = 1 \quad \text{for } a = 0$$
$$= 0 \quad \text{for } a \neq 0\ .$$

Taking the Laplace transform of x'(t) gives

$$X'(s) = \int_{o}^{\infty} x'(t)\ e^{-st}\ dt\ . \tag{3-26}$$

Substituting Equation (3-25) into Equation (3-26) results in

$$X'(s) = \sum_{m=0}^{\infty} x(m\ \Delta t)\ e^{-s(m\ \Delta t)}\ . \tag{3-27}$$

The Z-transform X(z) is equal to X'(s) if z is set equal to $e^{s\ \Delta t}$, and Equation (3-27) becomes

$$X(z) = X'(s) = \sum_{m=0}^{\infty} x_m \, e^{-m(s\,\Delta t)} \quad , \tag{3-28}$$

where

$$x_m = x(m\,\Delta t) \quad .$$

The transformation is now defined as a function Z,

$$X(z) = Z\,[\,x(t)\,] \quad . \tag{3-29}$$

Therefore, the transformation of $x(t + \Delta t)$ becomes

$$\begin{aligned} Z\,[\,x_{m+1}\,] &= \sum_{m=0}^{\infty} x_{m+1} \, z^{-m} \\ &= z\,\Big(\sum_{m=0}^{\infty} x_{m+1} \, z^{-(m+1)}\Big) \\ &= z\,\Big(\sum_{m=0}^{\infty} x_m \, z^{-m} - x_o\Big) \\ &= z\,(\,Z\,[\,x_m\,] - x_o\,) \end{aligned} \tag{3-30}$$

in the same manner it can be shown that the Z-transformation of $[\,x_{m+1} - x_m\,]$ is equal to

$$Z\,[\,x_{m+1} - x_m\,] = (z-1)\;Z\,[\,x_m\,] - z\;x_o \quad . \tag{3-31}$$

This equation can be used to determine x_{m+1} from x_m by the appropriate inverse transformation. The application of Equation (3-31) to simulate turbulence is as follows.

The basis of the Z-transform technique is to establish the difference equation for the output y_{n+1}. Therefore, if the Z-transform of the filter function h(t) in the system shown in Figure 3-2, page 35, can be found, then the output y_{n+1} can be calculated directly from the y_n and x_n values.

An example determination of the filter function h(t) for simulation of the Dryden spectrum is given in the following.

The Fourier transform is (see Chapter II, Equation (2-17))

$$H(\omega) = \frac{\sqrt{c_1}}{j\omega + a_1} ,$$

which also can be expressed in Laplace form by setting $s = j\omega$ (see [18])

$$H(s) = \frac{\sqrt{c_1}}{s + a_1} . \qquad (3\text{-}32)$$

Now, consider a unit step function x(t) as the input to the system where

$$\begin{aligned} x(t) &= 1 \quad t \geq 0 \\ &= 0 \quad t < 0 . \end{aligned} \qquad (3\text{-}33)$$

The Laplace transform x(t) can be obtained from Equation (3-24) as

$$X(s) = L[\, x(t) \,] = 1/s . \qquad (3\text{-}34)$$

For a linear system, the Laplace transform of the output is related to the input by

$$Y(s) = H(s) \cdot X(s) \ . \tag{3-35}$$

Therefore, the output Y(s) of passing a unit step input through a Dryden spectrum filter would be

$$Y(s) = \frac{\sqrt{c_1}}{s+a_1} \cdot \frac{1}{s} \ . \tag{3-36}$$

Partial fractions give

$$Y(s) = \frac{\sqrt{c_1}}{a_1} \left(\frac{1}{s} - \frac{1}{s+a_1} \right) . \tag{3-37}$$

Taking the inverse Laplace transformation provides the output y(t)

$$y(t) = L^{-1} [\, Y(s) \,] = \frac{\sqrt{c_1}}{a_1} \left(1 - e^{-a_1 t} \right) . \tag{3-38}$$

The Z-transform of the input x(t) and of the output y(t) can be obtained by substituting Equations (3-33) and (3-38) into Equation (3-23); hence,

$$X(z) = \frac{z}{z-1}$$

$$Y(z) = \frac{\sqrt{c_1}}{a_1} \left(\frac{z}{z-1} - \frac{z}{z-e^{-a_1 \Delta t}} \right) . \tag{3-39}$$

Since

$$H(z) = Y(z) / X(z) \quad , \tag{3-40}$$

the Z-transform of the Dryden spectrum filter function becomes

$$H(z) = \frac{\sqrt{c_1}}{a_1} \left(\frac{1-e^{-a_1 \Delta t}}{z-e^{-a_1 \Delta t}} \right) . \tag{3-41}$$

For a general input X(z) the output of the filter system can be written as

$$Y(z) = \frac{\sqrt{c_1}}{a_1} \left(\frac{1-e^{-a_1 \Delta t}}{z-e^{-a_1 \Delta t}} \right) X(z) \quad . \tag{3-42}$$

Cross multiplication results in

$$(z-A)Y(z) = BX(z) \quad , \tag{3-43}$$

where

$$A = e^{-a_1 \Delta t} \quad , \quad B = \frac{\sqrt{c_1}}{a_1} \left(1-e^{-a_1 \Delta t} \right) .$$

Now, applying Equation (3-31) and setting y(0) = 0, the left-hand part of Equation (3-43) becomes

$$\begin{aligned} Z_1 [y_{m+1} - A y_m] &= (z-A) Z [y_m] \\ &= (z-A) Y(z) \quad . \end{aligned} \tag{3-44}$$

Hence, Equation (3-43) becomes

$$Z\left[y_{m+1} - Ay_m\right] = B\,Z\left[x_m\right] . \tag{3-45}$$

Taking the inverse Z-transformation, Equation (3-45) becomes

$$y_{m+1} - Ay_m = Bx_m$$

and

$$y_{m+1} = Ay_m + Bx_m . \tag{3-46}$$

This equation for calculating the discrete output y(t) is simple and very convenient for digitized data. Also, because the coefficients A and B are predetermined, this approach does not require calculation of the filter function, H, over all values of frequency in each computational step, as required in the FFT technique. For these reasons, the Z-transformation method is even more efficient than the FFT method. Only 2N real multiplications and N real additions are required to simulate N discrete components of a given time history. If N equals 1024, for example, the FFT method requires ten times more multiplications than does the Z-transform technique.

C. General Consideration in Digitization and Discrete Transformation Calculation

There are several required operations for the processing of random data. They are heavily dependent upon the physical phenomenon represented by the data and the desired engineering goals. In this section, the basic considerations associated with digital simulation are discussed.

Cut-Off Frequency

Sampling a time history for digital data analysis is usually performed at equally spaced intervals of time. Care must be taken in determining an appropriate sampling interval Δt. If sampling points are taken too close together, they will yield correlated and highly redundant data, thus unnecessarily increasing the labor and cost of calculations. On the other hand, sampling at points which are too far apart will lead to confusion between the low- and high-frequency components in the original time history; this is so-called aliasing. Generally, at least two samples per cycle are required to define a frequency component in the data. Hence, the highest frequency which can be defined by sampling at the rate of $1/\Delta t$ samples per second is $1/2\Delta t$ cps. This is called the Nyquist frequency.

$$f_c = 1/2\Delta t \ . \qquad (3\text{-}47)$$

Frequencies in the original data above $1/2\Delta t$ cps will be folded back into the range from 0 to $1/2\Delta t$ cps, and be confused with data in the frequency range below this value.

One way to avoid the aliasing problem is to choose Δt sufficiently small, that is, f_c large, that it is physically unrealistic for data to exist above f_c. In general, it is a good rule (see [17]) to select f_c to be one and one-half to two times greater than the maximum anticipated frequency. For example, for atmospheric turbulence simulation, the energy spectrum (as shown in Figure 2-7, page 19) indicates most of the kinetic energy is in the range below 1 cps. Therefore, a meaningful Δt is about 0.1 to 0.5 sec.

The Quantization Error

Since the magnitude of each data sample must be expressed by some fixed number of digits, only a fixed set of levels is available for approximating the infinite number of levels in the continuous data. For typical analog to digital conversion, the quantization error will have a uniform probability distribution with a standard deviation of approximately 0.29 Δx (see [17], where Δx is the quantization increment. This is demonstrated as follows:

Let P(x) be the quantization error probability density function defined by

$$P(x) = 1 \qquad -0.5 \leq x \leq 0.5$$

$$= 0 \qquad \text{otherwise} .$$

The variance of the error

$$\sigma_x^2 = \int_{-\infty}^{\infty} (x-\bar{x})^2 \; P(x) \; dx .$$

Since $\bar{x} = 0$,

$$\sigma_x^2 = \int_{-0.5}^{0.5} x^2 \, dx = \frac{1}{12} ,$$

the standard deviation is

$$\sigma_x = \sqrt{1/12} \simeq 0.29 \quad \text{scale unit} . \tag{3-48}$$

In practice, the quantization error is usually unimportant relative to other sources of error in the data processing. For example, for simulated turbulence, the quantization increment Δx is usually chosen as 0.01 m/sec. Therefore, the standard deviation of the quantization error is approximately equal to 0.0029 m/sec, and is small enough to be neglected. However, care must be exercised to assure that the range of quantization is small enough to assure the accuracy desired.

The Bias Error

All of the power spectral density algorithms considered herein use the discrete Fourier transform. The finite length of time, $T = N \cdot \Delta t$, influences the spectral function. The estimated spectrum ϕ_e is calculated by the finite length time history $x_T(t)$, which is the product of a "boxcar" function $b_T(t)$ and the original time history $x(t)$.

$$x_T(t) = b_T(t) \cdot x(t) \ , \tag{3-49}$$

where

$$\begin{aligned} b_T(t) &= 0 \quad t < T/2 \\ &= 1 \quad -T/2 \leq t \leq T/2 \\ &= 0 \quad t > T/2 \ . \end{aligned}$$

The Fourier transform of $b_T(t)$ gives

$$\begin{aligned} B_T(f) &= \int_{-\infty}^{\infty} b_T(f) \ e^{-j2\pi ft} \ dt \\ &= T \left(\frac{\sin(\pi fT)}{\pi fT} \right) \end{aligned} \tag{3-50}$$

this is called a window function.

Thus, the true spectrum ϕ_t will be different than the spectrum ϕ_e estimated by the finite Fourier transformation. The two functions are related by the convolution integral

$$\phi_e(f) = \int_{-\infty}^{\infty} \phi_t(f_1)\ B_T(f-f_1)\, df_1$$

$$= \int_{-\infty}^{\infty} \phi_t(f_1)\ T\left(\frac{\sin(\pi(f-f_1)T)}{\pi(f-f_1)T}\right) df_1 \quad . \tag{3-51}$$

The difference between ϕ_e and ϕ_t is defined as the bias error. The strongest objection to the boxcar window is "leakage through the side lobes," as shown in Figure 3-4. The side lobes are those portions of the window between 1/T and 2/T, between T/2 and 3/T, and so forth.

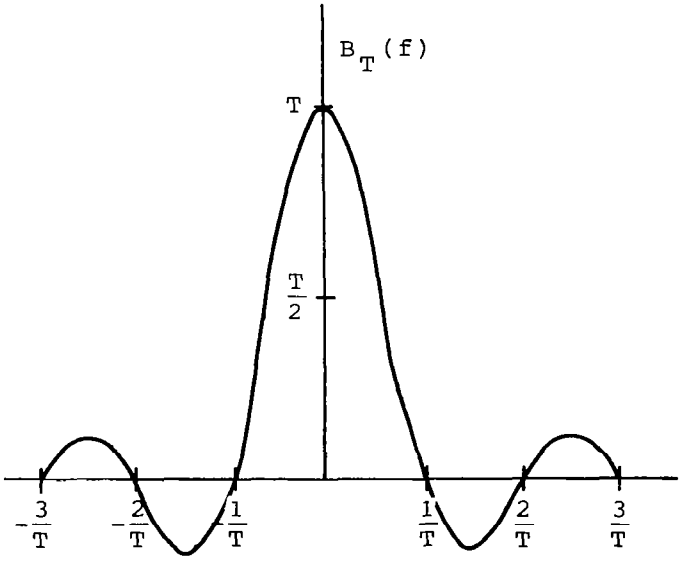

Figure 3-4. The spectral window for boxcar weighting function.

This deficiency in the boxcar window can be overcome largely by using a tapered window which tapers the ends of the time history. For example, the Hanning window

is defined as

$$h_T(t) = 0 \qquad \text{for } t < -T/2$$

$$= \frac{1}{2}\left[1 + \cos\left(\frac{2\pi t}{T}\right)\right] \qquad -T/2 \leq t \leq T/2 \qquad (3\text{-}52)$$

$$= 0 \qquad t > T/2 \ .$$

Then the Fourier transform of $h_T(t)$ gives the Hanning window function $H_T(f)$ where

$$H_T(f) = \frac{1}{4} B_T(f - f_o) + \frac{1}{2} B_T(f) + \frac{1}{4} B_T(f + f_o) \ , \qquad (3\text{-}53)$$

where

$$f_o = 1/T \ .$$

The Hanning window function is shown in Figure 3-5, the side lobes of which are greatly reduced.

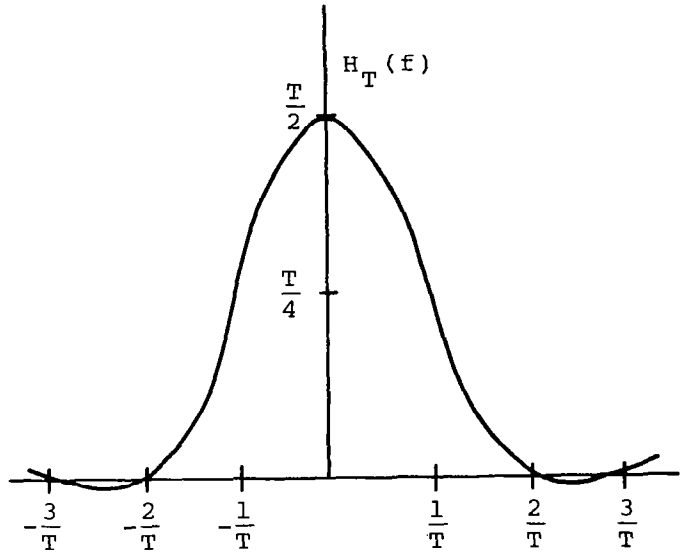

Figure 3-5. The spectral function of Hanning window function.

CHAPTER IV

RESULTS AND DISCUSSION OF SIMULATION

Chapter IV discusses simulation of turbulence employing the various filter techniques described in Chapter III. Included in the discussion are simulated turbulence time histories, probability density functions, power spectrum functions, and coherence functions. Some of the simulated results are compared with turbulence properties measured in the atmosphere. The atmospheric data were measured at NASA Marshall Space Flight Center, Atmospheric Boundary Layer Facility [19].

A. Random Number Generation

A 12-term equation (see Equation (3-6)) is used for generation of the Gaussian random numbers. These numbers used as input for the simulations described later are shown in Figure 4-1.

Figure 4-1. Gaussian distributed random signals with zero mean and unity standard deviation (2048 data).

By using the computer subroutine GAUSS, as described in Chapter III, Section A, and shown in Appendix A, Section A-1, ten sets of data, each set having 2048 digitized points, are generated. The first starting value, IX in subroutine GAUSS, is arbitrarily chosen as 65549. The starting value for the successive sets is taken as the last output value, IX, from the previous set. The input mean value $\bar{x}$ and the standard deviation σ are selected as zero and unity, respectively. The properties of each of the ten sets of output are shown in Table 4-1.

Table 4-1. The Variance, σ, and Mean Value of Random Signal Generated by Equation (3-6)

Set No.	Starting Value	Variance	σ	Mean
1	65 549	0.975	0.99	-0.02
2	1 873 182 733	0.962	0.98	-0.01
3	525 074 445	0.961	0.98	-0.02
4	250 707 981	0.976	0.99	-0.01
5	1 050 083 341	0.983	0.99	-0.03
6	775 716 877	1.062	1.03	0.04
7	1 575 092 237	0.960	0.98	0.02
8	1 300 725 773	0.978	0.99	0.00
9	2 100 101 133	0.981	0.99	0.00
10	1 825 734 669	1.041	1.02	0.03
Average		0.988	0.994	0.00

Table 4-1 shows that the generated standard deviations and mean values are very close to the designed values.

To examine the probability density function of the data set, the computer program PDF is used (see Appendix A, Section A-2). This computer program is based on the following equations.

The probability density function P(x) can be defined as (see [17])

$$P(x_o)\ \Delta x = \text{Prob}\ [\ (x_o - \tfrac{\Delta x}{2}) < x(t) \leq (x_o + \tfrac{\Delta x}{2})\ ]\ , \qquad (4\text{-}1)$$

where the function Prob [A] represents the probability that Statement A is true. More precisely,

$$P(x_o) = \lim_{\Delta x \to 0} \frac{\text{Prob}\ [(x_1 - \tfrac{\Delta x}{2}) < x(t) \leq (x_o + \tfrac{\Delta x}{2})\ ]}{\Delta x}\ . \qquad (4\text{-}2)$$

For digitized data, x_n, $n = 1,2,\ldots,N$, the probability that x_n falls within the range $[\ x_o \pm x/2\ ]$ can be calculated as

$$\text{Prob}\ [\ (x_o - \tfrac{\Delta x}{2}) < x_n \leq (x_o + \tfrac{\Delta x}{2})\ ] = \frac{N_{x_o}}{N}\ , \qquad (4\text{-}3)$$

where N_{x_o} is the number of digitized values which lie in the range $[\ x_o \pm \Delta x/2\ ]$.

The probability density function defined in Equation (4-2) can thus be written as

$$P(x_o) = \lim_{\Delta x \to 0} \frac{N_{x_o}}{N\ \Delta x} \ . \tag{4-4}$$

Rather than using the limiting process for digital simulation, a small, finite value of Δx is used which gives

$$\hat{P}(x_o) = \frac{N_{x_o}}{N\ \Delta x} \ . \tag{4-5}$$

Figure 4-2 shows the calculated $\hat{P}(x_o)$ for Data Set 1, using $\Delta x = 0.3$, compared with the theoretical Gaussian distribution defined in Equation (3-4). Figure 4-3 shows the same $\hat{P}(x_o)$ computed by using a Δx value of $\Delta x = 0.2$. Comparison of the two figures shows that the variation in Δx has little influence on the agreement of the $\hat{P}(x_o)$ function with the theoretical distribution to be simulated. Figure 4-4 shows the influence of using $\Delta x = 0.2$ and of increasing the sample size, N. Using the total 20480 datum points, the estimate of $\hat{P}(x_o)$ agrees considerably better with the actual Gaussian distribution.

As mentioned previously, a Gaussian distributed white noise input is required for the proposed simulations. The power spectrum for white noise is constant for all frequencies. The power spectrum for the generated random signal input was computed to confirm that it was, indeed, constant.

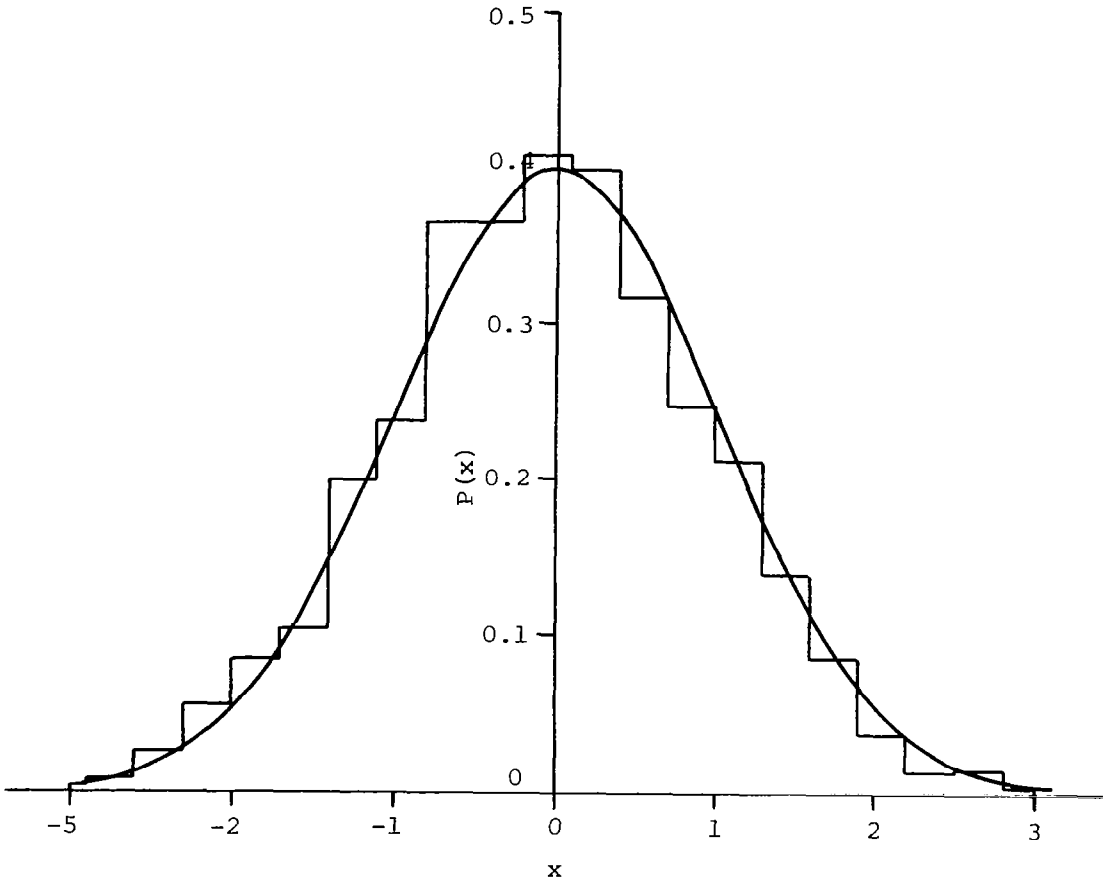

Figure 4-2. The estimated probability density function of the 2048 random numbers, shown in Figure 4-1, compared with the theoretical Gaussian distribution ($\Delta x = 0.3$).

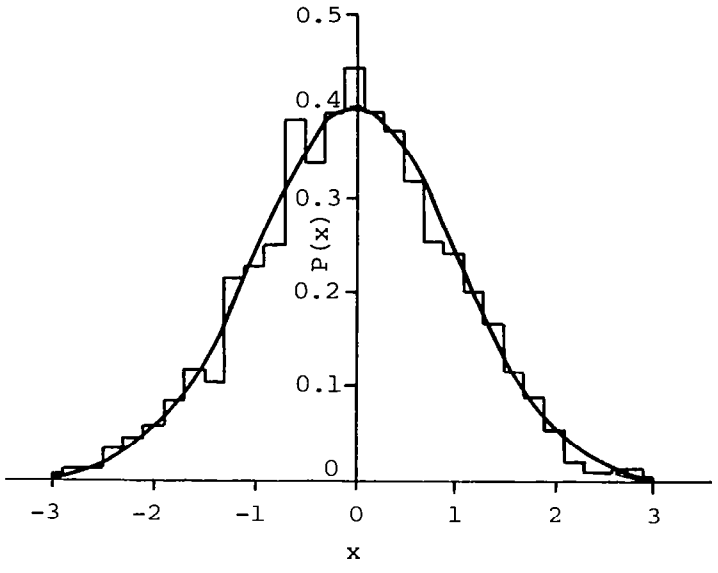

Figure 4-3. Probability density function of the data set used in Figure 4-2, computed with $\Delta x = 0.2$.

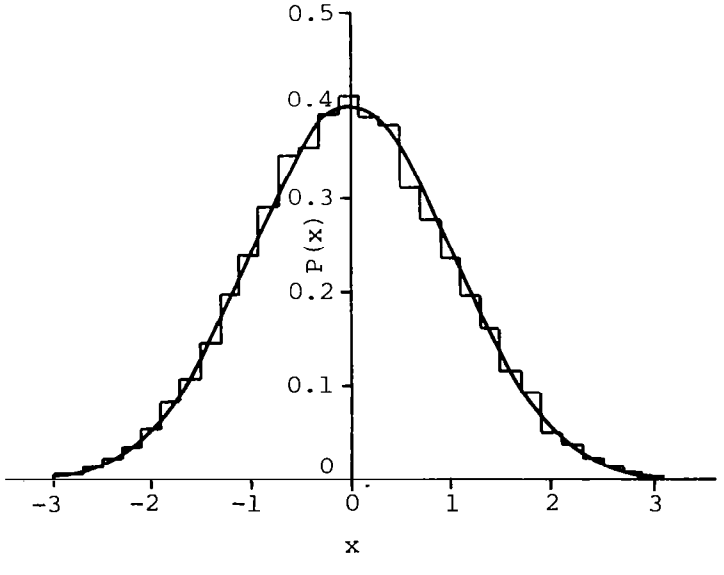

Figure 4.4. Probability density function computed with total 20480 data points ($\Delta x = 0.2$).

A raw estimate of the power spectrum is defined as (see [17]),

$$\phi(f) = \frac{2}{T} |X(f,t)|^2 , \qquad (4\text{-}6)$$

where $T = N \cdot \Delta t$, and $X(f,T)$ is the Fourier transform of $x(t)$ for discrete frequency values shown in Equation (3-15),

$$X_m = \frac{X(f_m,T)}{\Delta t} \qquad m = 0,1,2,\ldots,N-1 . \qquad (4\text{-}7)$$

Hence, the discrete power spectrum becomes

$$\phi_m = \frac{2\Delta t}{N} |X_m|^2 . \qquad (4\text{-}8)$$

To transform the time history x_n to the frequency domain X_m, the fast Fourier transform computer subroutine FFT (see Appendix A, Section A-3) is used. The estimated discrete power spectrum is then calculated from Equation (4-8). The computer subroutine for this purpose is called SPEC (see Appendix A, Section A-4). The estimated spectrum of Data Set 1 as generated by this subroutine is shown in Figure 4-5(a).

Since the estimated spectrum is for bandwidth-limited input data, estimates at a frequency spacing of 1/T will be essentially uncorrelated. Hence, smoothing or averaging techniques are required to obtain a representative spectrum function. One smoothing technique consists

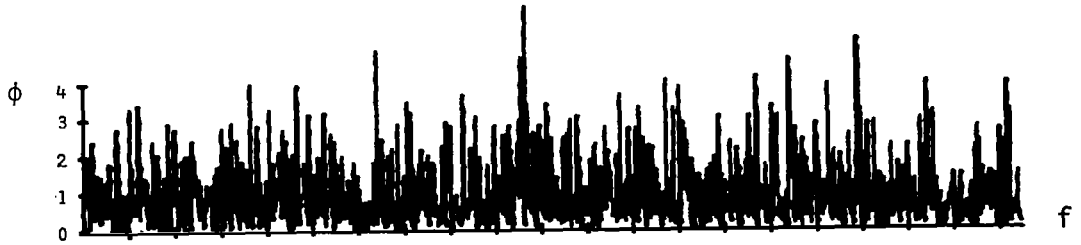

(a) Estimated raw spectrum

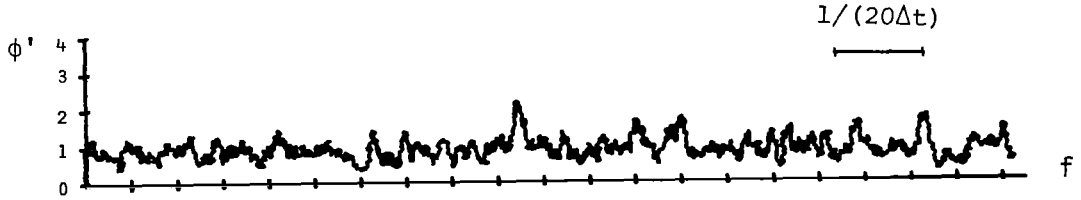

(b) Ten-point frequency smoothed spectrum

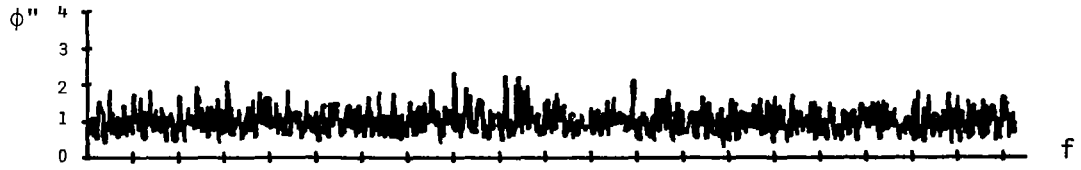

(c) Segment-averaged spectrum for ten data sets

Figure 4-5. The estimated raw and smoothed spectra of Data Set 1 (Figure 4-1, page 54) (Δt = 0.1 sec).

of averaging n neighboring frequency components of the raw spectrum estimates (see [17]),

$$\phi'_m = \frac{1}{n} [\, \phi_m + \phi_{m+1} + \ldots + \phi_{m+n-1} \,] . \qquad (4\text{-}9)$$

Figure 4-5(b) shows the frequency smoothed value ϕ'_m of the ϕ_m given in Figure 4-5(a).

A second technique of smoothing is averaging the results from n separate time slices, segment averaging, where each slice is of length T such that the original length is equal to n·T. The averaged spectrum is given by (see [17])

$$\phi''_m = \frac{1}{n} [\, \phi_{m,1} + \phi_{m,2} + \ldots + \phi_{m,n} \,] , \qquad (4\text{-}10)$$

where the second subscript indicates the slice number.

Figure 4-5(c) shows the segment-averaged values of ϕ''_m, as well as the average of the ϕ_m values calculated separately for each of the ten sets of data listed in Table 4-1. The computer subroutine for smoothing is called SMOOTH and is listed in Appendix A, Section A-5.

B. Simulated Turbulence

As discussed in Chapter II, various spectrum models can be simulated by different filter functions. A general form of H(f), which represents the Dryden filter and is a good approximation of the Kaimal and von Karman spectrum

filter, is given by

$$H(f) = \frac{c + jdf}{[a + jf]^2} , \qquad (4\text{-}11)$$

where the constants a, c, and d are different for each model, as listed in Table 4-2.

Equation (4-11) can be written as

$$H(f) = \frac{c + jdf}{[(a^2 - f^2) + 2jaf]}$$

$$= D[c(a^2 - f^2) + 2adf^2 + j[(a^2 - f^2)d - 2ac]f] , \qquad (4\text{-}12)$$

where

$$D = \frac{1}{(a^2 - f^2)^2 + 4a^2f^2} .$$

The real and imaginary parts of H(f) function are then given by the two functions

$$HR(f) = D[c(a^2 - f^2) + 2adf^2]$$

$$HI(f) = D[(a^2 - f^2)d - 2ac]f . \qquad (4\text{-}13)$$

A computer subroutine FILTER (see Appendix A, Section A-6) is available for the calculation of the real and imaginary parts of the filter function. This subroutine also calculates the output Y(f) from

Table 4-2. Coefficients a, c, and d for Different Spectrum Model

	a	b	c
Longitudinal component of Dryden spectrum (Equation (2-11))	$\frac{1}{2\pi}\left(\frac{V}{\Lambda}\right)$	$\frac{\sigma}{2\pi}\left(\frac{V}{\Lambda}\right)^{3/2}$	$\frac{\sigma}{\pi}\left(\frac{V}{\Lambda}\right)^{1/2}$
Lateral component of Dryden spectrum (Equation (2-11))	$\frac{1}{2\pi}\left(\frac{V}{\Lambda}\right)$	$\frac{3\sigma}{2\pi^2}\left(\frac{V}{2\Lambda}\right)^{3/2}$	$\frac{\sigma}{\pi}\left(\frac{V}{\Lambda}\right)^{1/2}$
Approximate Kaimal spectrum (Equation (2-20))	$0.155\left(\frac{V}{\Lambda}\right)$	$0.0432\ \sigma\left(\frac{V}{\Lambda}\right)^{3/2}$	$0.279\ \sigma\left(\frac{V}{\Lambda}\right)^{1/2}$
Approximate von Karman spectrum (Equation (2-23))	$0.286\left(\frac{V}{\Lambda}\right)$	$0.114\ \sigma\left(\frac{V}{\Lambda}\right)^{3/2}$	$0.398\ \sigma\left(\frac{V}{\Lambda}\right)^{1/2}$

$$YR(f) = HR(f)XR(f) - HI(f)XI(f)$$
$$YI(f) = HR(f)XI(f) + HI(f)XR(f) \qquad (4\text{-}14)$$

where XR(f) and XI(f) are the real and imaginary parts of the Fourier transform of the input x(t).

The frequency function Y(f) is transferred to the time domain, y(t), with the inverse FFT method.

The difference equation based on the Z-transformation technique can be derived for the filter of the spectrum given by Equation (4-11), as illustrated for the simple case in Chapter II, Section B. Thus, the discrete output y_{n+1} is related to y_n, y_{n-1}, x_n, and x_{n-1} by:

$$y_{n+1} = c_1 \cdot y_n + c_2 \cdot y_{n-1} + d_1 \cdot x_n + d_2 \cdot x_{n-1} \ , \qquad (4\text{-}15)$$

where

$$c_1 = 2 \exp [-2a\pi \ \Delta t]$$

$$c_2 = - \exp [-4a\pi \ \Delta t]$$

$$d_1 = d \left[\frac{c}{ba^2} + \frac{c_1}{2} \left(\left(\frac{a - c/b}{a} \right) \Delta t - \frac{c}{ba^2} \right) \right]$$

$$d_2 = d \left[\frac{c}{ba^2} \left(\frac{c_1}{2} - 1 \right) - \left(\frac{a - c/b}{a} \right) \Delta t \right] c_1/2 \ .$$

The constants a, c, and d are those listed in Table 4-2, and the constant $b = (2\pi)^{1/2}$.

A computer program employing the Z-transformation technique called DZT is given in Appendix A, Section A-7. The FFT/FILTER method and the DZT method are now used to simulate turbulence time histories having the different spectra described above.

Figures 4-6 and 4-7 show the simulated time histories for the four spectra as defined by the constants listed in Table 4-2, using both the FFT and DZT methods, respectively. All data shown in Figures 4-6 and 4-7 are normalized with σ to facilitate comparison. Smaller values of σ_{DZT} therefore give larger peaks, as shown in Figure 4-7.

Although the expected values of $\bar{x}$ and σ are zero and unity, respectively, the simulated mean value $\bar{x}$ and standard deviation σ are affected differently by the FFT and DZT methods. Tables 4-3 and 4-4 show values of $\bar{x}$ and σ determined statistically from the simulated turbulence time histories using Table 4-1, page 55, as the input. Table 4-3 shows that the value of $\bar{x}$ is approximately two times the input value for the FFT simulation, but almost exactly the input for the DZT method. The overall average value, however, is still in the acceptable range.

Table 4-4 indicates that the input variance is considerably altered by both techniques. This effect is strongly dependent on the time increment Δt.

To generate the correct variance, one must consider the difference between a continuous system before and after

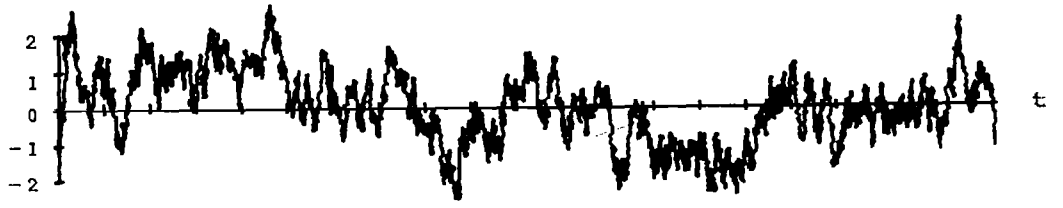

(a) Longitudinal component of Dryden spectrum model

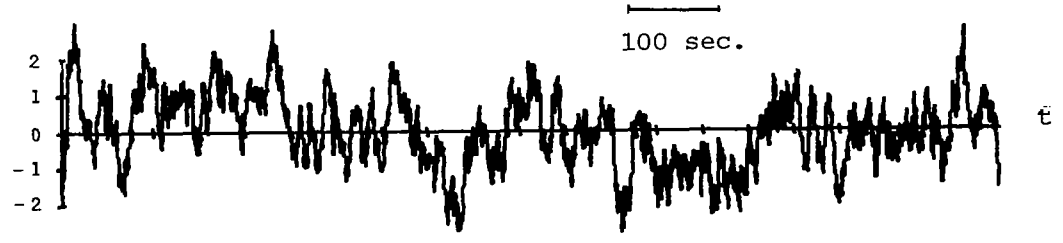

(b) Lateral component of Dryden spectrum model

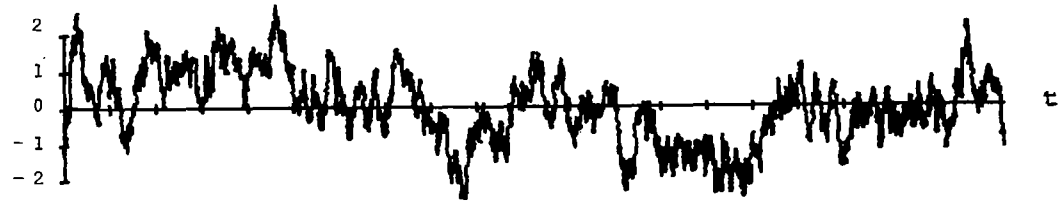

(c) Approximated Kaimal spectrum model

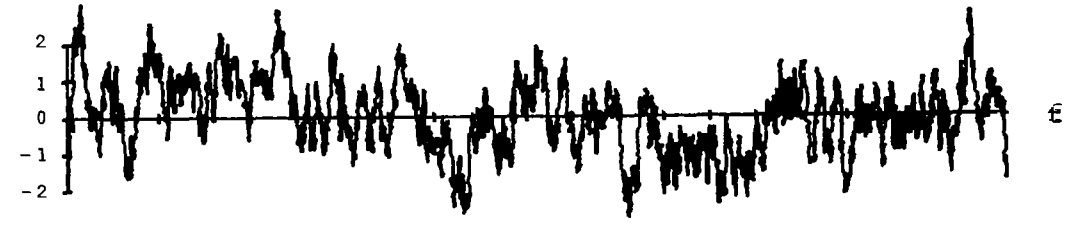

(d) Approximated von Karman spectrum model

Figure 4-6. The normalized time histories of simulated turbulence by the FFT method using Data Set 1 as input ($\Delta t = 0.5$, $N = 2048$).

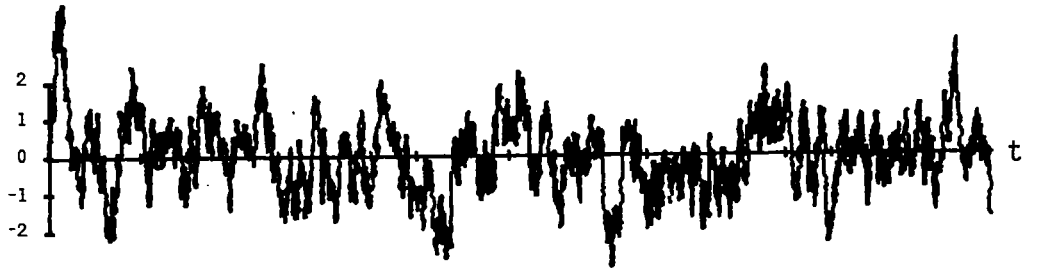

(a) Longitudinal component of Dryden spectrum model

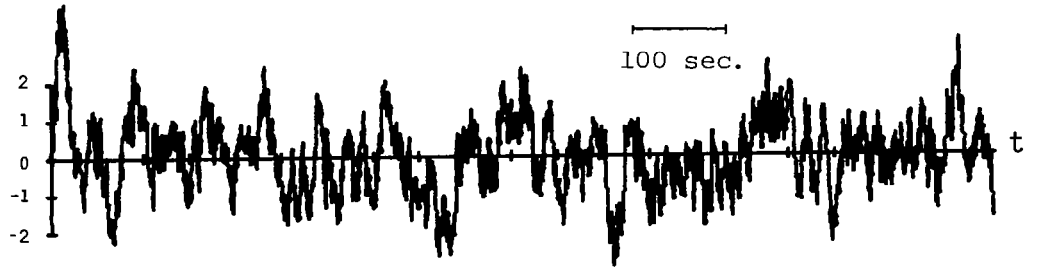

(b) Lateral component of Dryden spectrum model

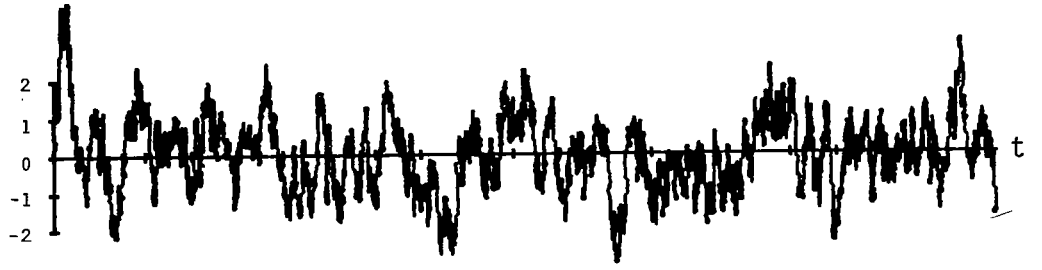

(c) Approximated Kaimal spectrum model

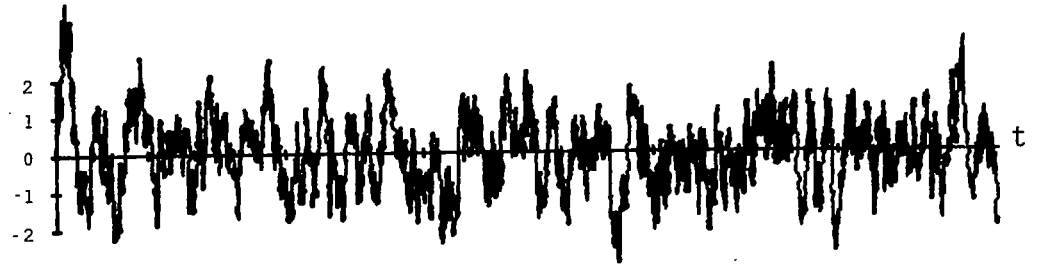

(d) Approximated von Karman spectrum model

Figure 4-7. The normalized time histories of simulated turbulence by the DZT method using Data Set 1 as input ($\Delta t = 0.5$, $N = 2048$).

Table 4-3. The Mean Value of the Simulated Turbulence

	Input	DZT	FFT
	-0.02	-0.02	-0.06
	-0.01	-0.01	-0.02
	-0.02	-0.02	-0.05
	-0.01	-0.01	-0.02
	-0.03	-0.04	-0.09
	0.04	0.04	0.09
	0.02	0.02	0.06
	0.00	0.00	0.00
	0.00	0.00	0.01
	0.03	0.03	0.07
Average	0.00	-0.01	-0.01

Table 4-4. The Standard Deviation σ of the Simulated Turbulence

Δt	0.1	0.2	0.5	1.0	2.0
Input	0.99	0.99	0.99	0.99	0.99
DZT	0.18	0.25	0.40	0.56	0.79
FFT	0.44	0.63	0.99	1.36	1.86

it is passed through a sampling and holding device. The sample and hold function $\hat{x}(t)$ is related to the continuous function $x(t)$ by

$$\hat{x}(t) = \sum_{n=0}^{\infty} x(n\Delta t) \left[s\left(t-n\Delta t\right) - s\left(t - (n+1)\Delta t \right) \right] , \quad (4\text{-}16)$$

where $s(t)$ is the step function defined

$$s(t) = 1 \qquad t \geq 0$$

$$= 0 \qquad t < 0 \ .$$

Taking the Fourier transform of Equation (4-16)

$$\hat{X}(\omega) = \sum_{n=0}^{\infty} x_n \left[\frac{e^{-jn\Delta t\omega} - e^{-j(n+1)\Delta t\omega}}{j\omega} \right]$$

$$= \sum_{n=0}^{\infty} x_n \, e^{-jn\Delta t\omega} \left[\frac{1 - e^{-j\Delta t\omega}}{j\omega} \right] \quad (4\text{-}17)$$

$$= X_m \left[\frac{1 - e^{-j\Delta t\omega}}{j\omega} \right] ,$$

where X_m is the discrete Fourier component of $x(t)$ (see Equation (3-16)). Equation (4-17) therefore becomes

$$\hat{X}(\omega) = X(\omega) \cdot s(\omega) \ , \quad (4\text{-}18)$$

where

$$s(\omega) = \frac{1}{\Delta t} \left[\frac{1 - \exp\left(- j\Delta t\omega\right)}{j\omega} \right] .$$

Let the continuous function input have a constant spectrum $\phi_x(f)$ and a variance of σ_x^2. Then the spectrum of the sample and hold output is

$$\hat{\phi}_x(f) = \phi_x(f) \cdot |s(f)|^2 . \tag{4-19}$$

Since the constant spectrum $\phi_x(f)$ can be replaced by

$$\sigma_x^2 = \int_0^{1/2\Delta t} \phi_x(f)\, df$$

$$\phi_x(f) = 2\Delta t\ \sigma_x^2 ,$$

it follows that

$$\hat{\phi}_x(f) = 2\Delta t\ \sigma_x^2 \left[\frac{\sin(\pi f \Delta t)}{\pi f \Delta t}\right] . \tag{4-20}$$

Using this sample and hold data as the input of the turbulence simulation system, the simulated output variance is

$$\hat{\sigma}_y^2 = \int_o^{\infty} \hat{\phi}_x(f)\ |H(f)|^2\, df , \tag{4-21}$$

and since the continuous system output ϕ_y is defined by $\phi_y = |H(f)|^2$, Equation (4-21) becomes

$$\hat{\sigma}_y^2 = \int_o^{\infty} 2\sigma_x^2\ \Delta t \left[\frac{\sin(\pi f \Delta t)}{\pi f \Delta t}\right]^2 \phi_y(f)\, df . \tag{4-22}$$

Assuming [sin(πfΔt) / πfΔt] to be approximately unity for the lower frequency (see Table 4-5) where the atmospheric turbulence has the most significant energy density, Equation (4-22) reduces to

$$\frac{\hat{\sigma}_y^2}{\sigma_x^2} = 2\Delta t \int_0^\infty \phi_y(f)df = 2\Delta t\ \sigma_y^2 \ . \qquad (4\text{-}23)$$

If σ_x^2 is equal to unity, then

$$\hat{\sigma}_y^2 = 2\Delta t\ \sigma_y^2 \ , \qquad (4\text{-}24)$$

or if σ_x^2 is selected equal to

$$\sigma_x^2 = \frac{1}{2\Delta t} \ , \qquad (4\text{-}25)$$

then

$$\hat{\sigma}_y^2 = \sigma_y^2 \ .$$

Table 4-5. Values of [sin(πfΔt) / πfΔt] for Low Frequency f (Δt = 0.1)

f	0.001	0.01	0.1	0.5	1.0	2.0	3.0
$[\frac{\sin(\pi f\Delta t)}{\pi f\Delta t}]$	0.999	0.999	0.999	0.995	0.983	0.935	0.858

Hence, by adjusting the input variance σ_x^2 through the relationship $1/2\Delta t$, the discrete system will have the desired output variance σ_y^2.

Considering now the difference equation of the Z-transformation, the output variable in terms of the input variables is

$$y_n = \sum_{i=1}^{n} \alpha_i \, x_i \ . \tag{4-27}$$

Since each value of x_i (or y_i) is independent, the variance can be given by

$$\hat{\sigma}_y^2 = \sigma_x^2 \lim_{n\to\infty} \sum_{i=0}^{n} \alpha_i^2 \ . \tag{4-28}$$

To find the α_i^2, one can write the initial terms of the difference equation for the first few inputs and then deduce the functional relationship between α_i and $\alpha_{(i+1)}$. The sum of the squares of these terms can then be split into geometric series and derivatives of geometric series, which are all summable. For example, the result for Equation (3-46) is (see Appendix B)

$$\hat{\sigma}_y^2 = \sigma_x^2 \left[\frac{2\sigma_y^2}{\pi a} \, \frac{(1 - e^{-a\Delta t})^2}{1 - e^{-2a\Delta t}} \right] , \tag{4-29}$$

where

$$a = \frac{V}{\Lambda} \ .$$

For small Δt, Equation (4-29) reduces to

$$\frac{\hat{\sigma}_y^2}{\sigma_x^2} = \frac{\Delta t}{\pi} \sigma_y^2 \quad . \tag{4-30}$$

With $\sigma_x^2 = 1$ the result is

$$\hat{\sigma}_y^2 = \frac{\Delta t}{\pi} \sigma_y^2 \quad . \tag{4-31}$$

Alternately, if the input is selected as

$$\sigma_x^2 = \frac{\pi}{\Delta t} \quad , \tag{4-32}$$

then the output variance $\hat{\sigma}_y^2$ of the difference equation will be equal to the desired output variance σ_y^2.

Figure 4-8 compares Equations (4-24) and (4-31) with the calculated standard deviations given in Table 4-4, page 69. In both cases good agreement with the theory in the small Δt range is observed. This is expected, since Equations (4-24) and (4-31) also assume small Δt. Hence, the variance can be simulated properly by applying Equations (4-25) and (4-32), respectively, to the input of the system. The computer program for generating the input array x_i with the adjusted variance is called INPUT, and is listed in Appendix A, Section A-8.

To compare the simulated turbulence with measured atmospheric turbulence, the value of the reference velocity V, the turbulence integral length scale Λ, and the

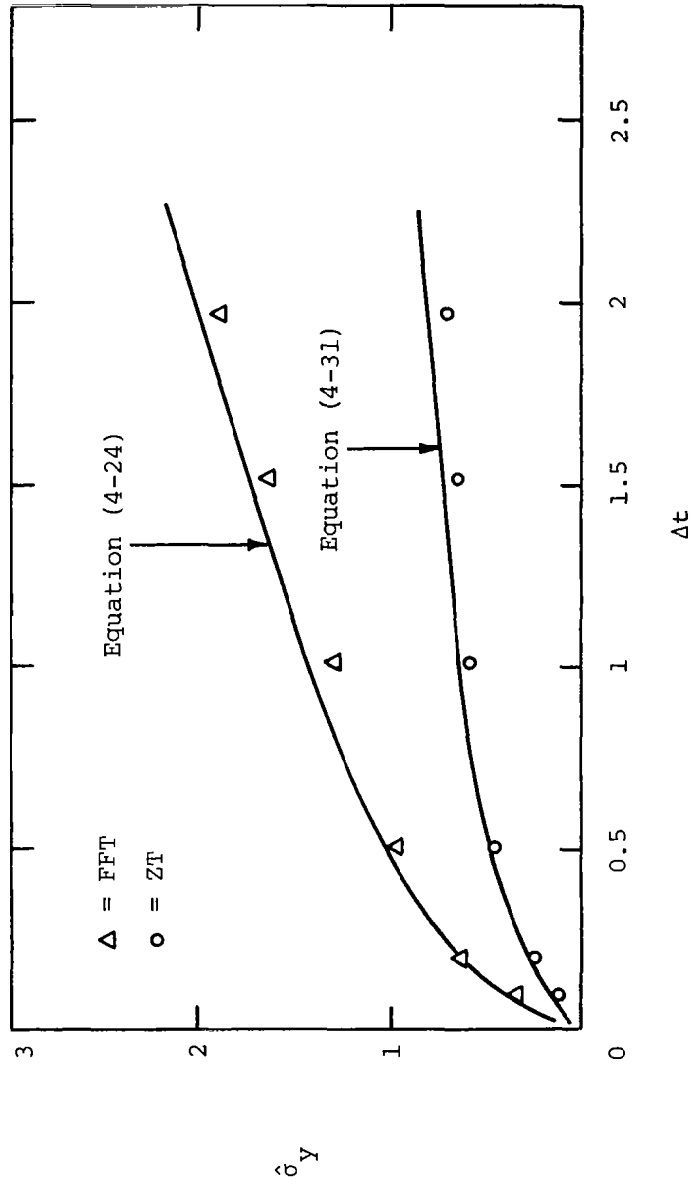

Figure 4-8. The output variance of discrete transformations for different sampling Δt.

turbulence intensity σ must be specified. The reference velocity is usually selected as the mean wind speed at the given height of the simulation. The Λ and σ values are functions of height, z, atmospheric stability conditions, $\psi(z/L)$, and surface roughness, z_o. The parameter L is the Monin Obukhov stability length. Equations for predicting the turbulence intensity values are given in [7] as:

$$\sigma_3 = 0.52\ U / \left[\ell n \left(\frac{z}{z_o} + 1 \right) + \psi(z/L) \right]$$

$$\sigma_2 = \sigma_3 \left[0.583 + 1.39 \times 10^{-3}\ z \right]^{-0.8} \qquad (4\text{-}33)$$

$$\sigma_1 = \sigma_3 \left[0.177 + 2.74 \times 10^{-3}\ z \right]^{-0.4}$$

The turbulence length scale for the Dryden spectrum is given in [16] as:

$$\Lambda_1 = \Lambda_2 = \begin{cases} 44.21(3.28\ z)^{1/2} & z \leq 533\text{m} \\ 533 & z > 533\text{m} \end{cases}$$

$$\Lambda_3 = \begin{cases} z & z \leq 533\text{m} \\ 533 & z > 533\text{m} \ . \end{cases} \qquad (4\text{-}34)$$

Figure 4-9 shows the comparison of the longitudinal velocity component time histories of simulated and measured atmospheric turbulence. The mean wind speed, U, and

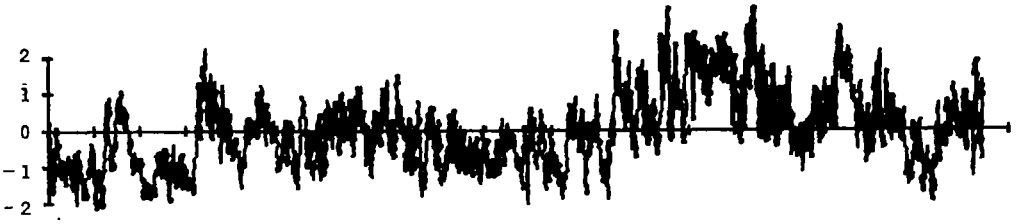

(a) Measured atmospheric turbulence (z = 24 m)

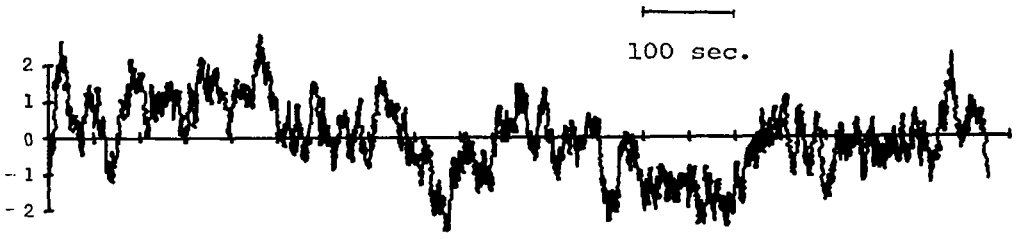

(b) Simulated Dryden spectrum turbulence

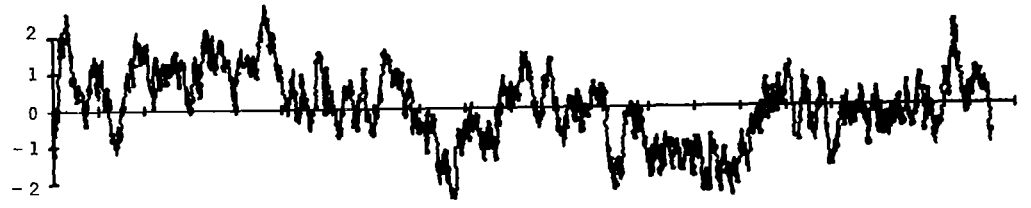

(c) Simulated turbulence of approximate Kaimal model

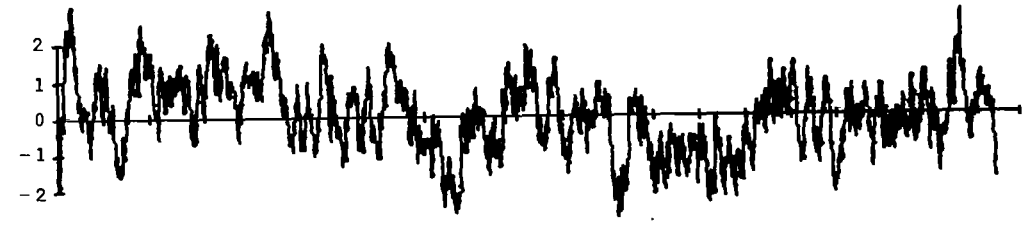

(d) Simulated turbulence of approximate von Karman model

Figure 4-9. The normalized time histories ($\Delta t = 0.5$, $N = 2048$).

turbulence intensity, σ, of the measured data are 7.52 m/s and 1.78 m/s, respectively. Based on this value and a height of 24 m for neutral stable conditions, the calculated value of σ_1 from Equation (4-33) is 1.26 m/s, which is the standard deviation used to simulate turbulence. Hence, the time histories shown in Figure 4-9 are normalized to facilitate comparison. From visual observation of the time histories, it appears that the measured data contain more high-frequency components than the simulated results. This is expected because the Dryden form of the spectrum results in a filter which generates less power at higher frequencies (see Figure 2-2, page 9).

The probability density functions (PDF) of the measured and simulated turbulence are given in Figure 4-10. All of the simulated turbulence is very nearly Gaussian distributed; however, the measured atmospheric turbulence has non-Gaussian characteristics, as discussed in Chapter II, Section C. Hence, the multi-filter system shown in Figure 2-8, page 20, and in Table 2-1, page 26, has been programmed (Appendix A, Section A-9) to provide better simulation of the non-Gaussian characteristics of atmospheric turbulence.

The calculated PDF's of this model for different values of r, the adjusting coefficient, are shown in Figure 4-11. A proper selected value of r is observed to provide a correct PDF for the simulated turbulence.

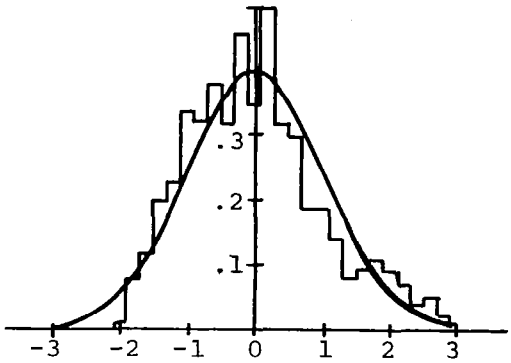

(a) Measured atmospheric turbulence

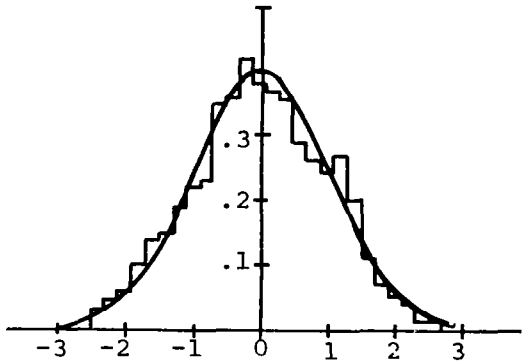

(b) Simulated Dryden spectrum turbulence

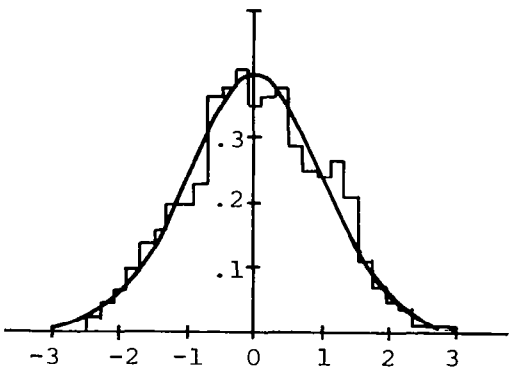

(c) Simulated turbulence of approximate Kaimal model

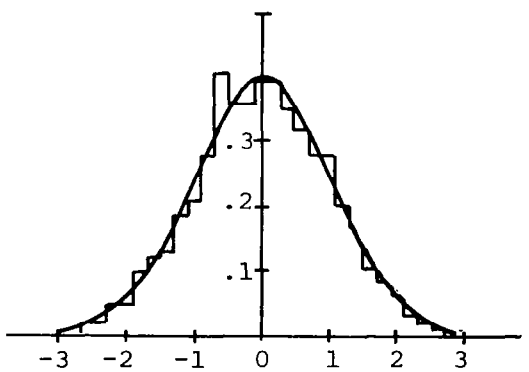

(d) Simulated turbulence of approximate von Karman model

Figure 4-10. The estimated PDF of the data of the different spectra techniques ($\Delta x = 0.2$).

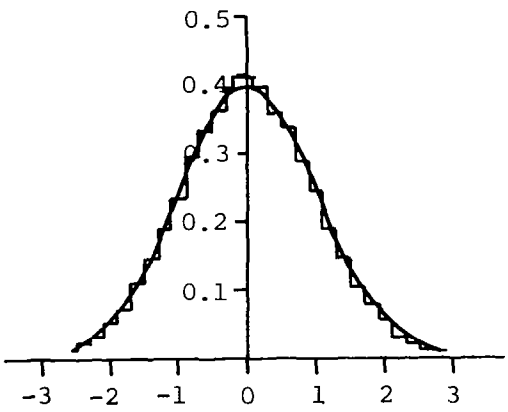

(a) r = 0.5

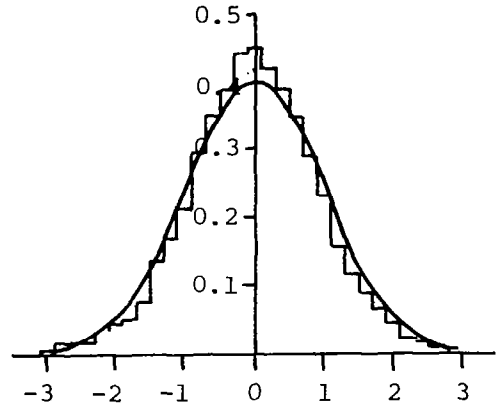

(b) r = 1.0

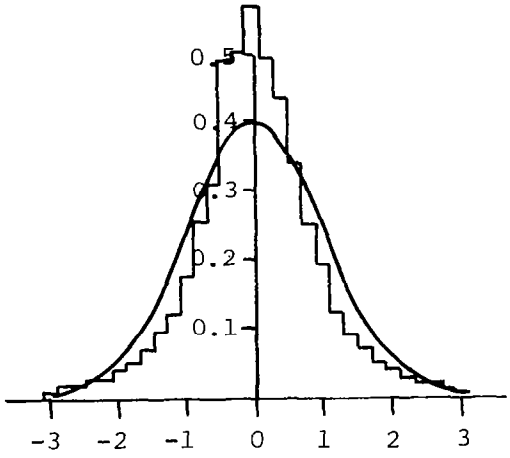

(c) r = 2.0

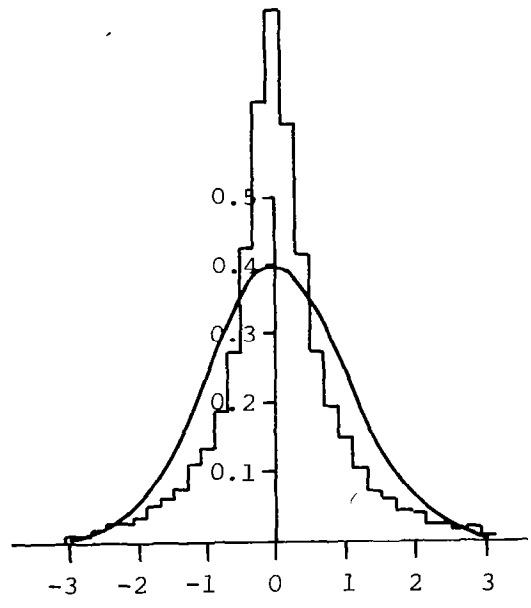

(d) r = 5.0

Figure 4-11. The calculated PDF using the non-Gaussian model ($\Delta x = 0.2$).

Figures 4-12 and 4-13 show the time histories and PDF's of the simulated non-Gaussian turbulence and of the measured atmospheric turbulence, respectively.

The PDF of the non-Gaussian model gives a peak shape similar to the measured data. This model also increases the number of sharp peaks relative to the Gaussian model; however, the number of overall high-frequency components is still much less than that for the measured atmospheric turbulence. This is to be expected because the non-Gaussian model still utilizes the Dryden spectrum filter.

In order to examine how well the simulation reproduces the input spectra functions, the discrete estimates were calculated from Equation (4-8). The segment-averaging technique, Equation (4-10), is applied to smooth the spectra.

The spectra estimates of turbulence are shown in Figures 4-14 and 4-15 for the FFT and DZT methods, respectively. Each plot is smoothed using 20 sets of data. The theoretical curves, based on Table 4-2, page 64, are also plotted for each case. Comparing these two figures shows that the FFT method provides a better spectrum simulation than the DZT method.

The spectrum of measured atmospheric turbulence was also computed and is compared with the von Karman spectrum (Equation 2-10)) and the Dryden spectrum (Equation (2-11)) in Figure 4-16. In this particular case, the measured spectrum agrees best with the von Karman spectrum.

(a) Measured atmospheric turbulence (z = 24 m)

(b) Simulated non-Gaussian Dryden spectrum model

Figure 4-12. The normalized time histories (r = 1.5).

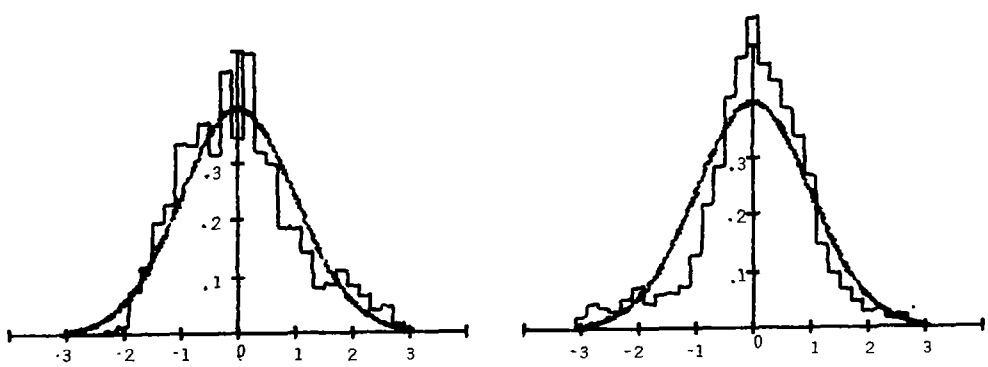

(a) Measured atmospheric turbulence (z = 24 m)

(b) Simulated non-Gaussian Dryden spectrum model (r = 1.5)

Figure 4-13. The estimated PDF of the non-Gaussian turbulence.

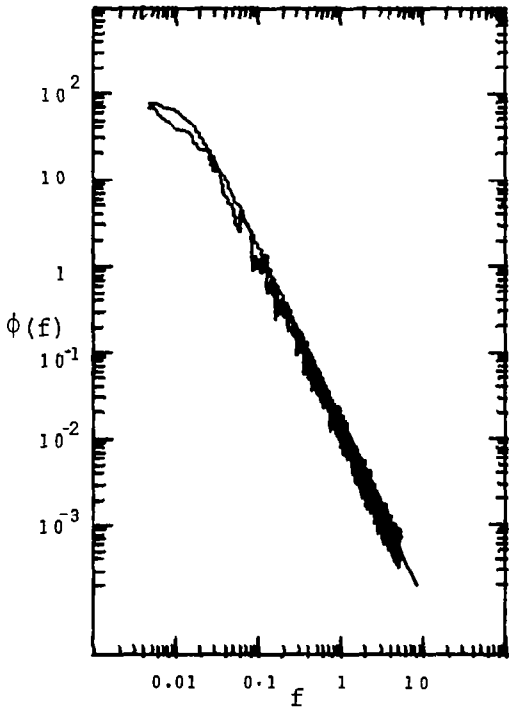

(a) Longitudinal component of Dryden spectrum model

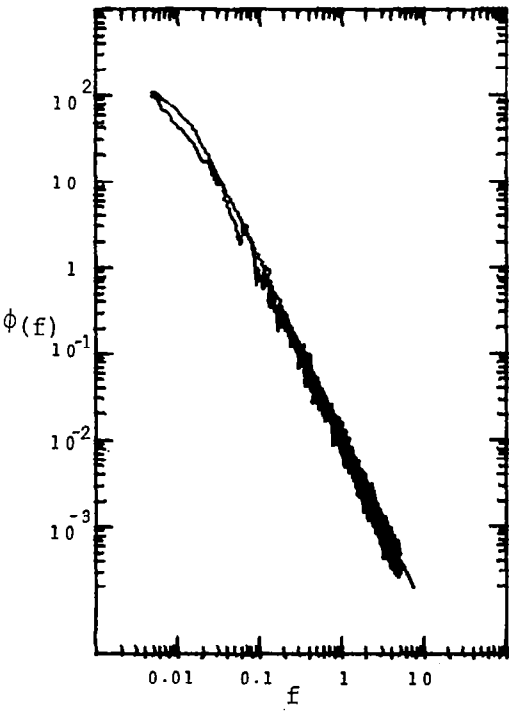

(b) Lateral component of Dryden spectrum model

Figure 4-14. Comparison of the theoretical and simulated spectra (by FFT method, $\Delta t = 0.5$, $N = 2048$, segment-average of ten sets).

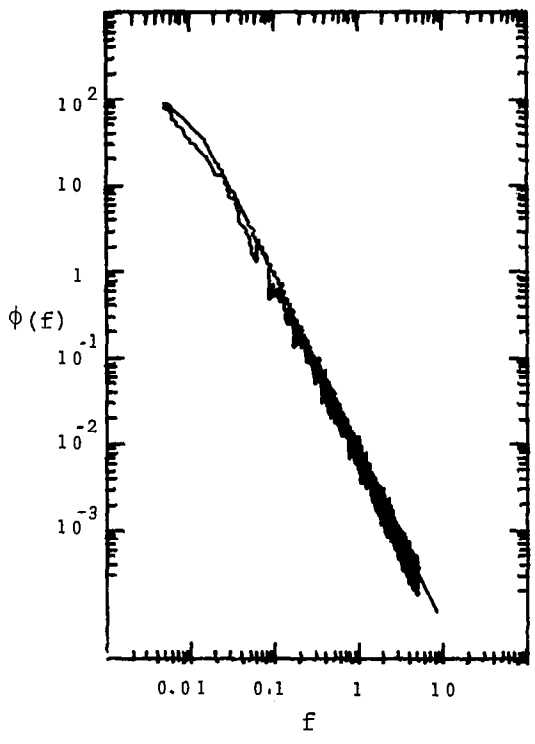

(c) Approximate Kaimal spectrum model

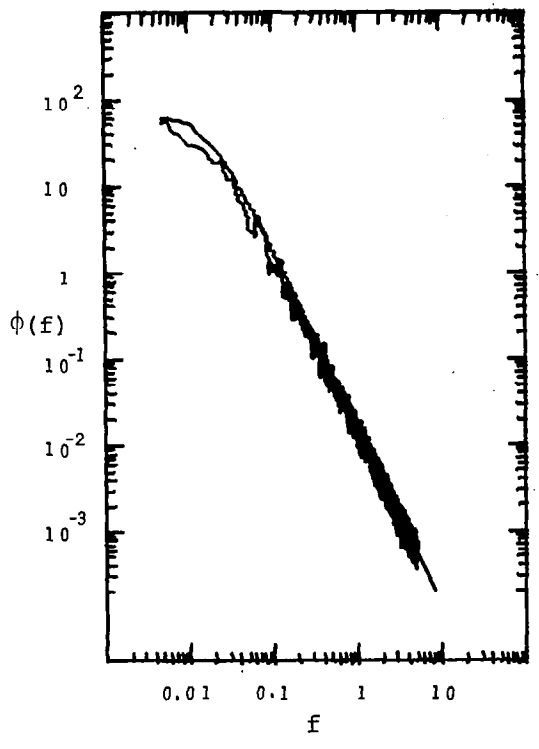

(d) Approximate von Karman spectrum model

Figure 4-14. (continued)

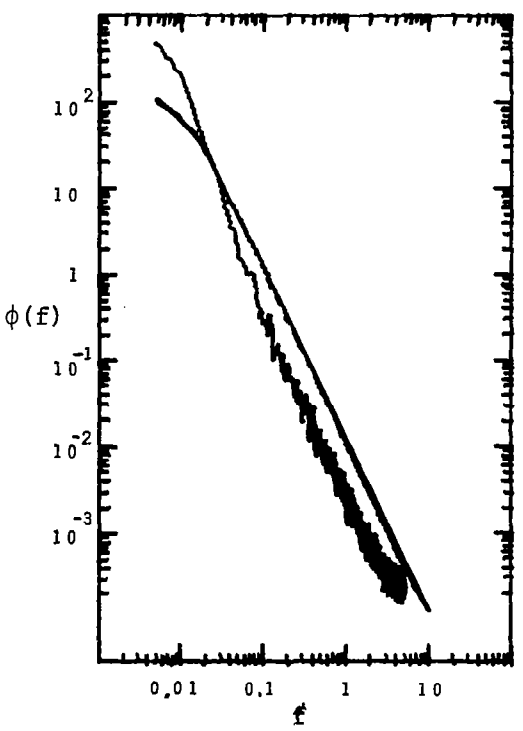

(a) Longitudinal component of Dryden spectrum model

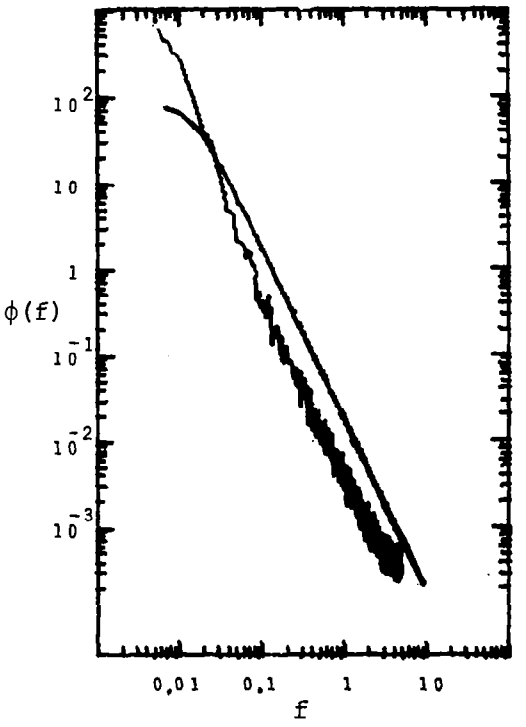

(b) Lateral component of Dryden spectrum model

Figure 4-15. Comparison of the theoretical and simulated spectra (by DZT method, $\Delta t = 0.5$, $N = 2048$, segment-average of ten sets).

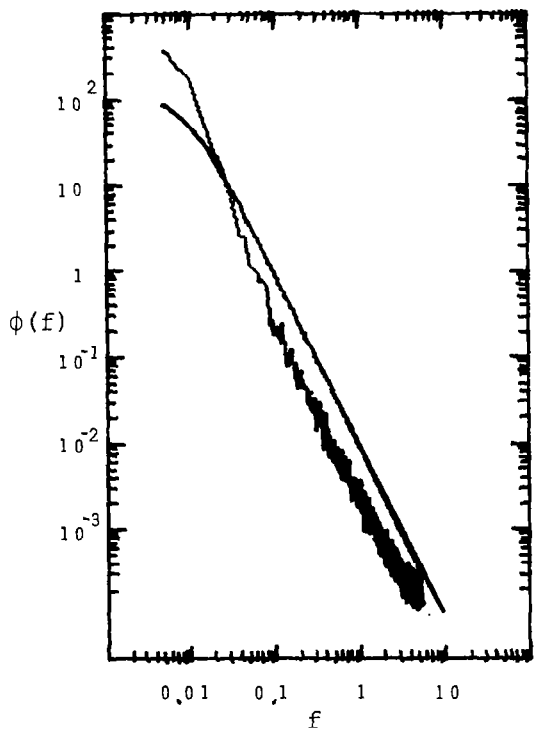

(c) Approximate Kaimal spectrum model

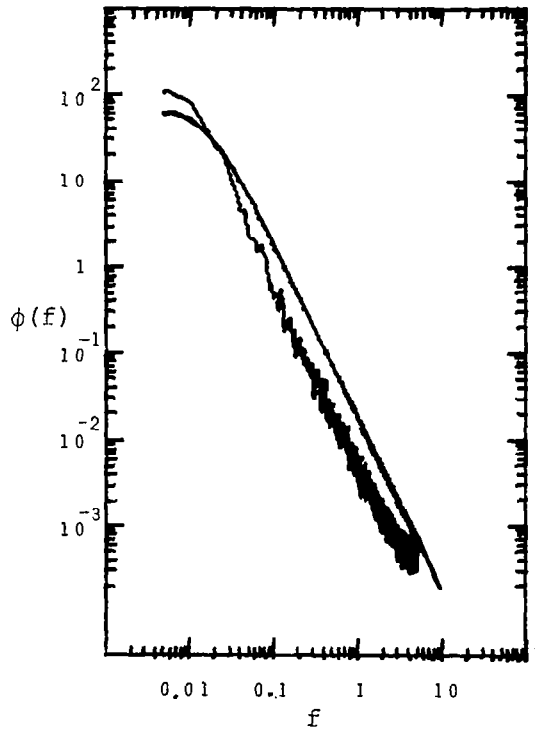

(d) Approximate von Karman spectrum model

Figure 4-15. (continued)

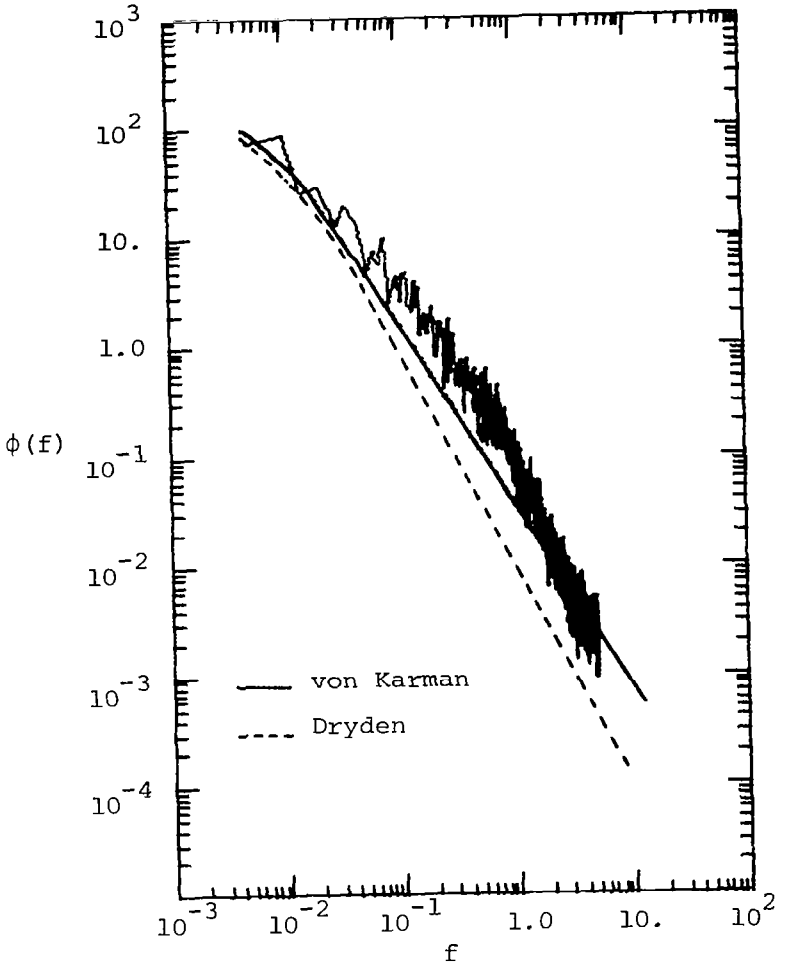

Figure 4-16. Comparison of two theoretical curves with the calculated spectrum of measured atmospheric turbulence ($z = 24$ m, $\Delta t = 0.5$, $N = 2048$).

It is well known that the von Karman spectrum more accurately describes atmospheric turbulence than does the Dryden spectrum (see Figure 2-2, page 9). For stable atmospheric turbulent flow conditions the Kaimal spectrum is required.

Because of the irrational nature of the von Karman and Kaimal spectrum functions, no real physical filter function can be obtained for simulation purposes. However, an exact solution of the filter function for these two spectra can be obtained. For the von Karman spectrum, the filter function is given as:

$$H_1(\omega) = \frac{c_1}{(a + j\omega)^{5/6}}$$

$$H_2(\omega) = \frac{b(j\omega + c_2)}{(a + j\omega)^{11/6}} \quad , \tag{4-35}$$

where

$$a = (0.74682)\frac{V}{\Lambda} \qquad b = (0.72236\,[\frac{\sigma_2 V^{1/3}}{\Lambda^{1/3}}]$$

$$c_1 = (0.62558)\,[\frac{\sigma_1 V^{1/3}}{\Lambda^{1/3}}] \quad , \quad c_2 = (0.4573)\frac{V}{\Lambda} \; .$$

For the Kaimal spectrum the filter section is:

$$H(f) = \frac{c}{a + j(f)^{5/6}} \quad , \tag{4-36}$$

where

$$a = (0.17241)\left[\frac{V}{\Lambda}\right]^{5/6} \quad , \quad c = (0.34482)\left[\frac{V}{\Lambda}\right]^{1/3}$$

Therefore, by using Equations (4-35) and (4-36) in conjunction with the FFT method as described in Equations (4-13) and (4-14), the exact von Karman or Kaimal turbulence spectra can be simulated. The computer program for simulation of these two spectrum functions is included in the subroutine FILTER (Appendix A, Section A-6).

In Figure 4-17 the time histories utilizing these more exact spectrum functions are compared with measured atmospheric turbulence. It can be seen from this figure that simulation of the high-frequency components is improved greatly over the Dryden and approximate filter simulations shown in Figure 4-9, page 77. The spectrum functions computed by Equation (4-8) for these two cases are shown in Figure 4-18, and the results agree very well with the theoretical curves.

Two disadvantages for these mathematical models are: first, due to the irrational form of the filter function, the DZT method cannot be used to establish the simple difference equation; and second, the correlation functions for both the von Karman and Kaimal spectra are much more complicated than the exponential function for the Dryden spectrum (see Equation (2-26)). For example, the correlation function for the von Karman spectrum is in the

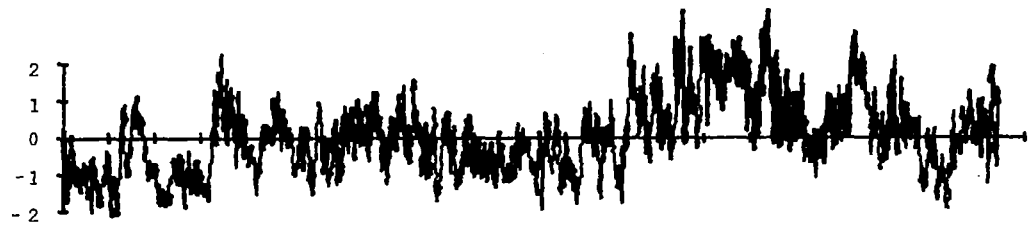

(a) Measured atmospheric turbulence (z = 24 m)

100 sec.

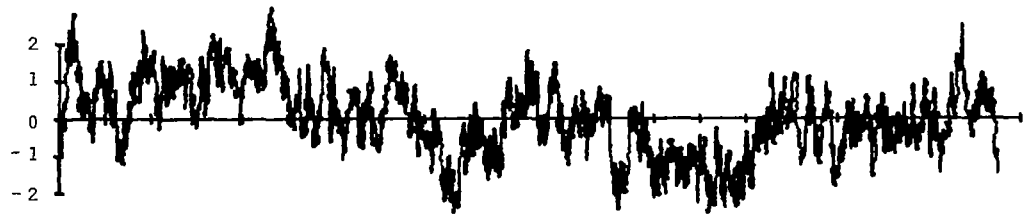

(b) Simulated von Karman spectral turbulence

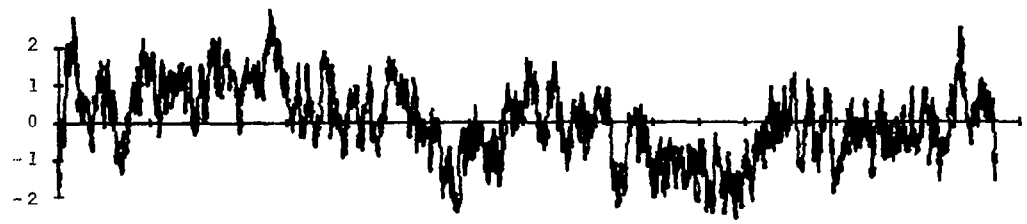

(c) Simulated Kaimal spectral turbulence

Figure 4-17. The time histories of non-linear system ($\Delta t = 0.5$, $N = 2048$).

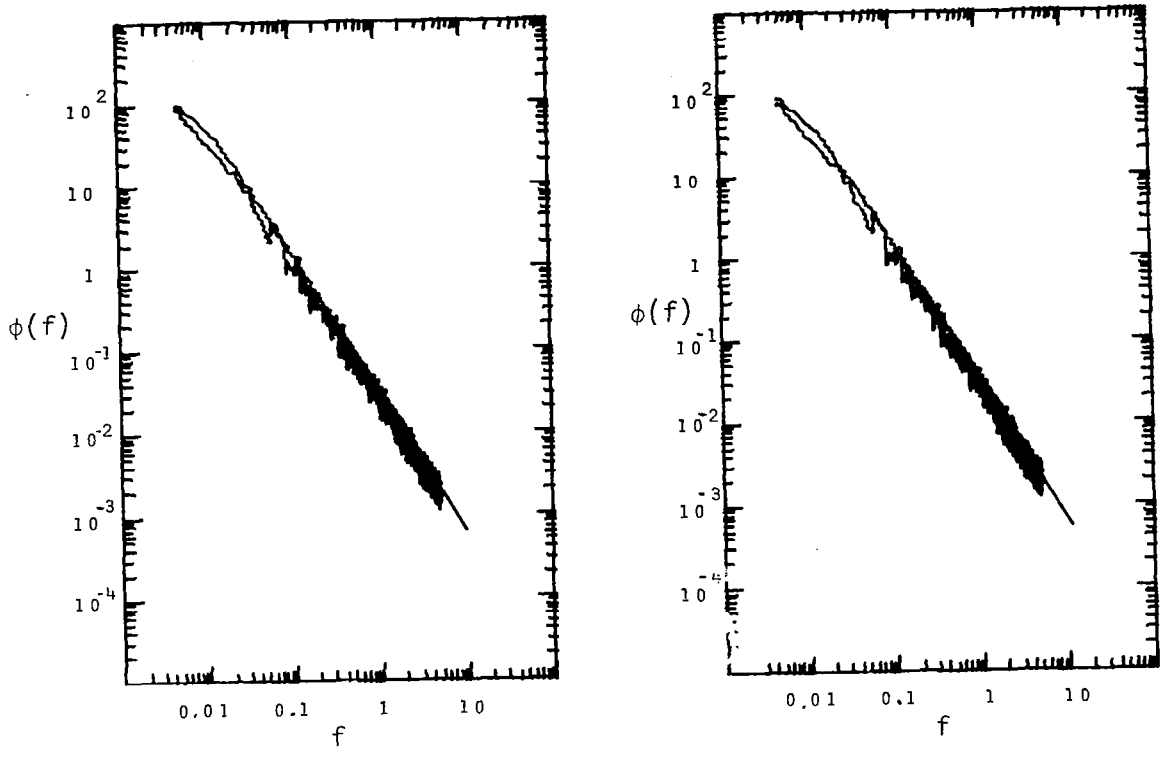

(a) von Karman spectral model

(b) Kaimal spectral model

Figure 18. Comparison of theoretical with simulated spectrum ($\Delta t = 0.5$, $N = 2048$, segment-average of ten sets).

form of modified Bessel function of the one-third order [5]. Thus, the von Karman and Kaimal spectra cannot be utilized for the multi-filter system to simulate the non-Gaussian character of atmospheric turbulence.

C. Simulation with Interlevel Coherence

In this section, simulated horizontal components of wind speed which include vertical coherence are discussed. Measured wind data recorded at the eight-tower Atmospheric Boundary Layer Facility, Atmospheric Sciences Division, NASA Marshall Space Flight Center, are also computed and presented for comparison.

The output transform, discussed in Chapter II and in reference [3], is given by

$$Y(K,z) = A\, H(K,z) \sum_{m=-M}^{M} D_m(K,z) X_m(K) \quad , \tag{4-37}$$

where the $D_m(K,z)$ was defined by Equation (2-38) as:

$$D_m(K,z) = c_m \exp [\, jKzm\pi / \varepsilon_o \,] \quad , \quad \varepsilon_o = (K\, \Delta z)_{max} \quad .$$

Substituting $D_m(K,z)$ into Equation (4-37) gives

$$Y(K,z) = H(K,z) \Big[\sum_{m=0}^{M} \left(e^{j\theta_m} X_m(K) + e^{-j\theta_m} X_{-m}(K) \right) B_m \Big] \quad , \tag{4-38}$$

where

$$B_0 = \frac{c_o A}{2} \quad , \quad B_m = c_m A \quad \text{for } m \neq 0$$

$$\theta_m = mKz\pi / \varepsilon_o \ .$$

Equation (4-38) can be reduced to

$$Y(K,z) = H(K,z)\ X'(K,z) \ , \tag{4-39}$$

where the

$$X'(K,z) = \sum_{m=0}^{M} \left(e^{j\theta_m} X_m(K) + e^{-j\theta_m} X_{-m}(K) \right) B_m \ .$$

Thus, the transform of the output Y(K,z) can be calculated in the same manner as described in Equations (4-13) and (4-14). The computer program for calculation of these equations is listed in Appendix A, Section A-10 .

Simulated results are obtained by using 11 levels of random signal inputs (M equal to 5 in Equation (4-37)) and the Dryden spectrum filter function for H(K,z). Figures 4-19 and 4-20 compare the time histories and auto-spectra of simulated coherent turbulence with the measured values for the 24 m and 12 m levels. Both figures show simularly shaped curves of equal magnitude.

As also mentioned in Chapter II, the atmospheric turbulence near the ground shows a coherence which behaves as

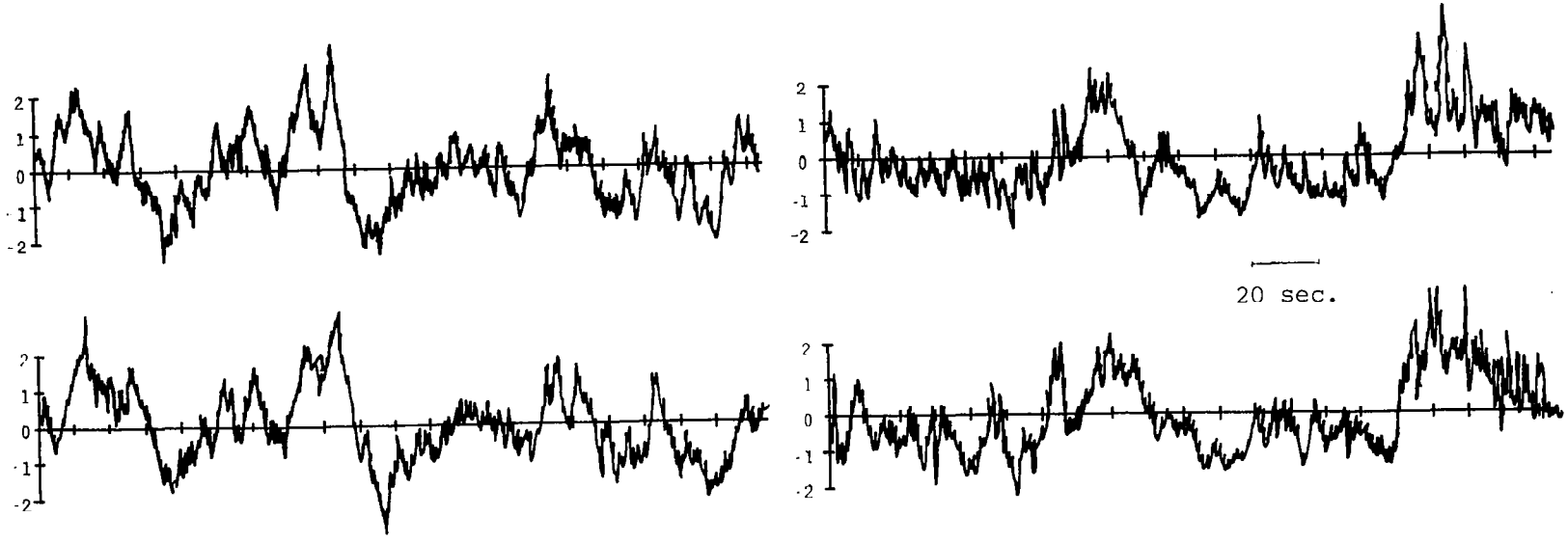

(a) Simulated interval coherence turbulence at z equal to 24 m and 12 m, respectively

(b) Measured atmospheric turbulence at z equal to 24 m and 12 m, respectively

Figure 4-19. The time histories of level coherence turbulence ($\Delta t = 0.1$, $N = 2048$).

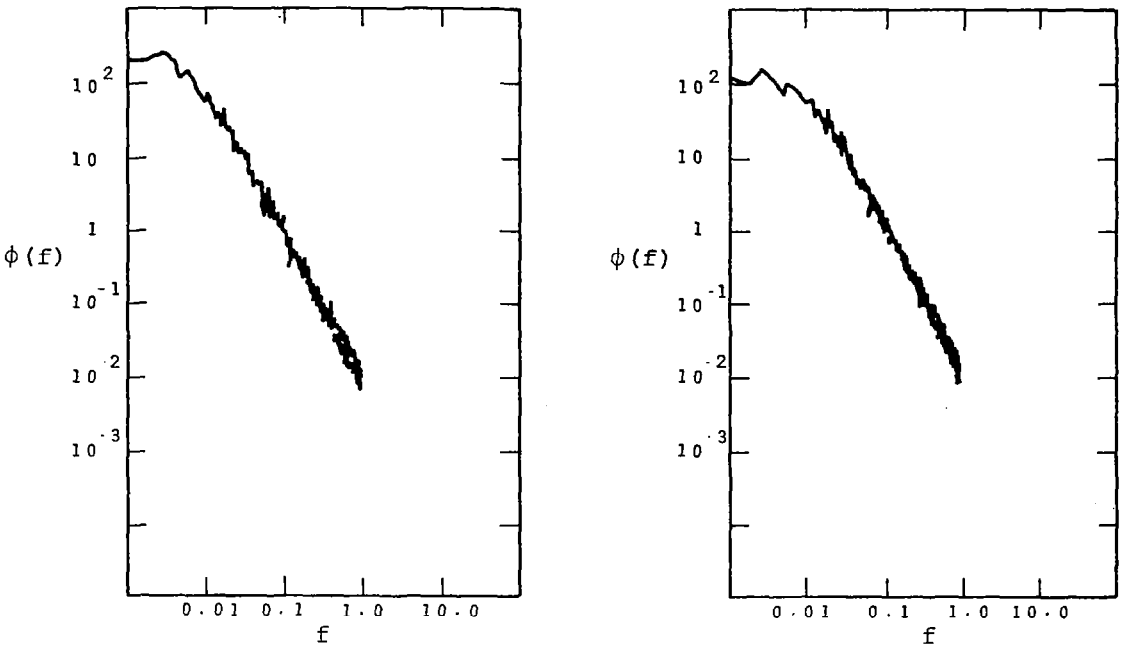

(a) Simulated interlevel coherence turbulence at z equal to 24 m and 12 m, respectively (Δt = 0.1)

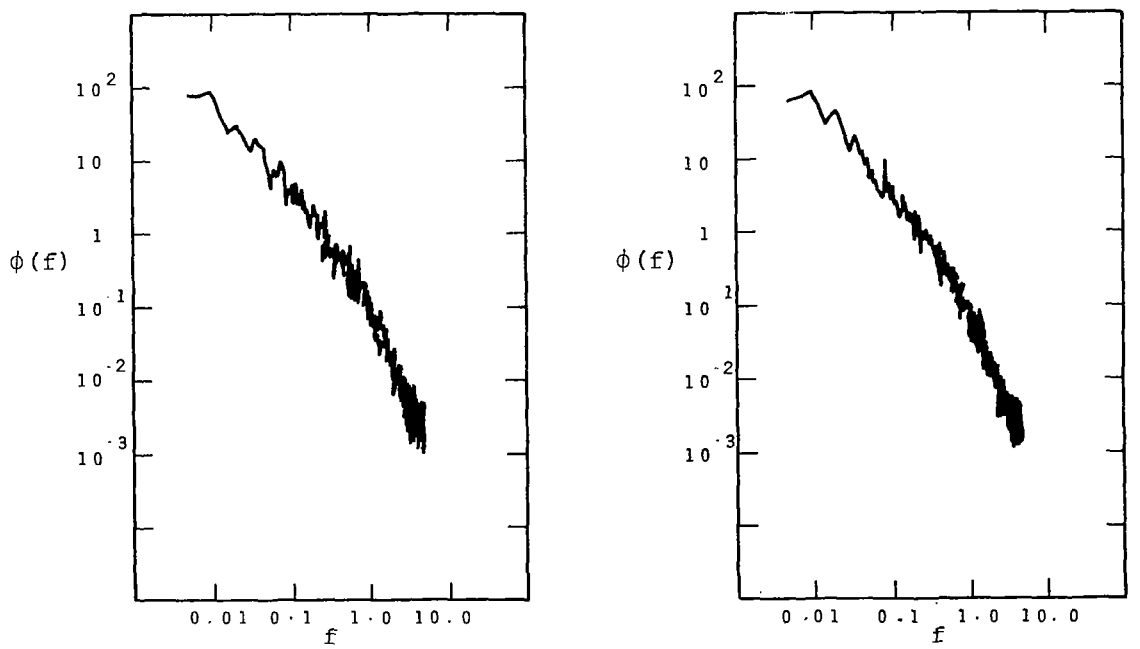

(b) Measured atmospheric turbulence at z equal to 24 m and 12 m, respectively (Δt = 0.5)

Figure 4-20. The spectrum estimated of level coherence turbulence (N = 2048).

$$\gamma_o(\eta) = \exp[-a\eta] \ , \qquad (4\text{-}40)$$

where

$$\eta = \frac{\Delta z \ f}{V} \ .$$

This expression for $\gamma_o(\eta)$ was originally proposed by Davenport [13] as a simple scaling law to describe the coherence of the vertical interlevel winds. He found a to be equal to 15.4 (note some reports use 7.7 for the square root coherence function). Stegen and Thorpe [12] show this is approximately correct. Work by Pielke and Panofsky [21] and Brook [11], however, provides values for the coefficient, a, which are dependent on stable conditions, as shown in Table 4-6.

Table 4-6. The Estimates of the Coefficient, a, of Different Stable Condition [11]

Component	η Range	Stable	Neutral Stable	Unstable
Longitudinal	all - η	16.8	17.0	16.8
	$\eta < 0.12$	13.4	13.2	16.8
Lateral	all - η	12.5	12.8	10.4
	$\eta < 0.12$	14.4	13.4	11.6

The coherence function is usually calculated from spectra as follows (note: here the x and y simply indicate two different time histories):

$$\gamma_{xy}(\eta) = \frac{|\phi_{xy}(\eta)|^2}{\phi_x(\eta)\ \phi_y(\eta)} , \tag{4-41}$$

where the cross-spectrum is defined as:

$$\phi_{xy}(\eta) = \frac{2\Delta t}{N} [\, X(\eta)\ Y^*(\eta)\ ] . \tag{4-42}$$

By using this equation and Equation (4-8) for the auto-spectra, the coherence function for a multi-input system as shown in Equation (4-37) can be calculated as:

$$\gamma(\eta) = \frac{[\, c_0^2 + 2 \sum_{m=0}^{M} c_m^2 \cos(m\eta\pi/\eta_{max})\,]^2}{[\, c_0^2 + 2 \sum_{m=0}^{M} c_m^2\,]^2} , \tag{4-43}$$

where

$$\eta_{max} = \frac{\Delta z_{max}\ f_{max}}{V} .$$

The value of f_{max} is taken as the cut-off frequency (Nyquist frequency) for the discrete transformation. In order to reproduce accurately the coherence function γ_o given in Equation (4-40), the value of Δz_{max} must be selected appropriately. Figure 4-21 shows the exponential curve with a = 17 compared with Equation (4-43) for

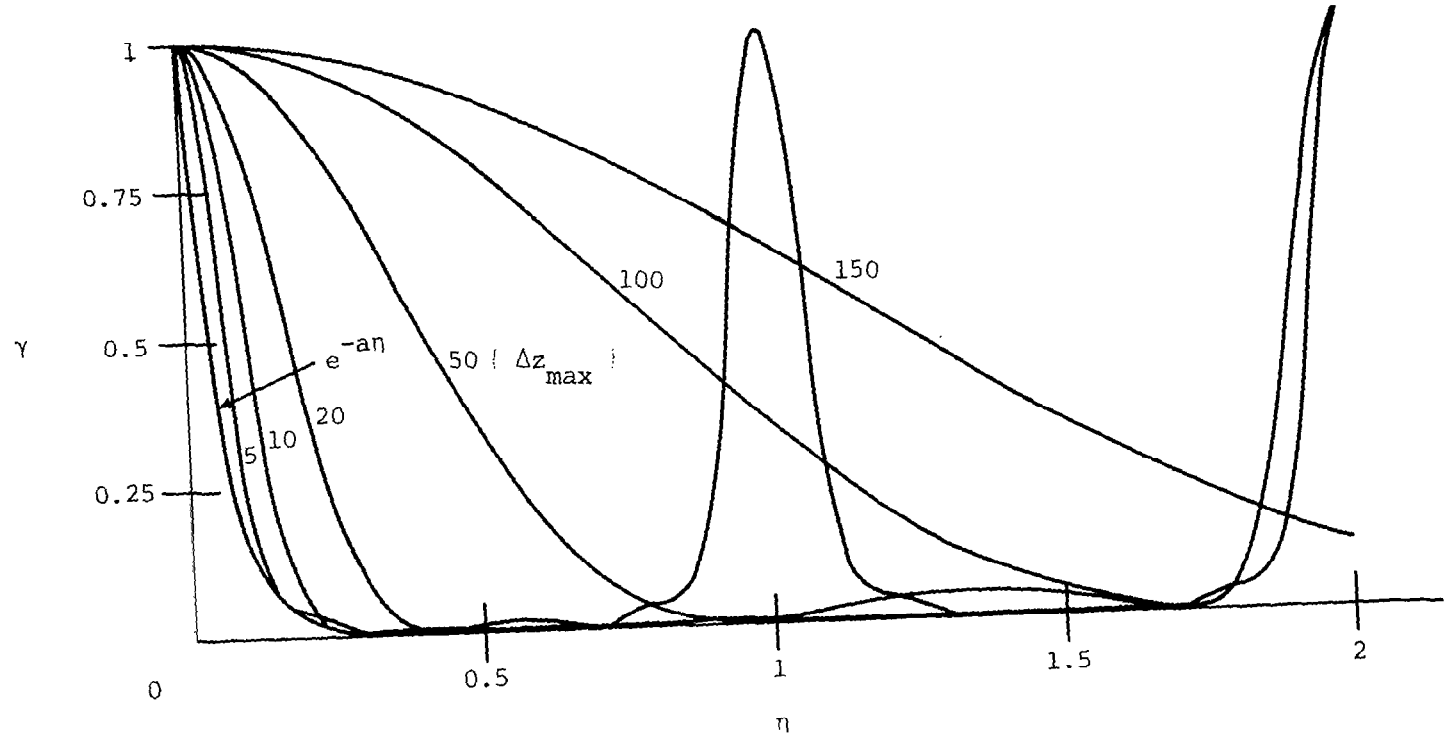

Figure 4-21. The coherence function, Equation (4-43), computed for different values of Δz_{max} as compared with γ_o, given by Equation (4-40) (a = 17).

different values of Δz_{max}. This figure indicates that small values of Δz_{max}, approximately equal to 2 or 3, represent reasonable values to describe the exponential curve. Note that Equation (4-43) produces a second peak after one period at

$$\eta / \eta_{max} \simeq 2.0 \ ; \qquad (4\text{-}44)$$

therefore, in programming the coherence model, the undesired cyclic peaks occurring at high frequencies must be truncated. A critical frequence η_c is defined by

$$\eta_c = \eta_{max} \ . \qquad (4\text{-}45)$$

This critical frequency defines the upper limit of the coherence function in Equation (4-43); hence,

$$\gamma(\eta) = \gamma(\eta_c) \qquad \text{for all } \eta > \eta_c \ . \qquad (4\text{-}46)$$

Figure 4-22 compares the calculated coherence functions of simulated and measured turbulence with the exponential curve given by Equation (4-40). This figure shows that the model behaves very much like the atmospheric turbulence and, at the same time, indicates that the calculated coherence functions are described appropriately by the exponential curve.

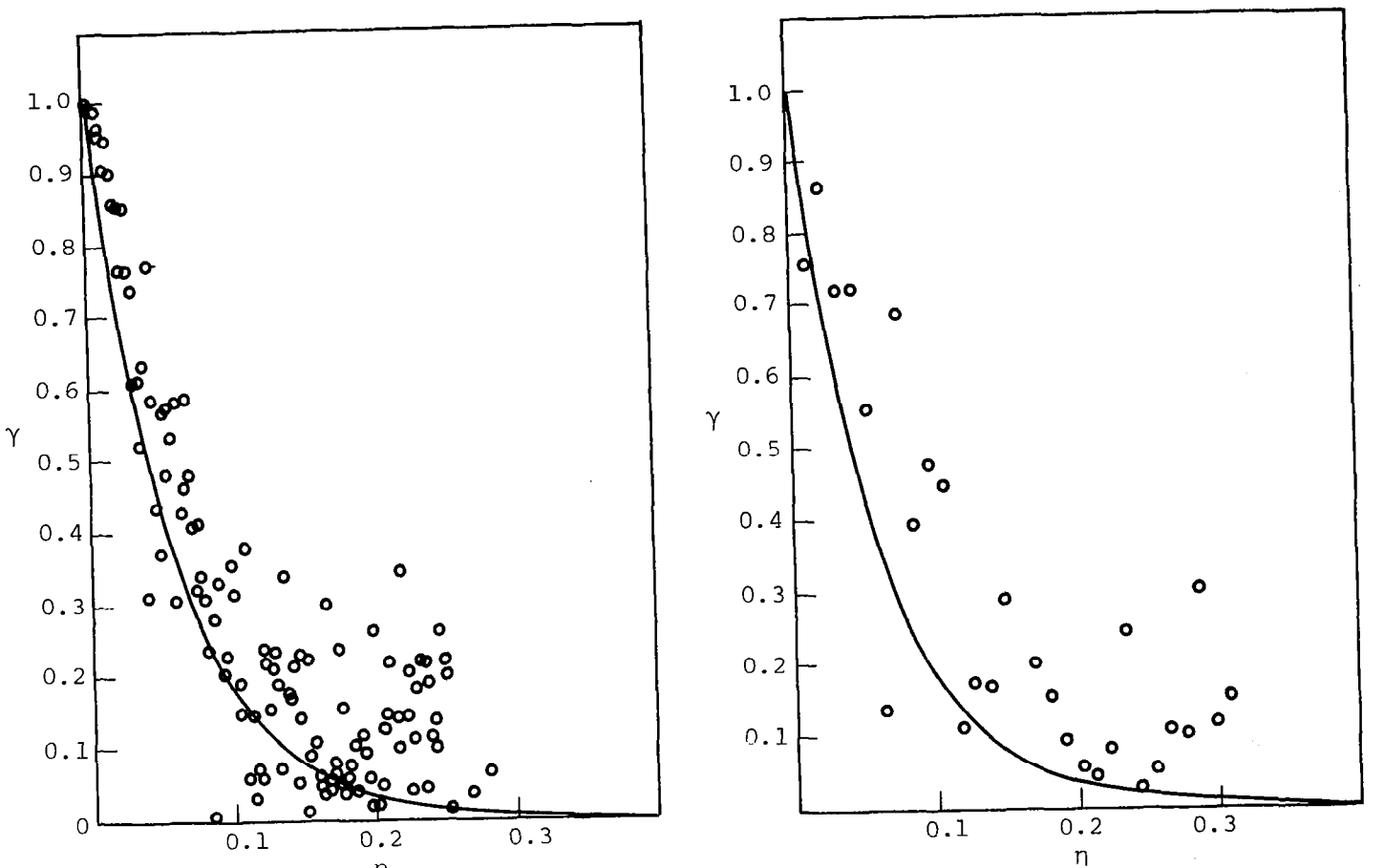

(a) Simulated turbulence

(b) Measured atmospheric turbulence

Figure 4-22. Statistical coherence estimates of simulated and measured atmospheric turbulence compared with Equation (4-40) ($a = 17$, $\Delta z_{max} = 3$).

The coherence of the simulated time histories was computed using statistical techniques. Considerable care must be taken in evaluating the coherence function because the statistical estimate has a rather complex sampling distribution. The coherence estimate must be smoothed by either ensemble or frequency averaging in order to suppress the random error to acceptable levels. Otherwise, even for the case of totally incoherent data, the estimated coherence will be unity for the entire frequency range. It should be noted, in particular, that the smoothing must be carried out separately for the real and imaginary terms of the cross-spectrum shown in Equation (4-42). Therefore, $\phi_{xy}(\eta)$ can be represented by

$$\phi_{xy}(\eta) = \phi'_{xy}(\eta) + j\phi''_{xy}(\eta) \quad , \tag{4-47}$$

where the ϕ'_{xy} and ϕ''_{xy} are the real and imaginary parts of ϕ_{xy}, called the co-spectrum and the quad-spectrum, respectively. To smooth the cross-spectrum, the averaging technique must be applied to each term individually. Therefore,

$$\overline{\phi}_{xy}(\eta) = \overline{\phi}'_{xy}(\eta) + j\overline{\phi}''_{xy}(\eta) \quad , \tag{4-48}$$

where the bar indicates the averaged value. Then the coherence $\gamma_{xy}(\eta)$ can be calculated by

$$\overline{\gamma}_{xy}(\eta) = \frac{|\overline{\phi}_{xy}(\eta)|^2}{\overline{\phi}_x(\eta)\ \overline{\phi}_y(\eta)} \quad . \tag{4-49}$$

It is re-emphasized that the average must be taken before the absolute function of the cross-spectrum is computed. This is because the value of the spectrum function is small relative to the high variation created by the discrete transformation. Therefore, the magnitude of the standard deviation of the variate is much greater than the magnitude of the mean. Thus, smoothing the absolute value of the spectrum is, in effect, just averaging the variance. The variance is always positive; therefore, the average is very large. By averaging ϕ'_{xy} and ϕ''_{xy} separately, the positive and negative values reduce the magnitude of the average. The computer program for calculation of the coherence function and the smoothing techniques is listed in Appendix A, Section A-11.

CHAPTER V

APPLICATION AND CONCLUSION

The purpose of this chapter is to describe how the different turbulence simulation techniques influence computer-simulated landings of aircraft having the characteristics of a DC-8. A three-degree-of-freedom dynamic model of an aircraft during approach is utilized with different models of simulated turbulence imposed as atmospheric gusts. The development of the model of the airplane dynamics and a description of the computer program are discussed in detail by Frost and Reddy [22] and Frost and Crosby [23].

The three-degree-of-freedom airplane computer model uses Runge-Kutta integration to solve the system of time-dependent, second-order ordinary differential equations (see Appendix C). The flight simulation program incorporates an automatic control system in which the basic control inputs are thrust and pitch angle and the control variables are speed and flight path height. The model selector automatically selects the proper control modes in sequence according to the predetermined flight path. The four modes are hold, capture, track, and flare, as shown in Figure 5-1.

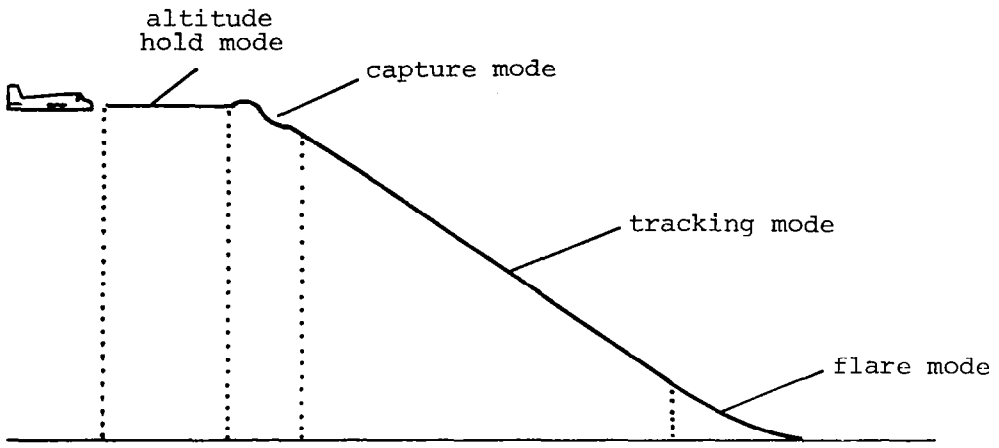

Figure 5-1. Automatic landing control modes.

A. Method of Inputting Wind

For input to the dynamic equations, the actual wind speed U at location (x,z) and time (t) is calculated by

$$U_i(x,z,t) = \bar{U}_i(z) + u_i(x,z,t) \ , \qquad (5\text{-}1)$$

where the mean wind speed, $\bar{U}$, upon which the turbulence is superimposed, is described by a logarithmic function of altitude z. Thus,

$$\bar{U}_1(z) = \frac{u_*}{K_o} \ln \left[\frac{z + z_o}{z_o} \right] \quad , \quad \bar{U}_2 = 0 \ , \qquad (5\text{-}2)$$

where

u_* is the friction velocity

K_o is the von Karman constant

z_o is the surface roughness length .

To utilize the simulated turbulence described in the preceding chapters for analysis of landing aircraft, $u_i(x,z,t)$ is replaced by the discrete signals. Inputting the discrete data into the computer program requires some special attention:

1. Simulation calculates N values for a given height z.
2. The airplane is descending, so z is changing with each time step.
3. A set of signals from a given transformation is generated for a period of 12.8 seconds, which is selected by using N equal to 128 (2^7) and Δt equal to 0.1 second.

It is assumed that the turbulence characteristics encountered by the airplane during that time period are uniform. However, as a second control, the program continuously checks altitude. If during the 12.8-second time period the aircraft has a sudden altitude change (in this case, 20 percent of the height z), the program automatically generates a new set of turbulence signals at the new height.

A second consideration is that the simulated turbulence is the discrete time history of wind fluctuations at a fixed point, and Taylor's hypothesis must be applied to establish a space and time relationship for calculating the effects due to location change, as shown in Figure 5-2. A

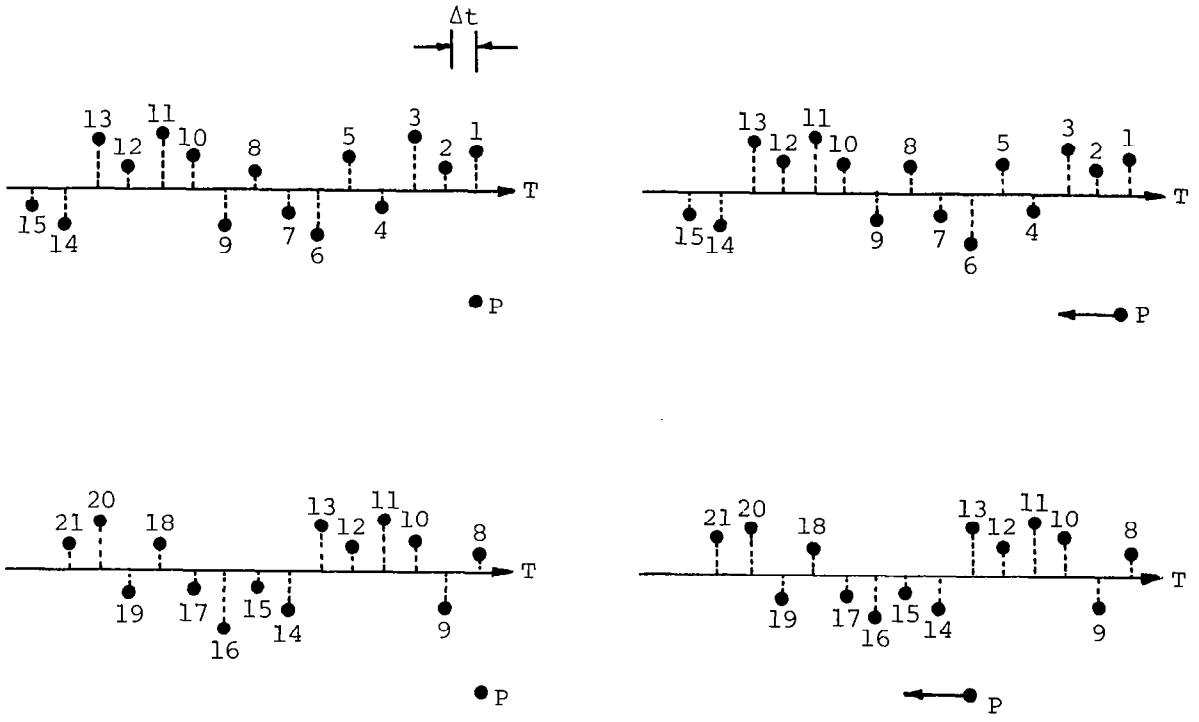

(a) A fixed point P, after $7\Delta t$ time steps, will encounter the eighth turbulence signal

(b) A moving point P, after $7\Delta t$ time steps, will encounter the thirteenth turbulence signal

Figure 5-2. Effects of aircraft motion relative to atmospheric motion.

time scale, t_L defined in Equation (5-3), is therefore used to count the turbulence signals

$$t_L = t + \frac{d}{\bar{V}} = n\ \Delta t\ , \qquad (5\text{-}3)$$

where

t_L is the time scale for counting turbulence signals

t is the real time measured from the airplane entering the wind field

d is the distance moved by the airplane in time t

V is the airplane relative velocity .

Hence, the n^{th} one of N-generated data is chosen as the turbulence fluctuation u_i at the time t. The lift and drag (see Appendix C) on the airplane are therefore computed from the wind U_i, defined as

$$U_i(t) = \bar{U}_i + u_i(n\ \Delta t)\ . \qquad (5\text{-}4)$$

The wind also enters into the equation (as shown in Appendix C) by

$$\frac{dU_i}{dt} = \frac{\partial U_i}{\partial t} + \frac{\partial U_i}{\partial x}\frac{\partial x}{\partial t} + \frac{\partial U_i}{\partial z}\frac{\partial z}{\partial t}\ . \qquad (5\text{-}5)$$

Hence, each term becomes two parts. For example, the $\partial U_i/\partial x$ becomes

$$\frac{\partial U_i}{\partial x} = \frac{\partial \bar{U}_i}{\partial x} + \frac{\partial u_i}{\partial x}\ . \qquad (5\text{-}6)$$

Because the Taylor hypothesis is used, the gradient $\partial u_i/\partial x$ of Equation (5-6) is represented by

$$\frac{\partial u_i}{\partial x} = [\, u_i\,(\,(n+1)\Delta t\,) - u_i(n\,\Delta t)\,] \,/\, (V\,\Delta t)\ . \qquad (5\text{-}7)$$

The computer program which provides the wind field data and the gradients for the aerodynamic equations is listed in Appendix A, Section A-12. Since the vertical motion of the airplane is relatively small compared with the horizontal motion, the gradient terms in the Z - direction can therefore be neglected.

B. Simulated Landings

The simulated landing begins at an altitude of 300 meters and a distance of 7 km from the runway in the altitude hold mode. Although this height is somewhat low for an actual landing case, it has been used to save computer calculation time. The glide slope angle is 2.7 deg and the initial trimmed airspeed is 70 m/s.

The major aircraft landing error is the touch-down position shifting, which is mainly affected by mean wind shear and turbulence. The mean wind shear is dependent upon the parameters u_* and z_o, as described in Equation (5-2). For a no-turbulence case, the simulated results of landing positions are plotted against different values of u_* and z_o in Figures 5-3 and 5-4, respectively. A head

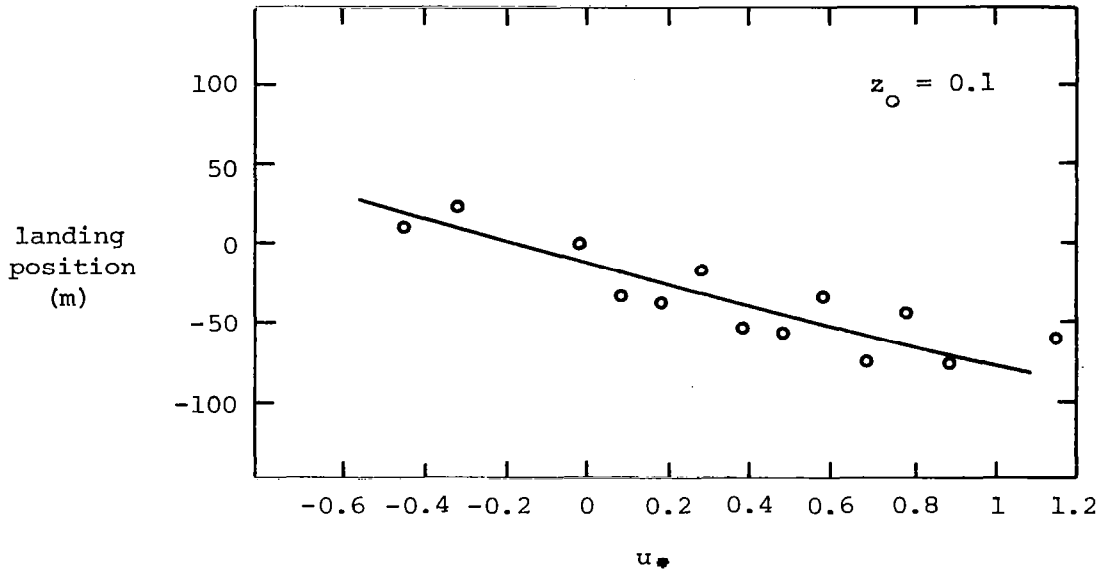

Figure 5-3. The landing position for different values of u_* with no turbulence.

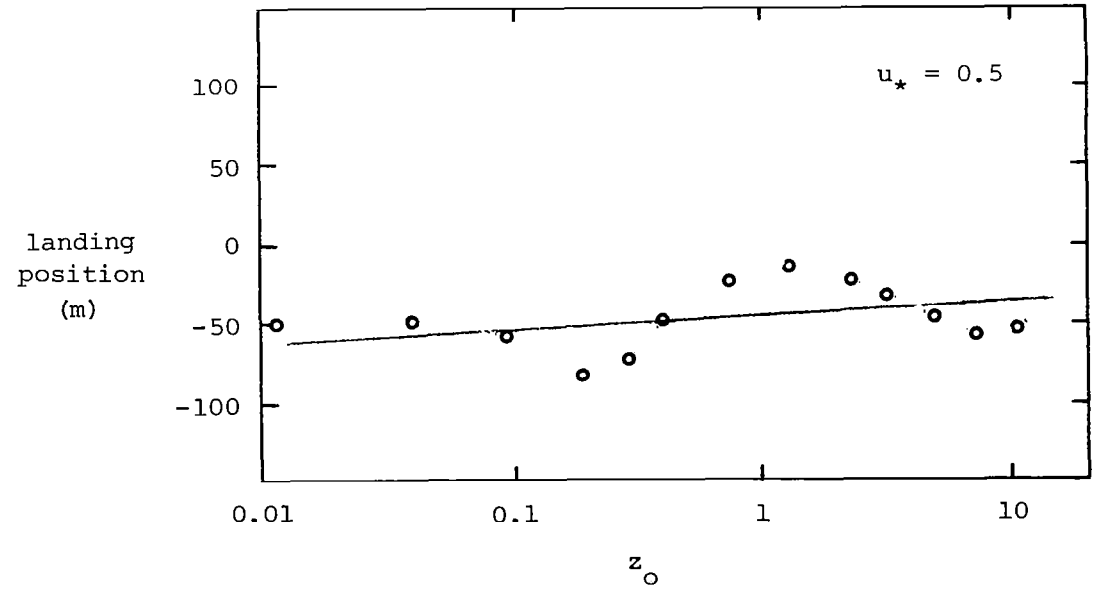

Figure 5-4. The landing position for different values of z_o.

wind decreasing vertically toward the ground causes the plane to land short of the runway, whereas a tail wind decreasing vertically toward the ground causes the plane to overshoot the landing point. The scatter in results as seen in Figures 5-3 and 5-4 is probably due to the over-response of the automatic control system.

In the landing simulation in which turbulence is the main cause of landing position error, different turbulence models have been applied. The statistical result for each model is based on a sample of 20 simulated landings. For the simple turbulence model with a Dryden spectrum, the statistical results of landing position are shown in Table 5-1.

The turbulence intensity, σ, strongly influences scatter in the landing position about the mean; i.e., landing position error. In the discrete transformation the output standard deviation, $\hat{\sigma}$, can easily be adjusted by using Equation (4-23) or Equation (4-30) to give a constant ratio of the original calculated turbulence intensity. It is not realistic of changing turbulence intensity without changing the value of u_*. The assumption has been made for only showing the influence of different values of σ.

The error in the average landing position with respect to the no-turbulence condition, defined as the average error, and the standard deviation for a plane landing in Gaussian and non-Gaussian turbulence with a

Table 5-1. Twenty Landings for Simple Turbulence Model using a Dryden Spectrum with $u_* = 0.5$ and $z_o = 0.1$ (FFT Method)

Run No.	Landing Position		Distance from Average Touchdown Point
1	6919.07		30.71
2	6883.52		-66.26
3	6950.17		0.39
4	7000.64		50.86
5	7001.87		52.09
6	6969.55		19.77
7	6988.47		38.69
8	6992.39		42.61
9	6907.23		-42.55
10	6948.49		-1.29
11	6956.65		6.87
12	7070.36		120.58
13	6970.75		20.97
14	6945.24		-4.54
15	6900.77		-49.01
16	6922.49		-27.29
17	6910.08		-39.70
18	6891.43		-58.35
19	6893.70		-56.08
20	6972.73		22.95
Average	6949.78	S.D.	46.37

Note: The results for non-Gaussian, Dryden spectrum, and for the Gaussian, von Karman spectrum turbulence landing simulation are listed in Appendix D.

Dryden spectrum, and in Gaussian turbulence with a von Karman spectrum, are shown in Figures 5-5 and 5-6. Both figures show the direct relation of turbulence intensity to deviation in landing position.

Another important factor relative to landing performance is the touchdown sink rate. From Figures 5-7 and 5-8 one can conclude that the turbulence intensity has little influence on the average touchdown sink rate for the automatic control system used in this analysis. However, the variability of sink rate, i.e., standard deviation, does increase with increasing turbulence intensity. This occurs because the touchdown sink rate is very sensitive to the turbulence fluctuation after the flare mode is started. Near the ground $\bar{U}$ becomes small, and if an increased head wind due to turbulence is experienced followed by a large reduction, or even a tail wind near the runway, a sudden loss of lift occurs and causes a very hard landing. Also, as noted in Figure 5-8, when σ is over 3 to 4 m/sec, the standard deviation of sink rate approaches 30 percent of the mean sink rate. Thus, the chance of a hard landing becomes high.

The influence of different turbulence models for this landing simulation can also be seen in Figures 5-5 through 5-8. The average values of position error and sink rate are affected little by using different turbulence models, whereas the standard deviation in touchdown

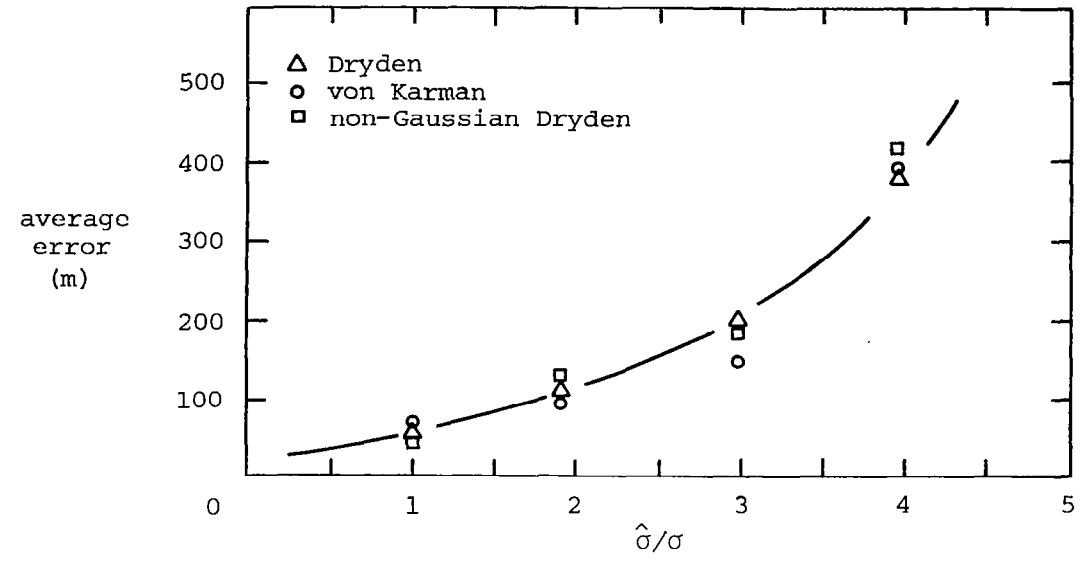

Figure 5-5. The average landing error for different turbulence models ($u_* = 0.5$, $z_o = 0.1$).

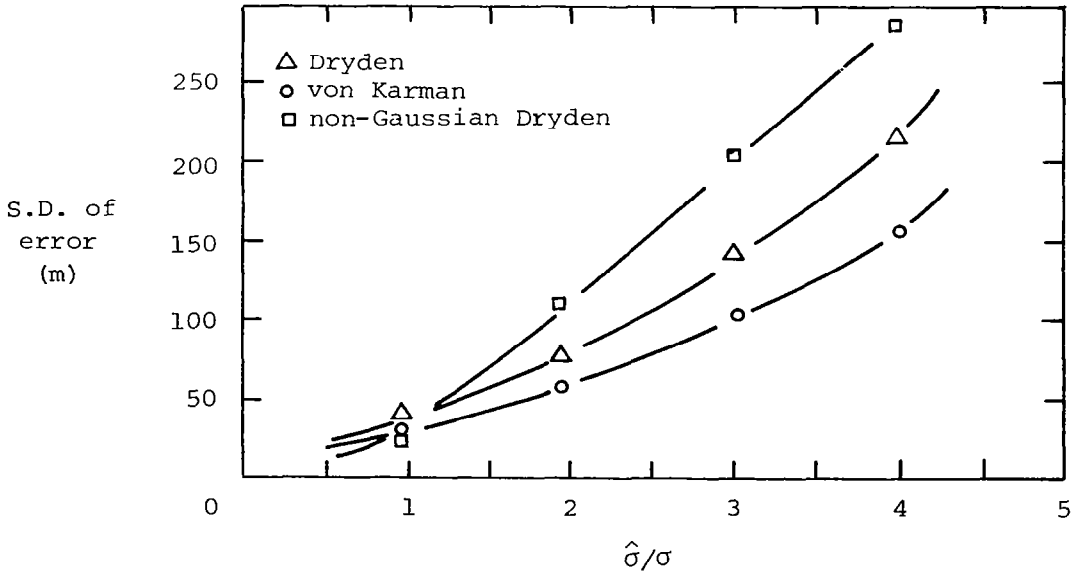

Figure 5-6. The standard deviation of error for different turbulence models ($u_* = 0.5$, $z_o = 0.1$).

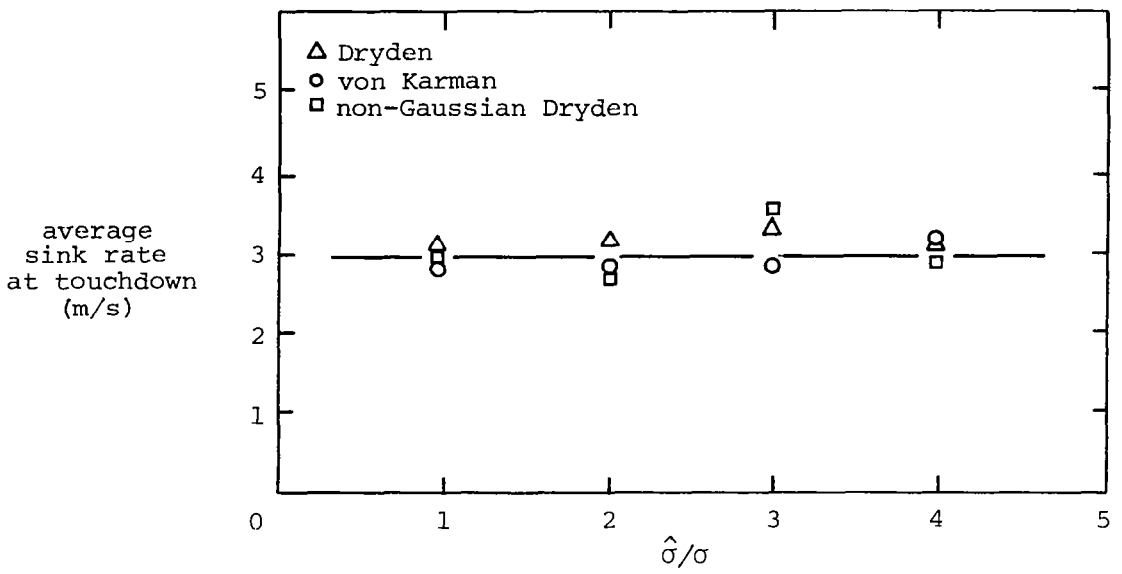

Figure 5-7. The average sink rate for different turbulence models ($u_* = 0.5$, $z_o = 0.1$).

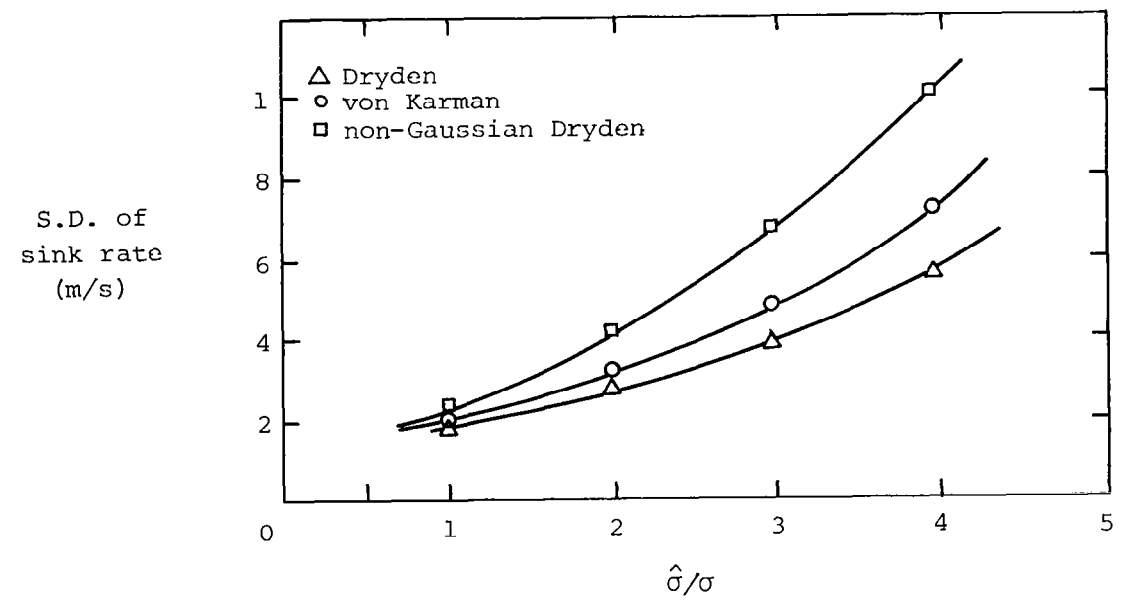

Figure 5-8. The standard deviation of sink rate for different turbulence models ($u_* = 0.5$, $z_o = 0.1$).

position is influenced significantly by the different turbulence models.

For the same spectrum function, a non-Gaussian turbulence model produces the higher degree of touchdown variability. It should also be noted that when different spectrum functions are used, the von Karman model induces a smaller standard deviation in position error than the Dryden model. These flight simulation results indicate that for a DC-8-type airplane, the turbulence energy contained by the higher frequency fluctuation affects the landing position little. The sharp peaks of the non-Gaussian model represent the most dangerous events which can cause the airplane to lose control during the approach. Hence, it is important to simulate properly the non-Gaussian nature of the atmosphere.

The DZT method for turbulence generation and the interlevel coherence turbulence model were also used to carry out flight simulation. As expected, the statistical results are essentially the same for the DZT method as they are for the FFT method. Also, the interlevel coherence model was found to give approximately the same results as the one-point spectrum model. The reason for this is that the airplane, when flying along the 2.7-deg glide slope, travels relatively longer distances in the horizontal direction than in the vertical direction. The coherence between vertical levels has little effect on the two-point

separation over relatively large horizontal distances. Therefore, the coherence turbulence model shows no significant difference from the one-point spectrum model for this landing simulation.

C. Conclusion

This study has been concerned with the problems of modeling continuous atmospheric turbulence by discrete transformation and with application to flight analysis. Different spectrum models have been used to generate turbulence. The results show that the von Karman spectrum more accurately describes atmospheric turbulence than does the Dryden spectrum. Both the interlevel coherence of vertical layers and the non-Gaussian nature of atmospheric turbulence, which are important in airplane analysis, can be simulated properly by different models. Two discrete transformation techniques, FFT and DZT, work fairly well. Although the FFT method provides better spectrum simulation, the DZT method is faster for computation.

On the other hand, the disadvantage of the von Karman spectrum model is that the non-Gaussian nature of atmospheric turbulence cannot be simulated simultaneously. For both the von Karman and the Kaimal spectra, only the FFT method can be used for the complex irrational filter function.

Overall, this study has provided a general discussion of statistical theories of atmospheric turbulence, the detailed description of both random signal analysis and digital simulation technique, and the application to the simulated turbulence to atmospheric flight analysis.

BIBLIOGRAPHY

BIBLIOGRAPHY

1. Neuman, F., and J. Foster. "Investigation of a Digital Automatic Aircraft Landing System in Turbulence," National Aeronautics and Space Administration TN-D-6066, Ames Research Center, Moffett Field, California, October, 1970.

2. Reeves, P. M., R. G. Joppa, and V. M. Ganger. "A Non-Gaussian Model of Continuous Atmospheric Turbulence for Use in Aircraft Design," National Aeronautics and Space Administration CR-2639, Ames Research Center, Moffett Field, California, January, 1976.

3. Perlmutter, M., W. Frost, and G. H. Fichtl. "Three Velocity Component, Nonhomogeneous Atmospheric Boundary-Layer Turbulence Modeling," AIAA Journal, 15(No. 10):1444-1454, October, 1977.

4. Frost, W., and T. H. Moulden. Handbook of Turbulence. Vol. 1. New York: Plenum Publishing Corp., 1977.

5. Hinze, J. O. Turbulence. New York: McGraw-Hill, 1975.

6. Kaimal, J. C. "Turbulence Spectra, Length Scales and Structure in the Stable Surface Layer," Boundary Layer Meterology. Vol. 4. Dordrecht, Holland: D. Reidel Publishing Co., 1973. Pp. 289-309.

7. Frost, W., B. H. Long, and R. E. Turner. "Engineering Handbook on the Atmospheric Environmental Guidelines for Use in Wind Turbine Generator Development," National Aeronautics and Space Administration Technical Paper 1359, Marshall Space Flight Center, Huntsville, Alabama, December, 1978.

8. Busch, N. E., and S. E. Larsen. "Spectra of Turbulence in the Atmospheric Surface Layer," Danish Atomic Energy Commission, Riso Research Establishment Report NO.256, [n.p.], 1972.

9. Otnes, R. K., H. A. Nathans, and L. V. Enochson. "A Procedure for Computing Power Spectral Density of Gust Data," Report for FDTR Contractor MAC 705-03, Wright-Patterson Air Force Base, Ohio, September, 1968.

10. Mather, G. K. "Some Measurements of Mountain Waves and Mountain Wave Turbulence Made Using the NAE T-33 Turbulence Research Aircraft," DME/NAE Quarterly Bulletin No. 2, National Research Council of Canada, Ottawa, 1967.

11. Brook, R. R. "A Note on Vertical Coherence of Wind Measured in Urban Boundary Layer," Boundary Layer Meteorology. Vol. 9. Dordrecht, Holland: D. Reidel Publishing Co., 1975. Pp. 11-20.

12. Stegen, G. R., and R. L. Thorpe. "Vertical Coherence in the Atmospheric Boundary Layer," National Science Foundation GK 35885, [n.p.], 1978.

13. Davenport, A. G. "The Spectrum of Horizontal Gustiness Near the Ground in the High Winds," Quarterly Journal of Royal Meteorological Society, 87:194-211, 1961.

14. Chambers, J. M. Computational Method for Data Analysis. New York: John Wiley and Sons, Inc., 1977.

15. Hamming, R. W. Digital Filters. Englewood Cliffs, New Jersey: Prentice-Hall, Inc., 1977.

16. Barr, N. M., Dagfinn Gangaas, and D. R. Schaeffer. "Wind Models for Flight Simulation Certification of Landing and Approach Guidance and Control Systems," Federal Aviation Agency FAA-RD-74-206, System Research and Development Service, Washington, D.C., December, 1974.

17. Bendat, J. S., and A. G. Piersol. Random Data Analysis and Measurement Procedures. New York: John Wiley and Sons, Inc., 1971.

18. Churchill, R. V. Operational Mathematics. New York: McGraw-Hill Book Co., Inc., 1973.

19. Frost, W., and A. M. Shahabi. "A Field Study of Wind Over a Simulated Block Building," National Aeronautics and Space Administration CR-2804, Marshall Space Flight Center, Huntsville, Alabama, March, 1977.

20. Brigham, E. O. The Fast Fourier Transform. Englewood Cliffs, New Jersey: Prentice-Hall, Inc., 1974.

21. Pielke, R. A., and H. A. Panofsky. "Turbulence Characteristics Along Several Towers," Boundary Layer Meteorology. Vol. 1. Dordrecht, Holland: D. Reidel Publishing Co., 1970. Pp. 115-130.

22. Frost, W., and K. R. Reddy. "Investigation of Aircraft Landing in Variable Wind Fields," National Aeronautics and Space Aministration CR-3073, Marshall Space Flight Center, Huntsville, Alabama, December, 1978.

23. Frost, W., and W. Crosby. "Investigation of Simulated Aircraft Flight through Thunderstorm Outflows," National Aeronautics and Space Administration CR-3052, Marshall Space Flight Center, Huntsville, Alabama, September, 1978.

24. Frost, W., D. W. Camp, and S. T. Wang. "Wind Shear Modeling for Aircraft Hazard Definition," Federal Aviation Agency FAA-RD-78-3, System Research and Development Service, Washington, D.C., February, 1978.

25. Crutcher, H. L., and L. W. Falls. "Multivariate Normality," National Aeronautics and Space Administration TN-D-8226, Marshall Space Flight Center, Huntsville, Alabama, May, 1976.

26. Harnett, R. M. "Validation of Automated Uniform Random Number Generators for the IBM 7044 and the UNIVAC 1108." Report prepared under National Aeronautics and Space Administration Contract No. NAS8-20082, Marshall Space Flight Center, Huntsville, Alabama, July, 1970.

27. Houbolt, J. C. "Atmospheric Turbulence," AIAA Journal, 11(No. 4):421-437, April, 1973.

28. Keisler, S. R., and R. H. Rhyne. "An Assessment of Prewhitening in Estimating Power Spectra of Atmospheric Turbulence at Long Wavelengths," National Aeronautics and Space Administration TN-D-8288, Langley Research Center, Hampton, Virginia, November, 1976.

29. Etkin, B. Dynamics of Atmospheric Flight. New York: John Wiley and Sons, Inc., 1972.

30. Dryden, H. L., and A. M. Kuethe. "Turbulence," National Advisory Committee for Aeronautics Technical Reports. No. 342. [n.p., n.n.], 1930.

31. von Karman, T. "Karman Theory." Proceedings of National Academy of Sciences, U.S. Vol. 34. [n.p., n.n.], 1948.

32. Dryden, H. L., G. B. Schubauer, W. C. Mick, and Skramstad, H. "Turbulence Spectra," National Advisory Committee for Aeronautics Technical Reports. No. 581. [n.p., n.n.], 1931.

APPENDIXES

APPENDIX A

COMPUTER PROGRAM

A-1. Subroutine GAUSS (IX, SIG, XB, XDP)

Subroutine GAUSS uses Equation (3-1), congruential method, to generate random numbers. The value of a in Equation (3-3) is selected equal to 65539. Also, the Central Limit theorem with 12 terms is applied to generate Gaussian distributed random numbers, Equation (3-6).

Nomenclature

IX	Seed number (input and output)
SIG	Desired standard deviation (input)
XB	Desired mean value (input)
XDP	Normalized Gaussian random number (output)

Listing

```
    SUBROUTINE GAUSS(IX,SIG,XB,XDP)
    REAL*8 XP
    A=0.0
    DO 30 I=1,12
    IY=IX*65539                    ┐
    IF(IY) 10,20,20                │
10  IY=IY+2147483647+1             ├ RANDU
20  XP=IY                          │
    XP=XP*0.4656613D-9             │
    IX=IY                          ┘
30  A=A+XP
    XDP=(A-6.0)*SIG+XB
    RETURN
    END
```

A-2. Subroutine PDF (N, DX, ND, X, P)

Subroutine PDF computes the probability density function of a discrete data set $\{x_i\}$, i = 1,2,...,N by using Equation (4-5).

Nomenclature

N	Dimension number for array X (input)
DX	Increment Δx (input)
ND	Dimension number for array P (input)
X	Discrete data set $\{x_i\}$ (input)
P	Calculated PDF of data set $\{x_i\}$ (output)

Listing

```
      SUBROUTINE PDF(N,DX,ND,X,P)
      DIMENSION X(N),P(ND),NP(2048)
      XS=-DX*((ND-1)/2+1.5)
      DO 30 I=1,ND
      NP(I)=0.
      XS=XS+DX
      XE=XS+DX
      DO 20 J=1,N
      IF(X(J).GE.XS.AND.X(J).LT.XE) NP(I)=NP(I)+1
   20 CONTINUE
   30 CONTINUE
      DO 40 I=1,ND
      P(I)=1.*NP(I)/(DX*N)
   40 CONTINUE
      RETURN
      END
```

A-3. Subroutine FFT (N, NP, NC, XR, XI)

Subroutine FFT is based on the Fast Fourier Transform algorithm and computes the Fourier transformation (or Inverse) of discrete data.

Nomenclature

N	Dimension number (must be a power of 2) (input)
NP	Power to which 2 is raised, i.e., $N = 2^{NP}$ (input)
NC	Control number (input)
	1 for Fourier transform
	2 for Inverse Fourier transform
XR	Real part of the data set (input and output)
XI	Imaginary part of the data set (input and output)

Listing

```
      SUBROUTINE FFT(N,NP,NC,XR,XI)
      DIMENSION XR(N),XI(N)
      IF(NC.EQ.1) GO TO 120
      DO 110 I=1,N
  110 XI(I)=-XI(I)
  120 N2=N/2
      NU1=NP-1
      K=0
      DO 150 L=1,NP
  130 DO 140 I=1,N2
      P=IBITR(K/2**NU1,NP)
      ARG=6.283185*P/FLOAT(N)
      C=COS(ARG)
      S=SIN(ARG)
      K1=K+1
      K1N2=K1+N2
      TR=XR(K1N2)*C+XI(K1N2)*S
      TI=XI(K1N2)*C-XR(K1N2)*S
      XR(K1N2)=XR(K1)-TR
      XI(K1N2)=XI(K1)-TI
      XR(K1)=XR(K1)+TR
      XI(K1)=XI(K1)+TI
  140 K=K+1
      K=K+N2
      IF(K.LT.N) GO TO 130
      K=0
      NU1=NU1-1
  150 N2=N2/2
      DO 160 K=1,N
      I=IBITR(K-1,NP)+1
      IF(I.LE.K) GO TO 160
      TR=XR(K)
      TI=XI(K)
      XR(K)=XR(I)
      XI(K)=XI(I)
```

```
      XR(I)=TR
      XI(I)=TI
  160 CONTINUE
      IF(NC.EQ.1) GO TO 180
      DO 170 I=1,N
      XR(I)=XR(I)/N
      XI(I)=XI(I)/N
  170 CONTINUE
  180 RETURN
      END
      FUNCTION IBITR(J,NU)
      J1=J
      IBITR=0
      DO 200 I=1,NU
      J2=J1/2
      IBITR=IBITR*2+(J1-2*J2)
  200 J1=J2
      RETURN
      END
```

A-4. Subroutine SPEC (N, NP, DT, XR, XI, SP)

Subroutine SPEC uses the FFT method to calculate estimated spectrum of the input x_n time history, see Equation (4-6).

Nomenclature

N	Dimension number (input)
NP	Power of 2 (input)
DT	Time increment Δt (input)
XR	Real part of data array (input)
XI	Imaginary part of data array (input)
SP	Spectrum estimated array (output)

Listing

```
      SUBROUTINE SPEC(N,NP,DT,XR,XI,SP)
      DIMENSION XR(N),XI(N),SP(N)
      RT=(2.*DT)/N
```

```
      CALL FFT(N,NP,1,XR,XI)
      DO 10 I=1,N
      SP(I)=RT*(XR(I)*XR(I)+XI(I)*XI(I))
   10 CONTINUE
      RETURN
      END
```

A-5. Subroutine SMOOTH (N, NS, NM, SP)

Subroutine SMOOTH is the computer program to smooth the raw estimate data after discrete transformation. Two basic methods, the Frequency Averaging and Segment Averaging methods are included. (See Equations (4-9) and (4-10).)

Nomenclature

N	Dimension number (input)
NS	Number of samples for average (input)
NM	Control number (input)
	1 for the Frequency averaging method
	2 for the Segment averaging method
SP	Raw estimate data (input)
	Smoothed data (output)

Listing

```
      SUBROUTINE SMOOTH(N,NS,NM,SP)
      DIMENSION SP(N,NS)
      IF(NM-2) 100,200,300
  100 ND=N-NS
      DO 150 I=1,ND
      SUM=0.
```

```
      DO 140 J=1,NS
      K=I+J-1
      SUM=SUM+SP(K,1)
  140 CONTINUE
      SP(I,1)=SUM/NS
  150 CONTINUE
      GO TO 300
  200 DO 250 I=1,N
      SUM=0.
      DO 240 J=1,NS
      SUM=SUM+SP(I,J)
  240 CONTINUE
      SP(I,1)=SUM/NS
  250 CONTINUE
  300 RETURN
      END
```

A-6. Subroutine FILTER (N, NM, DT, Z, V, XR, XI)

Subroutine FILTER calculates the filter function for the different models described in Chapter IV and computes Equations (4-13) and (4-14) for the frequency components of the output signal. There are three subroutines called by FILTER which are SAL (see A-6(a)), COEF1 (see A-6(b)), and COEF2 (see A-6(c)).

Nomenclature

N Dimension number (input)

NM Control number for selecting different spectrum model (input)

1 for Dryden spectrum longitudinal component

2 for Dryden spectrum vertical component

3 for approximate Kaimal spectrum

4 for approximate von Karman spectrum

5 for Kaimal spectrum

6 for von Karman spectrum longitudinal component

7 for von Karman spectrum vertical component

DT Time increment Δt (input)

Z Height (input)

V Reference velocity (input)

XR Real part of the data set (input and output)

XI Imaginary part of the data set (input and output)

Listing

```
      SUBROUTINE FILTER(N,NM,DT,Z,V,XR,XI)
      DIMENSION XR(N),XI(N),SIG(3),AL(3)
      COMMON/SI1/A2,A24,AC2,AD2
      COMMON/SI2/PW,PT,B2,C2,A3
      CALL SAL(Z,AL,SIG,V)
      TN=1./(N*DT)
      NHF=N/2+1
      IF(NM.GE.5) GO TO 200
      CALL COEF1(NM,A,C,D,AL,SIG,V)
      DO 100 I=1,NHF
      F=(I-1)*TN
      F2=F*F
      AMF=A2-F2
      DD=1./(AMF*AMF+A24*F2)
      HR=DD*(C*AMF+AD2*F2)
      HI=DD*(D*AMF-AC2)*F
      CALL MULTI(HR,HI,XR(I),XI(I))
  100 CONTINUE
      GO TO 300
  200 CONTINUE
      CALL COEF2(NM,A,B,C,AL,SIG,V)
      IF(NM-6) 270,210,210
  210 DO 250 I=1,NHF
      F=TN*(I-1)
      F2=F*F
      RR=A3+F2
      DD=((B2*F2+C2)**0.5)/(RR**(0.5*PW))
      TH=ATAN(F/B)+PT*(ATAN(F/A))
      HR=DD*(COS(TH))
      HI=DD*(SIN(TH))
      CALL MULTI(HR,HI,XR(I),XI(I))
  250 CONTINUE
      GO TO 300
  270 DO 280 I=1,NHF
      F=(TN*(I-1))**PW
      DD=C/(A3+F*F)
      HR=DD*A
      HI=-DD*F
      CALL MULTI(HR,HI,XR(I),XI(I))
  280 CONTINUE
```

```
300 NTT=N+2
    DO 400 I=2,NHF
    J=NTT-I
    XR(J)=XR(I)
    XI(J)=-XI(I)
400 CONTINUE
    RETURN
    END
    SUBROUTINE MUTI(HR,HI,YR,YI)
    YYR=HR*YR-HI*YI
    YI=HR*YI+HI*YR
    YR=YYR
    RETURN
    END
```

A-6(a). Subroutine SAL (Z, AL, SIG, V)

Subroutine SAL computes the turbulence intensity σ and the length scale Λ by using Equations (4-33) and (4-34).

Nomenclature

Z	Height (input)
AL	Length scale Λ_i, i = 1,2,3 (output)
SIG	Turbulence intensity σ_i, i = 1,2,3 (output)
V	Reference velocity (input)

Listing

```
    SUBROUTINE SAL(Z,AL,SIG,V)
    DIMENSION AL(3),SIG(3)
    Z0=0.1
    SIG(3)=0.52*V/(ALOG(Z/Z0+1))
    SIG(2)=SIG(3)/((0.583+0.00139*Z)**(0.8))
    SIG(1)=SIG(3)/((0.177+0.00274*Z)**(0.4))
    IF(Z.GT.533) GO TO 100
    AL(1)=44.21*(SQRT(3.28*Z))
    AL(2)=AL(1)
    AL(3)=Z
    GO TO 200
100 AL(1)=533.
    AL(2)=533.
    AL(3)=533.
200 RETURN
    END
```

A-6(b). Subroutine COEF1 (NM, A, C, D, AL, SIG, V)

Subroutine COEF1 computes the coefficients a, c, and d listed in Table 4-2, page 64, for Dryden's form spectrum filter function.

Nomenclature

NM	Control number (input) 1 for Dryden spectrum longitudinal component 2 for Dryden spectrum vertical component 3 for approximate Kaimal spectrum 4 for approximate von Karman spectrum
A	Coefficient a (output)
C	Coefficient c (output)
D	Coefficient d (output)
AL	Length scale Λ_i (input)
SIG	Turbulence intensity σ_i (input)
V	Reference velocity (input)

Listing

```
      SUBROUTINE COEF1(NM,A,C,D,AL,SIG,V)
      DIMENSION SIG(3),AL(3)
      COMMON/ST1/A2,A24,AC2,AD2
      VOA=V/AL(1)
      PI=3.141596
      PI2=PI*2.
      IF(NM.EQ.4) GO TO 400
      IF(NM-2) 100,200,300
  100 A=VOA/PI2
      C=SIG(1)/(PI2*PI)*(VOA**1.5)
      D=SIG(1)/PI*(VOA**0.5)
      GO TO 500
  200 VOA=V/AL(2)
      A=VOA/PI2
      C=SIG(2)/(PI*PI)*((VOA/2.)**1.5)
      D=SIG(2)/PI*((VOA*3./2.)**0.5)
      GO TO 500
```

```
300 A=0.155*VOA
    C=0.0432*SIG(1)*(VOA**1.5)
    D=SIG(1)*0.279*(VOA**0.5)
    GO TO 500
400 A=0.286*VOA
    C=0.114*SIG(1)*(VOA**1.5)
    D=0.398*SIG(1)*(VOA**0.5)
500 CONTINUE
    A2=A*A
    A24=4.*A2
    AC2=2.*A*C
    AD2=2.*A*D
    RETURN
    END
```

A-6(c). Subroutine COEF2 (NM, A, B, C, AL, SIG, V)

Subroutine COEF2 computes the coefficients a, b, and c shown in Equations (4-35) and (4-36) for the von Karman and Kaimal spectra.

Nomenclature

NM	Control number (input)
	5 for Kaimal spectrum
	6 for von Karman spectrum longitudinal component
	7 for von Karman spectrum vertical component
A	Coefficient a (output)
B	Coefficient b (output)
C	Coefficient c (output)
AL	Length scale Λ_i (input)
SIG	Turbulence intensity σ_i (input)
V	Reference velocity (input)

Listing

```
      SUBROUTINE COEF2(NM,A,B,C,AL,SIG,V)
      DIMENSION SIG(3),AL(3)
      COMMON/ST2/PW,PT,B2,C2,A3
      VOA=V/AL(1)
      PI=3.141596
      PI2=PI*2.
      IF(NM-6) 100,200,300
  100 A=VOA/(PI2*1.339)
      B=0.
      C=SIG(1)*0.6255*((VOA/PI2)**0.333333)
      PW=5./6.
      GO TO 400
  200 AA=0.164*((1./0.041)**(5./3.))
      AS=SQRT(AA)
      BB=SQRT(0.164/0.041)
      A=(VOA**(5./6.))/AS
      B=0.
      C=SIG(1)/AS*(VOA**0.33333)*BB
      PW=5./6.
      GO TO 400
  300 VOA=V/AL(2)
      PW=11./6.
      A=VOA/(PI2*1.339)
      B=SQRT(2.*SIG(2)**2/VOA*(A**(PW*2)))
      C=B/(0.6123*A)
  400 PT=-PW
      A3=A*A
      B2=B*B
      C2=C*C
      RETURN
      END
```

A-7. Subroutine DZT (N, NM, DT, Z, V, X, Y)

Subroutine DZT computes Equation (4-15) for different models, and this is the Z-transformation technique for the filter system.

Nomenclature

N	Dimension number (input)
NM	Control number for setting different spectrum model
	1 for Dryden spectrum longitudinal component
	2 for Dryden spectrum vertical component
	3 for approximate Kaimal spectrum
	4 for approximate von Karman spectrum
DT	Time increment (input)
Z	Height (input)
V	Reference velocity (input)
X	Input array
Y	Output array

Listing

```
      SUBROUTINE DZT(N,NM,DT,Z,V,X,Y)
      DIMENSION X(N),Y(N),SIG(3),AL(3)
      PI=3.141593
      CALL SAL(Z,AL,SIG,V)
      CALL COEF1(NM,A,C,D,AL,SIG,V)
      C1=2.*EXP(-2.*PI*A*DT)
      C2=-(EXP(-4.*PI*A*DT))
      B=SQRT(2.*PI)
      C12=C1/2.
      CBA=C/(B*A*A)
      ACA=(A-C/B)/A
      D1=D*(CBA+C12*(ACA*DT-CBA))
      D2=D*C12*(CBA*(C12-1.)-ACA*DT)
      Y(1)=0.
      Y(2)=0.
      DO 30 I=3,N
      Y(I)=C1*Y(I-1)+C2*Y(I-2)+D1*X(I-1)+D2*X(I-2)
   30 CONTINUE
      RETURN
      END
```

A-8. Subroutine INPUT (N, NM, DT, IX, XR, XI)

Subroutine INPUT generates the random number array $\{x_i\}$, i = 1,2,...,N, which standard deviation σ is adjusted for FFT and DZT, as shown in Equations (4-25) and (4-32).

Nomenclature

N	Dimension number (input)
NM	Control number for selecting different method (input)
	1 for FFT method
	2 for DZT method
DT	Time increment Δt (input)
IX	Seed number for calling GAUSS (input and output)
XR	Real part of the array $\{x_i\}$ (output)
XI	Imaginary part of the array $\{x_i\}$ (output)

Listing

```
      SUBROUTINE INPUT(N,NM,DT,IX,XR,XI)
      DIMENSION XR(N),XI(N)
      IF(NM-2) 100,200,300
  100 SIG=SQRT(0.5/DT)
      GO TO 300
  200 SIG=SQRT(3.141596/DT)
  300 DO 400 I=1,N
      CALL GAUSS(IX,SIG,0.,XDP)
      XR(I)=XDP
      XI(I)=0.
  400 CONTINUE
      RETURN
      END
```

A-9. Subroutine NONGAU (N, NC, DT, Z, V, R, XR, XI)

Subroutine NONGAU generates the non-Gaussian turbulence based on the model of Reeves, et al. [2], and calculates the filter functions listed in Table 2-1, page 26. There are three subroutines called by NONGAU, which are INPUT (see A8), COEF3 (see A-9(a)), and FFT (see A-3).

Nomenclature

N	Dimension number (input)
NC	Control number for specifying the velocity component (input) 1 for longitudinal component 2 for lateral component 3 for vertical component
DT	Time increment (input)
Z	Height (input)
V	Reference velocity
R	PDF adjusting coefficient r (input)
XT	Real part of simulated turbulence (output)
XI	Imaginary part of simulated turbulence (output)

Listing

```
      SUBROUTINE NONGAU(N,NC,DT,Z,V,XR,XI,R)
      DIMENSION XR(N),XI(N),ALA(3),SIGS(3),QR(2048)
      COMMON/SI/AL,SIG,IP,A2,A24,AD2,AC2
      NT2=(ALOG(1.*N))/(ALOG(2.))
      NH=N/2
      TN=1./(N*DT)
      NHF=NH+1
      CALL SAL(Z,ALA,SIGS,V)
      AL=ALA(NC)
      SIG=SIGS(NC)
      QR=1./(SQRT(1.+R*R))
      ROR=R*QR
      NR=1
  100 CALL COEF3(Z,V,A,C,D,NC,NR)
      CALL INPUT(N,1,DT,IX,XR,XI)
      CALL FFT(N,NT2,1,XR,XI)
      DO 150 I=1,NHF
      F=(I-1)*TN
      F2=F*F
      AMF=A2-F2
      DD=1./(AMF*AMF+A24*F2)
      HR=DD*(C*AMF+AD2*F2)
      HI=DD*(D*AMF-AC2)*F
      XXR=XR(I)*HR-XI(I)*HI
      XI(I)=XR(I)*HI+XI(I)*HR
  150 XR(I)=XXR
      NTT=N+2
      DO 190 I=2,NH
      J=NTT-I
      XR(J)=XR(I)
  190 XI(J)=-XI(I)
      CALL FFT(N,NT2,2,XR,XI)
      IF(NR-2) 200,300,400
  200 DO 250 I=1,N
  250 QR(I)=XR(I)
      NR=NR+1
      GO TO 100
  300 DO 350 I=1,N
  350 QR(I)=QR(I)*XR(I)
      NR=3
      GO TO 100
  400 DO 450 I=1,N
  450 XR(I)=XR(I)*QR+QR(I)*ROR
      RETURN
      END
```

A-9(a). Subroutine COEF3 (Z, V, A, C, D)

Subroutine COEF3 computes the coefficients for the filter functions listed in Table 2-1, page 26.

Nomenclature

Z	Height (input)
V	Reference velocity (input)
A	Coefficient a (output)
C	Coefficient c (output)
D	Coefficient d (output)

Listing

```
      SUBROUTINE COEF3(Z,V,A,C,D,NC,NR)
      COMMON/ST/AL,SIG,IP,A2,A24,AD2,AC2
      VOA=V/AL
      W=SQRT(126)
      VOA2=0.5*VOA
      IF(NC-2) 100,200,200
  100 IF(NR-2) 110,140,170
  110 A=VOA2
      C=4.*SIG/VOA*A*A
      D=1.
      GO TO 400
  140 A=VOA2
      C=A*A
      D=1.
      GO TO 400
  170 A=VOL
      C=SIG*(SQRT(2./VOA))*A*A
      D=1.
      GO TO 400
  200 IF(NR-2) 210,240,270
  210 A=VOA2
      C=SIG*W/(VOA**2)*A*A
      D=1.
      GO TO 400
  240 A=VOA2
      C=0.
      D=A
      GO TO 400
  270 A=VOA
      C=SIG*A/(SQRT(VOA))
      D=C*1.732/VOA
  400 A2=A*A
      A24=4.*A2
      AC2=2.*A*C
      AD2=2.*A*D
      RETURN
      END
```

A-10. Subroutine COHER (N, Z, DZ, DT, Y1, Y2)

Subroutine COHER simulates two levels of turbulence Y1 and Y2 with the coherence relation described in Equation (4-43). There are five subroutines called by COHER: BETA (see A-10(a)), NTRA (see A-10(b)), VHAT (see A-10(c), FILTER (see A-6), and FFT (see A-3).

Nomenclature

N	Dimension number (input)
Z	Height of the level one (input)
DZ	Vertical separation for two levels (input)
DT	Time increment (input)
Y1	Simulated coherent turbulence at level 1 (output)
Y2	Simulated coherent turbulence at level 2 (output)

Listing

```
      SUBROUTINE COHER(N,Z,DZ,DT,Y1,Y2)
      DIMENSION Y1(N),Y2(N)
      DIMENSION RNR(11,512),RNI(11,512),XR(512),XI(512),B(11)
      COMMON/T2/PI,Z1,DX,EPO,A
      COMMON/T3/NP21,NHF,NT2
      UREF=5.0
      IX=65549
      NT2=(ALOG(1.*N))/(ALOG(2.))
      NH=N/2
      NHF=NH+1
      NP21=11
      PI=3.141593
      A=17./(2.*PI)
      Z1=Z
      DZM=3.
      IL=1
      EPO=DZM*PI/(UREF*DT)
      DX=UREF*DT/(PI*2.)
      CALL BETA(NP21,B)
      CALL NTRA(N,DT,IX,RNR,RNI,XR,XI)
  100 CALL VHAT(N,DT,RNR,RNI,XR,XI,B)
```

```
      CALL FILTER(N,NM,DT,Z,UREF,XR,XI)
      CALL FFT(N,NT2,2,XR,XI)
      IF(IL.EQ.2) GO TO 300
      DO 200 K=1,N
      Y1(K)=XR(K)
  200 CONTINUE
      Z=Z-DZ
      IL=IL+1
      GO TO 100
  300 DO 310 K=1,N
      Y2(K)=XR(K)
  310 CONTINUE
      RETURN
      END
```

A-10(a). Subroutine BETA (N, B)

Subroutine BETA computes the coefficients B_m of Equation (4-38) using Equations (2-45) and (2-42).

Nomenclature

N	Dimension number (input)
B	Coefficient array B_m (output)

Listing

```
      SUBROUTINE BETA(NP21,B)
      DIMENSION B(NP21)
      COMMON/T2/PI,Z1,DX,EPO,A
      NP1=(NP21-1)/2+1
      D=A*EPO/2.
      B(NP1)=0.5
      SUM=1.
      EXEO=EXP(-D)
      PE2=PI/D
      ANUM=(1.+EXEO)/(1.-EXEO)
      DO 300 I=1,NP1,2
      K=NP1-I
      B(K)=ANUM/(1.+(PE2*I)**2)
      IF(K.EQ.1) GO TO 100
      B(K-1)= 1./(1.+(PE2*(I+1))**2)
      SUM=SUM+2.*(B(K)+B(K-1))
      B(K-1)=SQRT(B(K-1))
      GO TO 200
  100 SUM=SUM+2.*B(K)
  200 B(K)=SQRT(B(K))
  300 CONTINUE
```

```
      DO 400 I=1,NP1
400   B(I)=B(I)/SQRT(SUM)
      RETURN
      END
```

A-10(b). Subroutine NTRA (N, DT, IX, RNR, RNI, XR, IX)

Subroutine NTRA generates 11 sets of random signals for the coherence model.

Nomenclature

M	Dim nsion number (input)
DT	Time increment (input)
IX	Seed number for calling GAUSS (input and output)
RNR	Real part of the random signal (output)
RNI	Imaginary part of the random signals (output)
XR, XI	Working space

Listing

```
      SUBROUTINE NTRA(N,DT,IX,RNR,RNI,XR,XI)
      DIMENSION RNR(11,512),RNI(11,512),XR(512),XI(512)
      COMMON/T3/NP21,NHF,NT2
      DO 300 J=1,NP21
      CALL INPUT(N,1,DT,IX,XR,XI)
      CALL FFT(N,NT2,1,XR,XI)
      DO 200 I=1,NHF
      RNR(J,I)=XR(I)
      RNI(J,I)=XI(I)
  200 CONTINUE
  300 CONTINUE
      RETURN
      END
```

A-10(c). Subroutine VHAT (N, DT, RNR, RNI, XR, XI, B)

Subroutine VHAT is a part of the coherence model, and computes the X'(k,z) in Equation (4-39).

Nomenclature

N	Dimension number (input)
DT	Time increment (input)
RNR, RNI	Real and imaginary part of random signal (input)
XR, XI	Real and imaginary part of calculated X' (output)
B	Coefficient array B_m in Equation (4-38) (input)

Listing

```
      SUBROUTINE VHAT(N,DT,RNR,RNI,XR,XI,B)
      DIMENSION RNR(11,512),RNI(11,512),XR(512),XI(512),B(11)
      COMMON/T2/PI,ZI,DX,EPO,A
      COMMON/T3/NP21,NHF,NT2
      N12=NP21+1
      PI2=PI*2.
      CRIT=DX*N*PI/10.
      BETA=PI*ZI/(EPO*DX*N)
      DO 200 K=1,NHF
      FKK=1.*(K-1)
      IF(FKK.GE.CRIT) FKK=CRIT
      XR(K)=0.
      XI(K)=0.
      DO 100 L=1,NP1
      AUG=BETA*(NP1-L)
      AUGN=(-AUG)*FKK
      AUGP=(AUG)*FKK
      CSN=COS(AUGN)
      CSP=COS(AUGP)
      SNN=SIN(AUGN)
      SNP=SIN(AUGP)
      XR(K)=XR(K)+(RNR(N12-L,K)*CSN+RNR(L,K)*CSP-RNI(N12-L,K)*
     *SNN-RNI(L,K)*SNP)*B(L)
      XI(K)=XI(K)+(RNI(N12-L,K)*CSN+RNI(L,K)*CSP+RNR(N12-L,K)*
     *SNN+RNR(L,K)*SNP)*B(L)
  100 CONTINUE
  200 CONTINUE
      RETURN
      END
```

A-11. Subroutine COHERS (N, NS, DT, Y1, Y2, CO)

Subroutine COHERS computes the coherence function of the two time histories Y1 and Y2 by using Equation (4-41).

Nomenclature

N	Dimension number (input)
NS	Sample size (input)
DT	Time increment (input)
Y1	Time history at level 1 (input)
Y2	Time history at level 2 (input)
CO	Estimated coherence of Y1 and Y2 (output)

Listing

```
      SUBROUTINE COHERS(N,NS,DT,Y1,Y2,CO)
      DIMENSION Y1(NS,N),Y2(NS,N),CO(N)
      DIMENSION XR(2048),XI(2048),COR(1024),COI(1024),SP(1024)
      DIMENSION CORR(1024),COII(1024)
      NT2=(ALOG(1.*N)/ALOG(2.))
      NH=N/2
      RT=DT/NH
      DO 90 K=1,NH
      CORR(K)=0.
      COII(K)=0.
   90 CONTINUE
      DO 300 L=1,NS
      DO 100 K=1,N
      XR(K)=Y1(K,L)
      XI(K)=0.
  100 CONTINUE
      CALL SPEC(N,NT2,DT,XR,XI,SP)
      DO 110 K=1,NH
      COR(K)=XR(K)
      COI(K)=XI(K)
      Y1(K,L)=SP(K)
  110 CONTINUE
      DO 200 K=1,N
      XR(K)=Y2(K,L)
      XI(K)=0.
  200 CONTINUE
      CALL SPEC(N,NT2,DT,XR,XI,SP)
      DO 210 K=1,NH
```

```
      CORR(K)=CORR(K)+COR(K)*XR(K)-COI(K)*XI(K)
      COII(K)=COII(K)+COR(K)*XI(K)+COI(K)*XR(K)
      Y2(K,L)=SP(K)
  210 CONTINUE
  300 CONTINUE
      DO 400 K=1,NH
      SUM1=0.
      SUM2=0.
      DO 350 L=1,NS
      SUM1=SUM1+Y1(K,L)
      SUM2=SUM2+Y2(K,L)
  350 CONTINUE
      Y1(K,1)=SUM1/NS
      Y2(K,1)=SUM2/NS
      CORR(K)=CORR(K)/NS
      COII(K)=COII(K)/NS
  400 CONTINUE
      DO 500 K=1,NH
      CO(K)=RT*RT*(CORR(K)**2+COII(K)**2)/(Y1(K,1)*Y2(K,1))
  500 CONTINUE
      RETURN
      END
```

A-12. Subroutine WIND (XP, ZP, T, V, KCK)

Subroutine WIND computes the turbulent wind velocity U_1 and U_2 (see Equations (5-1) and (5-2)).

Nomenclature

XP,ZP Aircraft position (input)

T Time (input)

V Aircraft speed (input)

KCK Starting number KCK = 1 (input)

COMMON/WINDS/

WX,WZ Wind velocities U_1, U_2 (output)

WXT,WZT Time gradient terms $\partial U_1/\partial t$, $\partial U_2/\partial t$ (output)

WXX,WXZ Spatial gradient terms $\partial U_1/\partial x$, $\partial U_1/\partial z$ (output)

WZX,WZZ Spatial gradient terms $\partial U_2/\partial x$, $\partial U_2/\partial z$ (output)

Listing

```
      SUBROUTINE WIND (XP,ZP,T,V,KCK)
      COMMON/WINDS/WX,WZ,WXT,WZT,WXX,WXZ,WZX,WZZ,ZO,USTAR
      COMMON/STSR/FAT,WDRI
   31 FORMAT(2X,'  ***POINT X = ',E13.6,' Z = ',E13.6,' IS OUTSIDE ')
      AKP=0.4
      IF(XP.LT.0..OR.ZP.LT.0.) GO TO  210
      UOK=WDRI*USTAR/AKP
      WX=-UOK*(ALOG((ZP+ZO)/ZO))
      WZ=0.
      WXX=0.
      WXZ=-UOK/(ZP+ZO)
      WZX=0.
      WZZ=0.
      WXT=0.
      WZT=0.
      CALL VELO(XP,ZP,T,V,KCK)
      GO TO 215
  210 WRITE(6,31) XP,ZP
  215 RETURN
      END
      SUBROUTINE VELO(XP,ZP,T,V,KCK)
      COMMON/TT1/DX,DT,NNN,NT2
      COMMON/TT2/GG(2,128)
      COMMON/TT4/IX,RR,METH
      COMMON/TT5/XPR,ZPR,TEND,ZOWR
      COMMON/WINDS/WX,WZ,WXT,WZT,WXX,WXZ,WZX,WZZ,ZO,USTAR
      DNN=DT*NNN
      WXR=ABS(WX)
      IF(ABS(WX).LT.0.0000001) WXR=0.00001
      IF(KCK-1) 101,101,103
  101 XPR=XP
      ZPR=ZP
      CALL ROMDUN(ZP)
      ZOWR=ZP/WXR
      TEND=DNN
      GO TO 105
  103 ZOW=ZP/WXR
      IF (ZP.LT.20.) GO TO 105
      RRR=ZOW/ZOWR
      DDD=ABS(1-RRR)
      IF(DDD.LT.0.2) GO TO 105
  104 CALL ROMDUN(ZP)
      ZOWR=ZOW
      XPR=XP
      ZPR=ZP
      TEND=T+DNN
  105 TRP=T+ABS((XP-XPR)/V)
      IF(TPP-TEND) 109,104,104
  109 ER=(TRP+DNN-TEND)/DT
      NT=ER+1
      NTR=NT+1
      IF(NTP.GT.128) GO TO 104
      UP=GG(1,NT)
      VP=GG(2,NT)
      WX=WX+UP
      WZ=WZ+VP
```

```
      DLD=V*DT
      WXX=WXX+(GG(1,NTP)-GG(1,NT))/DLD
      WZX=WZX+(GG(2,NTP)-GG(2,NT))/DLD
  120 CONTINUE
      RETURN
      END

      SUBROUTINE ROMDUN(ZP)
      COMMON/TT1/DX,DT,NNN,NT2
      COMMON/TT2/GG(2,128)
      COMMON/TT4/IX,RR,MEPH
      COMMON/FT/XGR(128),XGI(128)
      COMMON/STSR/FAT,WDRI
      COMMON/WINDS/WX,WZ,WXT,WZT,WXX,WXZ,WZX,WZZ,ZO,USTAR
      SIGX=SQRT(3.141596/DT)
      DO 110 I=1,2
      DO 105 J=1,NNN
      CALL GAUSS(IX,SIGX,0.,R)
      XGR(J)=R
  105 CONTINUE
      DO 108 J=1,NNN
      XGI(J)=0.
  108 CONTINUE
      CALL FFT(NNN,NT2,1)
      CALL FILTER(ZP,I)
      CALL FFT(NNN,NT2,2)
      WRITE(6,1) (XGR(K),K=1,NNN,5)
    1 FORMAT(1X,20F5.2)
      DO 109 J=1,NNN
      GG(I,J)=XGR(J)*FAT
  109 CONTINUE
  110 CONTINUE
      RETURN
      END

      SUBROUTINE FILTER(ZP,IOP)
      COMMON/TT1/DX,DT,NNN,NT2
      COMMON/FT/XGR(128),XGI(128)
      COMMON/WINDS/WX,WZ,WXT,WZT,WXX,WXZ,WZX,WZZ,ZO,USTAR
      PI=3.141596
      AL=ZP/(0.177+0.832/304.79*ZP)**1.2
      UMEAN=ABS(WX)
      IF(UMEAN.LT.0.0001) UMEAN=0.0001
      SIG3=0.52*UMEAN/((ALOG(ZP/ZO+1)))
      SIG=SIG3/((0.177+0.00274*ZP)**(0.4))
      IF(IOP.EQ.2) SIG=SIG3/((0.583+0.00139*ZP)**(0.8))
      AOV=AL/UMEAN
      NH=NNN/2
      NHF=NH+1
      TN=1./(NNN*DT)
  100 CONTINUE
      IF(IOP.EQ.2) GO TO 115
      A1=1./(1.339*AOV*2.*PI)
      C1=4.*AOV*SIG*SIG*(A1**1.000000)
      PO=5./12.
      C1S=SQRT(C1)
      FAC=-5./6.
      A12=A1*A1
      DO 110 K=1,NHF
```

```
      S2=S*S
      D=C1S/((A12+S2)**PO)
      ANG=FAC*(ATAN(S/A1))
      HR=D*(COS(ANG))
      HI=D*(SIN(ANG))
      XAR=XGR(K)*HR-XGI(K)*HI
      XGI(K)=XGI(K)*HR+XGR(K)*HI
      XGR(K)=XAR
  110 CONTINUE
      GO TO 300
  115 CONTINUE
      A=1./(1.339*AOV*2.*PI)
      C=A*(SQRT(3./8.))
      C2=C*C
      B2=2.*SIG*SIG*AOV*(A**(11./3.))/(C2)
      B=SQRT(B2)
      A2=A*A
      PW=11./12.
      PW2=11./6.
      DO 120 K=1,NHF
      S=(K-1)*TN
      S2=S*S
      D=B*(SQRT(C2+S2))/((A2+S2)**PW)
      ANG=ATAN(S/C)-PW2*(ATAN(S/A))
      HR=D*(COS(ANG))
      HI=D*(SIN(ANG))
      XAA=XGR(K)*HR-XGI(K)*HI
      XGI(K)=XGI(K)*HR+XGR(K)*HI
      XGR(K)=XAA
  120 CONTINUE
  300 N3=NMN+2
      DO 330 J=2,NH
      K=N3-J
      XGR(K)=XGR(J)
      XGI(K)=-XGI(J)
  330 CONTINUE
      RETURN
      END
```

APPENDIX B

VARIANCE OF DZT

An approach to derive exact equations for the output variance by using the DZT method is to calculate the variance directly by expressing the difference equation involving input and output variables in terms of the input variables only. Recall Equation (3-46):

$$y_{n+1} = Ay_n + Bx_n \ , \tag{B-1}$$

where

$$A = \exp(-a\Delta t) \quad , \quad B = \frac{\sqrt{c}}{a}\left(1 - \exp(-a\Delta t)\right)$$

$$a = \frac{V}{\Lambda} \quad , \quad c = \frac{2V\sigma_y^2}{\Lambda\pi} \ .$$

Rewrite Equation (B-1) so that

$$\begin{aligned} y_{n+1} &= Ay_n + Bx_n \\ y_n &= Ay_{n-1} + Bx_{n-1} \\ &\vdots \\ y_2 &= Ay_1 + Bx_1 \\ y_1 &= 0 \ . \end{aligned} \tag{B-2}$$

Substitute y_1 into y_2, y_2 into y_3,..., etc., which results in

$$y_{n+1} = A^{n-1} Bx_1 + A^{n-2} Bx_2 + \ldots + Bx_n$$

$$= \sum_{i=1}^{n} \alpha_i x_i ,$$

where

$$\alpha_i = B A^{i-1} .$$

Since x_i and y_i are independent, the variance can be calculated by

$$\hat{\sigma}_y^2 = \sigma_x^2 \lim_{n\to\infty} \sum_{i=1}^{n} \alpha_i^2$$

$$= \sigma_x^2 \frac{c}{a^2} \left(1 - e^{-\Delta t} \right)^2 \lim_{n\to\infty} \sum_{i=1}^{n} \left(e^{-a\Delta t} \right)^{i-1} \qquad \text{(B-4)}$$

Note that

$$\sum_{i=0}^{\infty} b^i = \frac{1}{1-b} .$$

Therefore, Equation (B-4) becomes

$$\frac{\hat{\sigma}_y^2}{\sigma_x^2} = \frac{2\sigma_y^2}{\pi a} \frac{\left(1 - e^{-a\Delta t} \right)^2}{1 - e^{-2a\Delta t}} . \qquad \text{(B-5)}$$

Consider the case for $a\Delta t$ very small,

$$\frac{(1 - e^{-a\Delta t})^2}{1 - e^{-2a\Delta t}} = \frac{(1 - 1 + a\Delta t - \frac{(a\Delta t)^2}{2!} + \ldots)^2}{1 - 1 + 2\,a\Delta t - \ldots}$$

$$\approx \frac{a\Delta t}{2} . \qquad \text{(B-6)}$$

Hence, Equation (B-5) reduces to

$$\frac{\hat{\sigma}_y^2}{\sigma_x^2} = \frac{\Delta t}{\pi}\,\sigma_y^2 . \qquad \text{(B-7)}$$

APPENDIX C

EQUATIONS OF MOTION FOR LANDING SIMULATION

The three-degree-of-freedom model for aircraft motion presented in this appendix follows the general form developed by Neuman and Foster [1], except the non-linear terms are retained. It accounts for both vertical and horizontal mean wind components having both time and spatial variations.

Figure C-1 illustrates the forces acting on the aircraft. These include:

$\vec{F}_T$ = thrust of the engines

$\vec{L}$ = lift

$\vec{D}$ = drag

$\vec{U}$ = wind vector

$\vec{mg}$ = gravitational force .

Figure C-1 shows the orientation of the forces with respect to the velocity relative to the earth V, the velocity relative to the air mass V_a, and the fuselage reference line FRT of the aircraft.

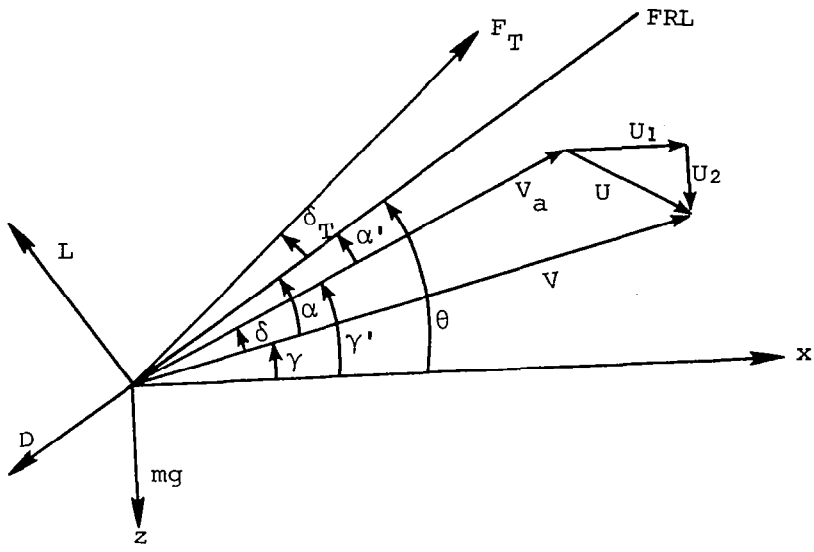

Figure C-1. The forces acting on the aircraft.

The basic variables are V, γ, q, α', x, and z, where

γ = angle between V and x-axis (flight path angle)

q = time derivative of θ (pitch rate)

α' = angle between V_a and the FRL (angle of attack)

From a direct force balance along each direction and basic kinematic relations, the equations of motion can be derived as

$$\dot{V} = -D_1 (c_D \cos \delta + c_L \sin \delta) V_a^2 - D_2 \sin \gamma + D_2 \sin \gamma + D_6 F_T \cos (\delta_T + \alpha)$$

$$\dot{\gamma} = \frac{D_1 V_a^2}{V} (c_L \cos \delta - c_D \sin \delta) - D_2 \frac{\cos \gamma}{V} + D_6 F_T \frac{\sin (\delta_T + \alpha)}{V}$$

$$\dot{q} = D_7 F_T + D_5 V_a^2 c_M$$

$$\dot{\alpha}' = q - D_1 c_L V_a + D_2 \frac{\cos \gamma'}{V_a} - D_6 F_T \frac{\sin (\delta + \alpha')}{V_a} - \frac{1}{V_a} (\dot{U}_1 \sin \gamma' + \dot{U}_2 \cos \gamma')$$

$$\dot{x} = V \cos \gamma$$

$$\dot{z} = -V \sin \gamma \ ,$$

where D_1, D_2, ... D_7 are the nondimensional coefficients and c_L, c_D, and c_M are the aerodynamic coefficients defined by

$$c_L = c_{L_o} + c_{L_a} \alpha' + c_{L_{\delta_E}} \delta_E + \frac{D_4}{V_a} [c_{L_q} q + c_{L_{\dot{a}}} \dot{\alpha}'] + c_{L_{GE}}$$

$$c_D = c_{D_o} + c_{D_a} \alpha' + c_{D_{a^2}} \alpha'^2 + c_{D_{GE}}$$

$$c_M = c_{M_o} + c_{M_a} \alpha' + c_{M_{\delta_E}} \delta_E + \frac{D_4}{V_a} [c_{M_q} q + c_{M_{\dot{a}}} \dot{\alpha}'] + c_{M_{GE}}$$

The wind is seen to enter the equations in the form of a gradient or wind shear $\dot{U}_1$ and $\dot{U}_2$. The expanded form of these equations is:

$$\dot{U}_1 = \frac{\partial U_1}{\partial t} + \frac{\partial U_1}{\partial x}\frac{dx}{dt} + \frac{\partial U_1}{\partial z}\frac{dz}{dt}$$

$$\dot{U}_2 = \frac{\partial U_2}{\partial t} + \frac{\partial U_2}{\partial x}\frac{dx}{dt} + \frac{\partial U_2}{\partial z}\frac{dz}{dt} \cdot$$

Thus, both spatial variations and temporal variations in atmospheric motion influence the equations in the wind coordinate system.

APPENDIX D

LANDING RESULTS

This appendix presents landing results for non-Gaussian, Dryden spectrum turbulence, and Gaussian, von Karman spectrum turbulence (Table D-1).

Table D-1. Landing Results

No.	Non-Gaussian, Dryden Spectrum Turbulence		Gaussian, von Karman Spectrum Turbulence	
	Landing Position	Standard Deviation	Landing Position	Standard Deviation
1	7033.13	62.41	6926.15	-35.97
2	6924.73	-46.0	6984.11	21.99
3	6983.23	12.51	6991.46	29.34
4	6933.35	-37.37	7009.88	47.76
5	6968.89	-1.83	6986.71	24.59
6	6998.80	28.08	6992.73	30.61
7	6977.84	7.12	7022.72	60.60
8	6917.63	-53.09	7016.62	54.50
9	7007.27	36.55	6909.70	-52.42
10	6920.63	-50.09	6923.54	-38.58
11	6976.52	5.8	6962.78	0.66
12	6939.20	-31.50	7008.04	45.92
13	7057.49	86.77	6951.11	-11.01
14	6974	5.03	6948.43	6.31
15	6969.15	-1.57	6914.48	-47.64
16	7009.27	38.55	6925.56	-36.56
17	6994.06	23.24	6927.14	-34.98
18	6944.93	-25.79	6896.60	-65.52
19	6946.49	-24.23	6960.51	-1.61
20	6936.05	-34.67	6964.12	2.00
Average	6970.72	37.51	6962.12	32.43

Note: $u_* = 0.5$, $z_o = 0.1$.

TECHNICAL REPORT STANDARD TITLE PAGE

1. REPORT NO.	2. GOVERNMENT ACCESSION NO.	3. RECIPIENT'S CATALOG NO.
NASA CR-3309		

4. TITLE AND SUBTITLE	5. REPORT DATE
Atmospheric Turbulence Simulation Techniques With Application to Flight Analysis	September 1980
	6. PERFORMING ORGANIZATION CODE
7. AUTHOR(S)	8. PERFORMING ORGANIZATION REPORT #
Show-Tien Wang and Walter Frost	
9. PERFORMING ORGANIZATION NAME AND ADDRESS	10. WORK UNIT NO.
	M-302
The University of Tennessee Space Institute Tullahoma, Tennessee 37388	11. CONTRACT OR GRANT NO. NAS8-32692
	13. TYPE OF REPORT & PERIOD COVERED
12. SPONSORING AGENCY NAME AND ADDRESS	Contractor Report
National Aeronautics and Space Administration Washington, D. C. 20546	14. SPONSORING AGENCY CODE

15. SUPPLEMENTARY NOTES

Marshall Technical Monitor: Dennis W. Camp
Final Report

16. ABSTRACT

Statistical modeling of atmospheric turbulence is discussed. The statistical properties of atmospheric turbulence, in particular the probability distribution, the spectra, and the coherence are reviewed. Different atmospheric turbulence simulation models are investigated, and appropriate statistical analyses are carried out to verify their validity.

The models for simulation are incorporated into a computer model of aircraft flight dynamics. Statistical results of computer simulated landings for an aircraft having characteristics of a DC-8 are reported for the different turbulence simulation techniques.

The significance of various degrees of sophistication in the turbulence simulation techniques on the landing performance of the aircraft is discussed.

17. KEY WORDS	18. DISTRIBUTION STATEMENT
Wind Shear Wind Turbulence Flight Simulation	Unclassified - Unlimited Subject Category 47

19. SECURITY CLASSIF. (of this report)	20. SECURITY CLASSIF. (of this page)	21. NO. OF PAGES	22. PRICE
Unclassified	Unclassified	170	A08

For sale by National Technical Information Service, Springfield, Virginia 22161

NASA-Langley, 1980